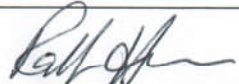
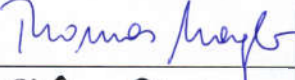


 	<p>SARSimHT-NG – Simulation of Hydroterra SAR System Performance in the Mediterranean and the Alps Based on Experimental Airborne SAR Data</p> <p>D1: Data Acquisition Report of SWE Experiment</p>	<p>Doc.: DLR-HR-TR-SARSimHT-NG-01 Issue: 2.0 Date: 25.11.2021 Page: 1 of 110</p>
--	---	---

D1: Data Acquisition Report of SWE Experiment

SARSimHT-NG – Simulation of Hydroterra SAR System Performance in the Mediterranean and the Alps Based on Experimental Airborne SAR Data
(EESA Contract 4000134680/21/NL/FF/an)

Reference: DLR-HR-TR-SARSimHT-NG-01

	Name	Date & Signature
Prepared by	Horn, Ralf	25.11.2021 
	Gracheva, Valeria	06.12.2021 
	Fischer, Jens	29.11.21 
	Nagler, Thomas	29/11/2021 
	Scheiblauer, Stefan	29/11/2021 
Released by	Reigber, Andreas	A. Reigber  <small>Digital signiert von Andreas Reigber DN: C=DE, O=Deutsches Zentrum fuer Luft- und Raumfahrt e.V. (DLR), CN=Andreas Reigber Grund: Ich genehmige dieses Dokument Ort: Seefeld Datum: 2021.12.06 11:42:52+01'00' Foxit PDF Editor Version: 11.0.0</small>

Approval and release information:

This document has been approved either by manual signatures or via electronic workflow.



 	<p>SARSimHT-NG – Simulation of Hydroterra SAR System Performance in the Mediterranean and the Alps Based on Experimental Airborne SAR Data</p> <p>D1: Data Acquisition Report of SWE Experiment</p>	<p>Doc.: DLR-HR-TR-SARSimHT-NG-01 Issue: 2.0 Date: 25.11.2021 Page: 2 of 110</p>
--	---	---

Document Preparation

The document on hand was prepared with contributions from the personnel listed below:

Name	Organization
Gracheva, Valeria	DLR-HR
Horn, Ralf	DLR-HR
Fischer, Jens	DLR-HR
Scheiblauer, Stefan	ENVEO IT
Nagler, Thomas	ENVEO IT

Distribution List

Name	Organization	Type
Alberto Moreira	DLR-HR	PDF
Andreas Reigber	DLR-HR	PDF
Julia Kubanek	ESA	DOCX, PDF

Document Change Details

Latest changes to the document are listed first.

Issue	Date	Modified Pages/Sections	Changes
2.0	25.11.2021	All	Final issue
1.0	03.09.2021	All	First issue (draft)

 	<p>SARSimHT-NG – Simulation of Hydroterra SAR System Performance in the Mediterranean and the Alps Based on Experimental Airborne SAR Data</p> <p>D1: Data Acquisition Report of SWE Experiment</p>	<p>Doc.: DLR-HR-TR-SARSimHT-NG-01 Issue: 2.0 Date: 25.11.2021 Page: 3 of 110</p>
--	---	---

Table of Contents

Table of Contents	3
List of Acronyms and Abbreviations	5
Documents	6
Applicable Documents.....	6
Reference Documents	6
1 Introduction and Purpose of the Document	7
2 Airborne SAR Measurements for SWE	8
2.1 The F-SAR System – Description and Measurement Settings.....	8
2.2 Flight Planning and Radar Geometry.....	9
2.3 21HTERRA SWE Campaign Execution	11
2.3.1 Acquisition Procedure for HYDROTERRA Simulation	13
3 Field Measurements	14
3.1 Description of Test site	14
3.2 Corner Reflectors	15
3.3 Devices	16
3.4 Methods for Snow Pit Measurements	16
3.5 Auxiliary datasets - DEM.....	16
3.6 Field measurements.....	17
3.6.1 Field campaign 02.03.2021	17
3.6.2 Field campaign 03.03.2021	21
3.6.3 Field campaign 06.03.2021	24
3.6.4 Field campaign 19.03.2021	27
3.6.5 FC Dates Wörgetal.....	33
3.7 Meteorological datasets	33
3.8 Database description	33
4 Processing Strategy and Inventory	35
4.1 Preparations.....	35
4.1.1 Digital Elevation Model and Tie Points.....	35
4.1.2 Ideal Track Assignment	37
4.1.3 Squint Angle Analysis.....	38
4.1.4 Processing Strategy	40
4.2 Processing Results	40
4.2.1 Processing Parameters.....	40
4.2.2 Overview and Image Geometries	41
4.2.3 Corner Reflectors in RGI Data	43
4.2.4 Radar Geometry Image (RGI) Product Generation.....	45
4.2.5 Geocoded and Terrain Corrected (GTC) Product Generation.....	46
4.2.6 Interferometric Image Product (INF) Product Generation	47
4.3 Calibration Check.....	55

 	<p>SARSimHT-NG – Simulation of Hydroterra SAR System Performance in the Mediterranean and the Alps Based on Experimental Airborne SAR Data</p> <p>D1: Data Acquisition Report of SWE Experiment</p>	<p>Doc.: DLR-HR-TR-SARSimHT-NG-01 Issue: 2.0 Date: 25.11.2021 Page: 4 of 110</p>
--	---	---

- 4.4 Inventory of Data Products 59
 - 4.4.1 Radar Geometry Image (RGI) Products 59
 - 4.4.2 Geocoded and Terrain Corrected (GTC) Products 59
 - 4.4.3 Interferometric (INF) Products 60
- 4.5 Summary of Data Products 69
- 5 Simulation of Hydroterra Products 70**
 - 5.1 Overview 70
 - 5.2 Simulation Procedure 71
 - 5.3 Simulated Geosynchronous SAR Products with F-SAR Resolution..... 72
 - 5.3.1 Simulation and Analysis of Geosynchronous SAR Image Products 72
 - 5.3.2 Interferometric Geosynchronous SAR Products..... 84
 - 5.4 Simulated Hydroterra Products 93
 - 5.5 Data Products Format..... 106
 - 5.6 Delivered Simulation Products..... 108
- 6 Summary 110**

 	<p>SARSimHT-NG – Simulation of Hydroterra SAR System Performance in the Mediterranean and the Alps Based on Experimental Airborne SAR Data</p> <p>D1: Data Acquisition Report of SWE Experiment</p>	<p>Doc.: DLR-HR-TR-SARSimHT-NG-01 Issue: 2.0 Date: 25.11.2021 Page: 5 of 110</p>
--	---	---

List of Acronyms and Abbreviations

DAR	Data Acquisition Report
DLR	Deutsches Zentrum für Luft- und Raumfahrt e.V., German Aerospace Center
DLR-HR	German Aerospace Center, Microwaves and Radar Institute
ENVEO IT	Environmental Earth Observation Information Technology GmbH
ESA	European Space Agency
InSAR	Interferometric SAR
NESZ	Noise Equivalent Sigma Zero
PRF	Pulse Repetition Frequency
ROSE-L	L-Band Radar Observation System for Europe
SAR	Synthetic Aperture Radar
Sentinel-1 NG	Sentinel-1 Next Generation
SLC	Single-Look Complex
SNR	Signal-to-Noise Ratio
SSM	Surface Soil Moisture
SWE	Snow Water Equivalent
WP	Work Package

 	<p>SARSimHT-NG – Simulation of Hydroterra SAR System Performance in the Mediterranean and the Alps Based on Experimental Airborne SAR Data</p> <p>D1: Data Acquisition Report of SWE Experiment</p>	<p>Doc.: DLR-HR-TR-SARSimHT-NG-01 Issue: 2.0 Date: 25.11.2021 Page: 6 of 110</p>
--	---	---

Documents

Applicable Documents

- [A1] Statement of Work. SARSimHT-NG – Simulation of Hydroterra SAR System Performance in the Mediterranean and the Alps Based on Experimental Airborne SAR Data. ESA-EOPSM-CAMP-SOW-3812, Issue 1, Revision 6, 04/02/2021.

Reference Documents

- [1] SARSimHT 2019: "Final Report", Technical Report: DLR-HR-TR-SARSimHT-2019-003, Oct. 2020.
- [2] Ralf Horn, Marc Jaeger, Martin Keller, Markus Limbach, Anton Nottensteiner, Matteo Pardini, Andreas Reigber, Rolf Scheiber (2017), "F-SAR – Recent Upgrades and Campaign Activities". In: 13th International Radar Symposium (IRS), 2017-06-28 - 2017-06-30, Prague, Czechia. CUVILLIER VERLAG. ISBN 978-3-7369-9542-0.)
- [3] Fierz, C., Armstrong, R.L., Durand, Y., Etchevers, P., Greene, E., McClung, D.M., Nishimura, K., Satyawali, P.K. and Sokratov, S.A. 2009. The International Classification for Seasonal Snow on the Ground. IHP-VII Technical Documents in Hydrology No. 83, UNESCO-IHP, Paris. 90 pp.
- [4] R. Scheiber, S.-K. Lee, K. P. Papathanassiou, N. Floury, "Extrapolation of Airborne Polarimetry and Interferometric SAR Data for Validation of Bio-Geo-Retrieval Algorithms for Future Spaceborne SAR Missions", Proc. IGARSS, Cape Town, 2009.
- [5] Description of Simulated Amplitude Results for Hydroterra (Technical Report: DLR-HR-TR-SARSimHT-2019-002).
- [6] Curlander, J. C., and R. N. McDonough, "Synthetic Aperture Radar: Systems and Signal Processing", 647 pp., John Wiley, New York, 1991.
- [7] Hydroterra Earth Explorer 10 Mission Candidate Mission Assumptions and Preliminary Technical Requirements (MATER).
- [8] DLR's Airborne SAR System F-SAR PRODUCT DESCRIPTION, Version: 3.2.

 	<p>SARSimHT-NG – Simulation of Hydroterra SAR System Performance in the Mediterranean and the Alps Based on Experimental Airborne SAR Data</p> <p>D1: Data Acquisition Report of SWE Experiment</p>	<p>Doc.: DLR-HR-TR-SARSimHT-NG-01 Issue: 2.0 Date: 25.11.2021 Page: 7 of 110</p>
--	---	---

1 Introduction and Purpose of the Document

This document gives an overview of the airborne SAR campaign conducted on the test site Wörgetal in the Austrian Alps in L- and C-band, the simultaneously collected ground truth data, processed radar data and simulated Hydroterra products. The data will be used to analyse the potential to retrieve the snow water equivalent (SWE) from geosynchronous SAR data. A retrieval will also be performed from conventional SAR data at L- and C-band to support the missions ROSE-L and Sentinel-1 NG.

The data described in this document will be used as basis for the SARSimHT-NG study requested by ESA. The main goal of this study is to perform an assessment of the potential to retrieve snow water equivalent (SWE) and surface soil moisture (SSM) from future SAR systems in geosynchronous orbits. For this analysis the results from the SARSimHT 2019 study [1] will be used. In 2019 airborne radar data of the F-SAR system of DLR were used for the first time to simulate geosynchronous SAR products of the system Hydroterra. Hydroterra has been considered as one of the three candidates for ESA's Earth Explorer 10 mission and its mission concept consists in placing a SAR system into a geosynchronous orbit.

This document focusses on the data acquisition for an assessment of SWE retrieval. This document is structured as follows: Chapter 2 describes the airborne campaign. The ground-truth measurements are documented in Chapter 3. The processing of the airborne data is described in Chapter 4 and an inventory is provided. The simulation procedure of Hydroterra products is outlined in Chapter 5.

	<p>SARSimHT-NG – Simulation of Hydroterra SAR System Performance in the Mediterranean and the Alps Based on Experimental Airborne SAR Data</p> <p>D1: Data Acquisition Report of SWE Experiment</p>	<p>Doc.: DLR-HR-TR-SARSimHT-NG-01 Issue: 2.0 Date: 25.11.2021 Page: 8 of 110</p>
---	---	---

2 Airborne SAR Measurements for SWE

This chapter summarises the airborne SAR measurements which were performed with DLR’s airborne radar system F-SAR over the ‘Woergetal’ test site in Austria to investigate capabilities of spaceborne SAR instruments of deriving measures on Snow-Water-Equivalent (SWE) in Alpine regions. The measurements were carried out in C- and L-bands in regard to SENTINEL and upcoming HYDROTERRA and ROSE-L space systems.

2.1 The F-SAR System – Description and Measurement Settings

F-SAR is a fully polarimetric and interferometric airborne radar system, which can operate in X-, C-, S-, L- and P-bands. See [2] for more details. It was developed to define the “state-of-the-art” in SAR technology and perform scientific flight campaigns for the preparation of new satellite missions.

F-SAR is certified airworthy on-board the DLR DO 228-212 aircraft. The DO 228 is a twin-engine short take-off and landing turbo-prop aircraft without pressurised cabin. Figure 2-1 shows the DO 228 aircraft equipped with the F-SAR system. All antennas are pointing to the right-hand side of the aircraft. The antenna footprints on ground overlap from 20° to 65° off-nadir.



Figure 2-1: The F-SAR instrument on-board a DLR Dornier DO 228 aircraft. Antennas are mounted behind the wing (X-C-S-L) and under the cockpit (P).

Data collection took place in March 2021 as part of the 21HTERRA campaign in cooperation with ENVEO IT. F-SAR was operated in a 4-channel, dual-frequency, C- and L-band, fully polarimetric mode to match the new HYDROTERRA and ROSE-L space missions. Relevant system settings are listed in Table 2-1 below. In each radar band F-SAR operates with a single TX and two parallel RX chains. It requires two pulses for a fully polarimetric measurement. Polarisation is switched on transmit. Here in particular an L-band pulse is transmitted simultaneously with every second C-band pulse.

Table 2-1: F-SAR system parameters used in the course of the 21HTERRA measurement flights.

F-SAR system parameters	C-band	L-band
RF centre frequency	5300 MHz	1325 MHz
Signal bandwidth	384 MHz	150 MHz
Type of signal	FM modulated pulse ('Down-Chirp')	
Pulse duration	10 μ s	
Pulse repetition frequency per channel	1811 Hz	905.5 Hz
System range delay	26.4 μ s	
Receive gate duration	25 μ s	

2.2 Flight Planning and Radar Geometry

The 'Woergetal' test site in Austria (see Figure 2-2) is located in the Stubai Alps approx. 35km west from the City of Innsbruck. It is oriented almost North-South. The valley is characterized by gentle topography and has three flat parts along the valley floor (at 2000m, 2150m, and 2300m elevation) separated by steeper slopes. It is surrounded by mountain ridges as high as 2600m.

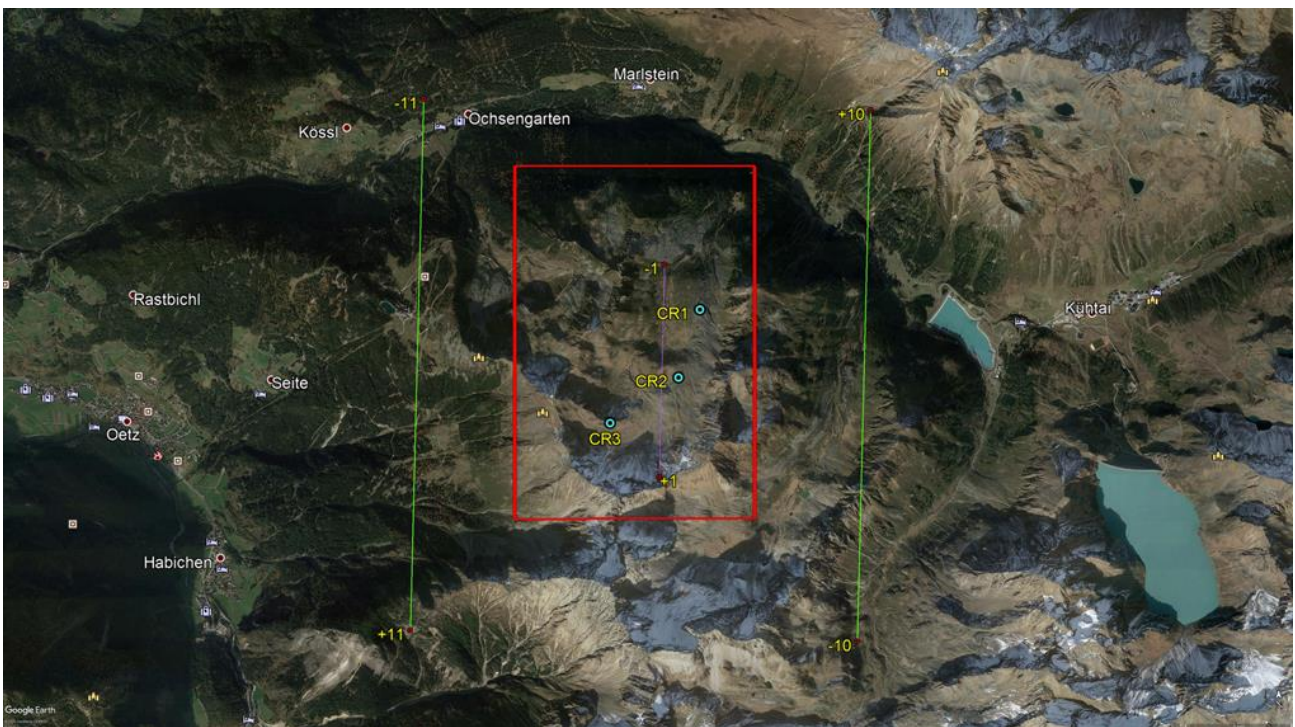


Figure 2-2: The 'Woergetal' test site situated in the Stubai Alps west of the City of Innsbruck (Austria). The red rectangle indicates the area to be imaged by F-SAR. Measurement flight tracks #10 and #11 are shown in green. Blue dots indicate positions of ground control points.

Figure 2-2 shows the 'Woergetal' SWE test site in the centre of the red rectangle. ENVEO IT recommended to illuminate the target area from opposite look directions, i.e. from east and from west. The valley floor (indicated by line #1 (purple)) should be imaged at an off-nadir angle of approx. 30° to 35° depending on look direction. Accordingly, two measurement flight tracks were planned offset east (#10)

and west (#11) from the valley floor line by approx. 1.9km and 2.3km, respectively. Each flight track is 5km long.

Flight planning is done in the WGS84 system in general. Hence, all altitudes are referenced to the WGS84 ellipsoid. The map base is Google Earth (GE). GE represents geographical coordinates in WGS84 and topographic heights are referenced to sea level. Therefore, in F-SAR flight planning we consider the local geoid height (from EGM96 or EGM2008) to obtain ellipsoidal terrain heights.

It is current practice to define F-SAR flight altitudes above ‘flat terrain’. This is basically a plane which cuts through the local topography at an average height above the WGS84 ellipsoid (see Figure 2-3).

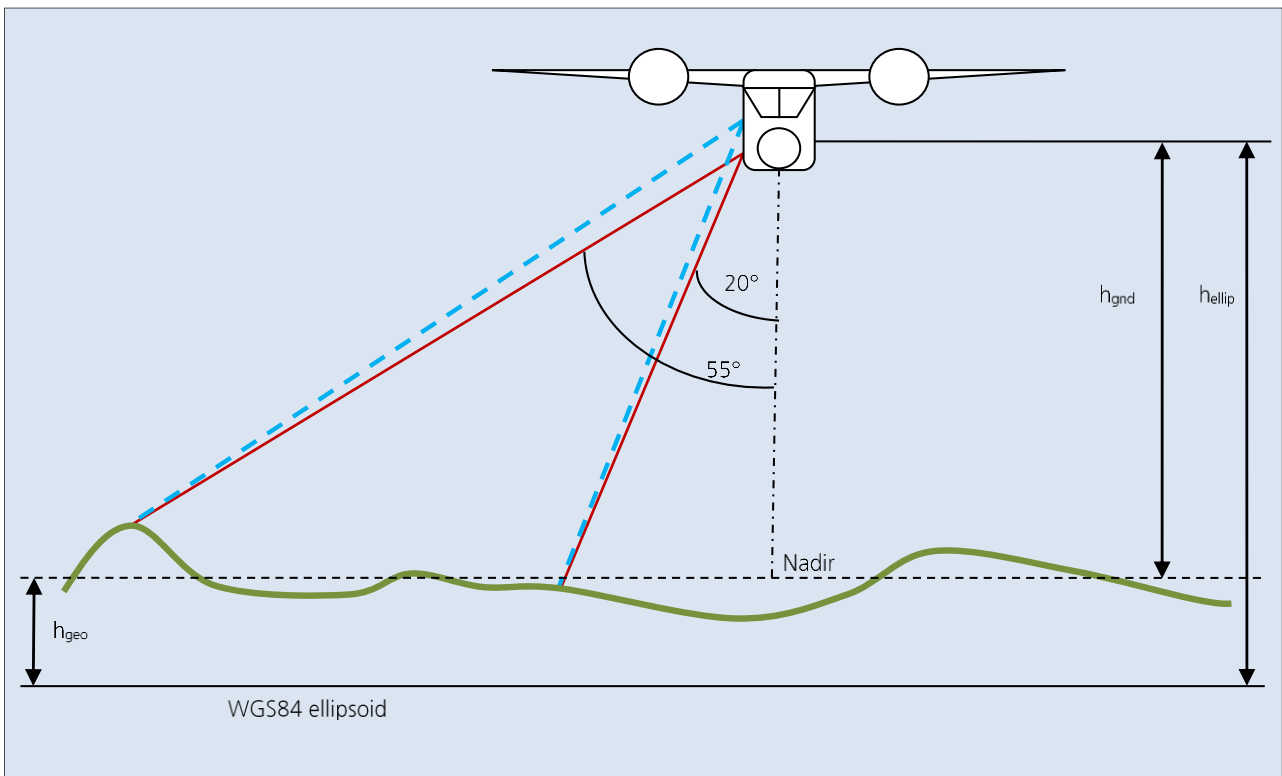


Figure 2-3: F-SAR standard flight geometry referenced to the WGS84 ellipsoid (GPS). Antennas are pointing to the right-hand side of the aircraft.

For the SWE measurement flights the geometry settings listed in Table 2-2 below were chosen.

Table 2-2: F-SAR flight geometry parameters used during 21HTERRA measurement flights.

Geometry parameters	Track #10	Track #11
Geoid height (EGM96)	50 m	
Average ‘terrain’ height above WGS84 ellipsoid (h_{geo})	2650 m	
Height above average ‘terrain’ (h_{gnd})	3050 m	
Flight altitude above WGS84 ellipsoid (h_{ellip})	5700 m or 18700 ft	
Approximate distance from valley centre line	1.9 km	2.3 km

The specifications in WGS84 for the flight tracks #10 and #11 are listed in Table 2-3.

	<p>SARSimHT-NG – Simulation of Hydroterra SAR System Performance in the Mediterranean and the Alps Based on Experimental Airborne SAR Data</p> <p>D1: Data Acquisition Report of SWE Experiment</p>	<p>Doc.: DLR-HR-TR-SARSimHT-NG-01 Issue: 2.0 Date: 25.11.2021 Page: 11 of 110</p>
---	---	--

Table 2-3: F-SAR flight track specification used during 21HTERRA measurement flights.

Track #	Start point coordinates		End point coordinates		Heading	Length
10	47N13.7771	010E59.3691	47N11.0792	010E59.2682	180°	5 km
11	47N11.1363	010E55.9321	47N13.8343	010E56.0302	0°	5 km

2.3 21HTERRA SWE Campaign Execution

The 21HTERRA SWE campaign was executed following a standard routine. F-SAR with its X-C-S-L instrument configuration was installed in DLR’s DO228 research aeroplane end of February 2021. The pre-campaign calibration flight over DLR’s calibration test site Kaufbeuren took place on Monday, March 1st 2021. From March 2nd until March 19th 2021 a total of eight measurement flights were performed over the ‘Woergetal’ test site. Details are listed in Table 2-4. Additional calibration flights were performed on March 3rd and March 24th.

Table 2-4: Listing of F-SAR measurement flights and passes executed during the 21HTERRA campaign.

Date	Time of departure	Flight duration	# of passes T10/T11	Drift T10/T11	Weather observations at flight level
02.03.21	07:20 CET	3.5 h	11 / 11	+2° / -2°	Wind 175°/12kt, no precip
03.03.21	07:30 CET	3.6 h	11 / 11	-2° / +2°	Wind 300°/4kt, no precip
04.03.21	07:30 CET	4 h	10 / 10	-6° / +8°	Wind 250°/33kt, no precip
04.03.21	13:35 CET	2.5 h	5 / 5	-9° / +10°	Wind 257°/35kt, no precip
06.03.21	12:30 CET	3.3 h	10 / 10	+2° / -2°	Wind 30°/18kt, 10+mm precip
08.03.21	13:40 CET	2.5 h	5 / 5	-5° / +4°	Wind 295°/23kt, no precip
09.03.21	11:00 CET	2.1 h	5 / 5	-5° / +6°	Wind 260°/20kt, no precip
19.03.21	10:25 CET	2 h	3 / 3	-4° / +3°	Wind 330°/15kt, 80+mm precip



Figure 2-4: Newly built foldable radar reflectors of 95cm inner leg-length inside transport box.

As listed in Table 2-4 we have had only two events of significant snowfall during the campaign, on March 5th and in the period from March 14th to March 18th. The weather history in March 2021 for the area (obtained from Meteoblue) is shown in Figure 2-5.

As further activity during the campaign, DLR provided six newly built foldable radar reflectors of 95cm inner leg length to ENVEO IT (see Figure 2-4). They were set up as pairs with opposite look directions at three locations indicated in Figure 2-2.

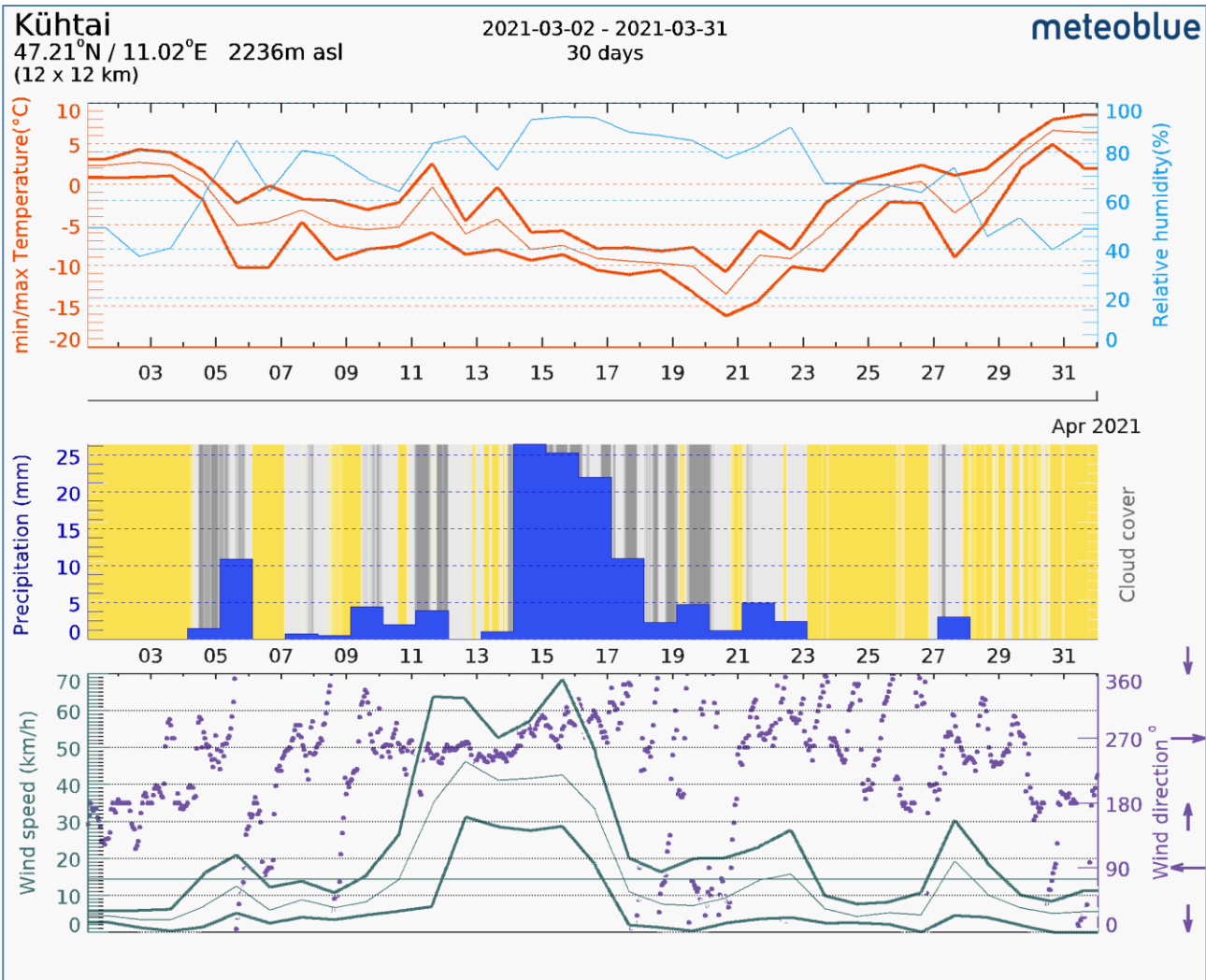


Figure 2-5: Weather history for the 'Woergetal' SWE test site (obtained from Meteoblue). Significant precipitation was registered at the nearby Kuehtai weather station on March 5th and from March 14 to March 18, 2021.

	<p>SARSimHT-NG – Simulation of Hydroterra SAR System Performance in the Mediterranean and the Alps Based on Experimental Airborne SAR Data</p> <p>D1: Data Acquisition Report of SWE Experiment</p>	<p>Doc.: DLR-HR-TR-SARSimHT-NG-01</p> <p>Issue: 2.0</p> <p>Date: 25.11.2021</p> <p>Page: 13 of 110</p>
---	---	--

2.3.1 Acquisition Procedure for HYDROTERRA Simulation

In order to simulate the long integration time of HYDROTERRA DLR used the same procedure as for the first experiment carried out in July 2019 [1]. The tracks #10 and #11 were flown one after the other as many times as possible during a measurement flight. Per flight two stacks, one per look direction, of up to 11 strip-map SAR data sets were acquired with zero-meter spatial baseline and an approx. 12-minute temporal baseline. In Figure 2-6 the principle of this acquisition procedure is visualized.

This procedure was applied for flights #1, #2, #3 and #5 (refer to Table 2-4). In total eight data sets were obtained covering a range of integration times from 1h50m up to 2h.

The temporal distance between flights #1, #2, #3 is 24 hours each. Flight #5 follows on #3 by 53 hours. Flight #4 was intended to follow #3 on the same day (diurnal set-up). Unfortunately, due to a failure in the autopilot system this flight had to be cut short. Nevertheless, an integration time of 1h10m has been achieved still.

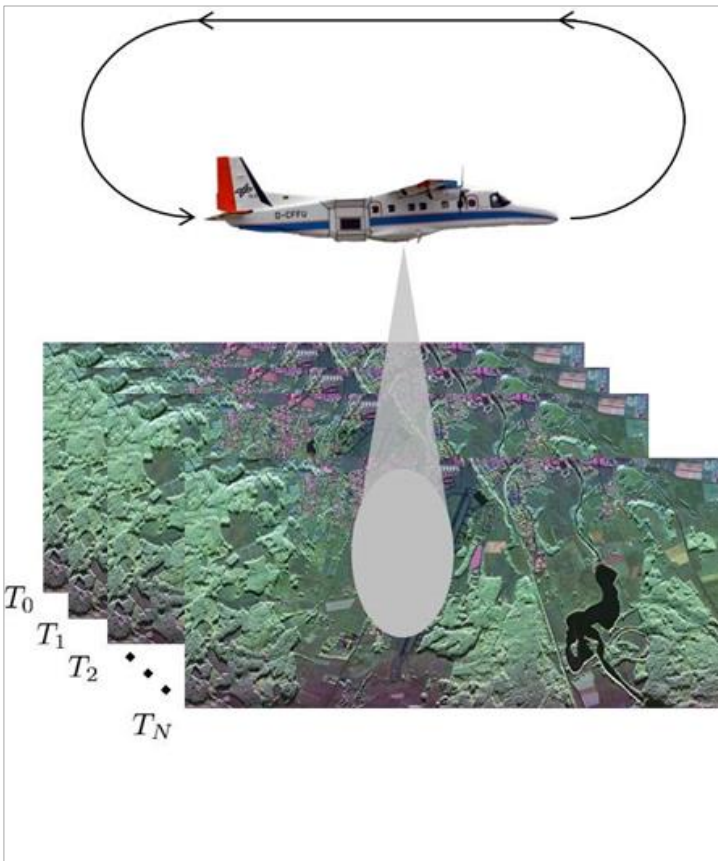


Figure 2-6: Typical acquisition procedure of a HYDROTERRA airborne experiment.

3 Field Measurements

For supporting the C- and L-band interferometric SAR acquisitions executed by DLR and the scientific analysis of the data set, the following field measurements were performed:

- Setting up of Trihedral Corner Reflectors
- Transects of the depth of the winter snowpack
- Vertical profiles of physical parameters of the winter snowpack within snow pits

The test area is the Wörgetal valley, Austrian Alps.

3.1 Description of Test site

The Wörgetal test site is located roughly 35 km southeast of Innsbruck, Austria, in the Tyrolean Alps. It is a 3 km north-south orientated side valley of the Needertal Valley. From the lower limit of the valley floor at 1900 m two escarpments lead from the Untere Böden to the Obere Böden (Figure 3-1) ranging from 2200 to 2400 m in elevation. The Untere Böden section is characterised by alpine grassland, scree and some boulder fields, and scattered mountain pines in its lower section. At the Obere Böden alpine meadows and scree dominate. Mountain ridges with an elevation up to 2722 m confine the valley.

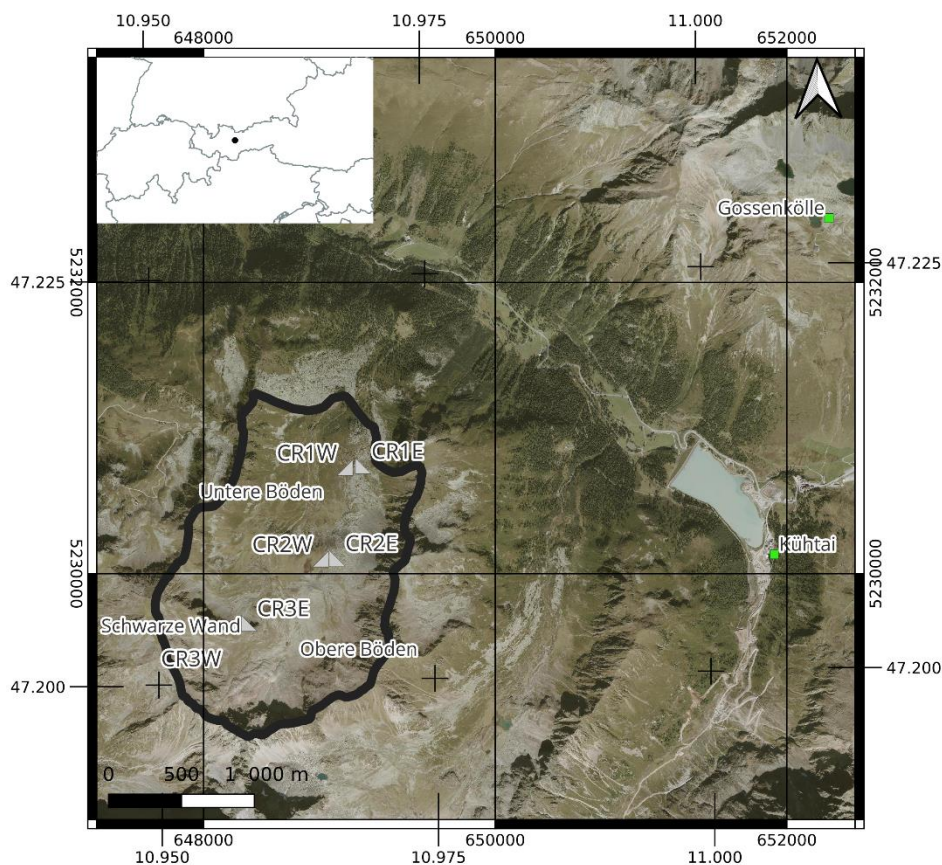


Figure 3-1: Overview of the test site. Wörgetal in the Tyrolian Alps southwest of Innsbruck (inset). The aerial photograph was taken in 2020. Mountain ridges which elevate up to 2722 m confine the Wörgetal valley (black solid line). Data of two automatic weather stations (green squares) are available starting from 01/10/2020 00:00 to 01/05/2021 00:00 sampled hourly.

3.2 Corner Reflectors

Six triangular trihedral corner reflectors provided by DLR were deployed within the test area at three locations at different elevations. Each reflector had a side-edge length of $l = 95$ cm. The CRs were installed pairwise at three locations, one CR pointing towards East and the other one towards West to serve both SAR flight tracks. All reflectors were deployed on stable bare surfaces and firmly fixed on boulders (Figure 3-2) in order to avoid any changes of their position and orientation during the field campaign due to wind or changing snow conditions. In the following figures and tables the corner reflectors are named with CR-1 E/W, CR-2 E/W and CR-3 E/W, where 1 refers to the pair at the lowest elevation, 2 to the middle one and 3 to the pair at the ridge of Schwarze Wand. E/W indicates the azimuth orientation, towards East (90 degrees) or West (270 degrees), respectively. In the azimuth orientation of all CRs a local magnetic declination of 3.5° has been considered.

A DGPS TRIMBLE R6 device and the Real Time Austrian Positioning Service (APOS) were used to measure the precise position of the reflector phase centre (Figure 3-2). Table 3-1 summarizes position and orientation of all corner reflectors.

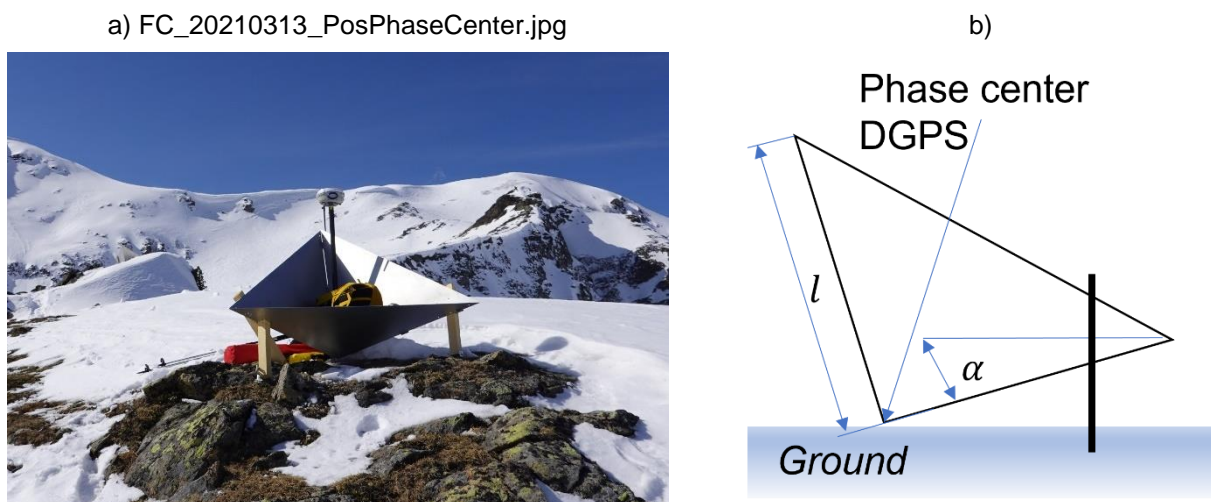


Figure 3-2: a) Corner Reflector CR3E mounted on rocks with angle irons and wooden rods. The location of the phase centre was measured with a DGPS TRIMBLE R6 device making use of the Real Time Austrian Positioning Service (APOS), b) The side-edge of the reflectors had a length $l = 95$ cm. The CRs were inclined with respect to the horizontal by a tilt angle α , [filename: FC_20210313_PosPhaseCenter.jpg].

Table 3-1: Summary of the position and orientation of the deployed corner reflectors.

Name	Azimuth [deg]	Tilt angle α [deg]	Elevation [m]	Phase Centre Easting [m]	Phase Centre Northing [m]	Latitude [deg]	Longitude [deg]
CR1E	0	31	2224.10	649041.85	5230685.237	47.212745	10.968272
CR1W	180	18	2224.88	649024.64	5230674.017	47.212648	10.968042
CR2E	0	28	2338.63	648862.504	5230052.503	47.207095	10.965695
CR2W	180	19	2339.39	648857.027	5230046.017	47.2070383	10.965621
CR3E	0	19	2473.17	648231.986	5229597.187	47.2031432	10.957224
CR3W	180	26	2467.51	648259.058	5229604.464	47.2032025	10.957583

	<p>SARSimHT-NG – Simulation of Hydroterra SAR System Performance in the Mediterranean and the Alps Based on Experimental Airborne SAR Data</p> <p>D1: Data Acquisition Report of SWE Experiment</p>	<p>Doc.: DLR-HR-TR-SARSimHT-NG-01 Issue: 2.0 Date: 25.11.2021 Page: 16 of 110</p>
---	---	--

3.3 Devices

The following parameters were measured utilizing the listed devices and instruments:

- **Snow and air temperature:** Commercial off-the-shelf (COTS) digital thermometer
- **Snow density** sampler: Aluminium tube (Ø 5.6 cm x 17.5 cm) and spring scale (standard equipment)
- **Stratigraphy:** snow crystal card and magnifying glass
- **Snow depth:** avalanche probe with depth scale
- **Position of phase centre:** DGPS TRIMBLE R6 device and the Real Time Austrian Positioning Service (APOS)

3.4 Methods for Snow Pit Measurements

The snow pit measurements follow the International Classification for Seasonal Snow on the Ground (Ref. [3]). The stratigraphy and structural properties are characterized by means of snow grain size and type, density and hardness. The hardness of the snow is based on the hand test, which grades the hardness into five classes according to the penetration. Snow density is measured with the snow density sampler, preferably inserting the tube horizontally in order to obtain higher vertical resolution of the density profile. The mean grain size and variance is estimated by using a grain size plate, and the shape is described according to Ref. [3]. In addition, the snow grains are photographically documented. The measurements recorded in the snow pits are reported in the following section.

Snow depth measurements along the transects were executed about every 50 m. At each location 5 snow depth measurements were taken using an avalanche probe following the sketch in Figure 3-3. Additionally, the centre location was measured with GPS.

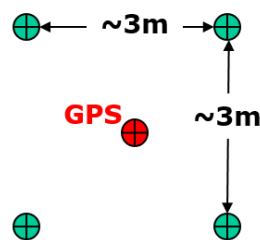


Figure 3-3: Sketch of probing the snow depth at each measurement point along the snow depth transect line. Four snow depth measurements at the corners of a ca. 3x3 m square and one at its centre point. GPS measurement is carried out at the centre point.

3.5 Auxiliary datasets - DEM

For the SAR processing and analysis of the results a Digital Elevation Model (DEM) of Tirol with 5 m resolution (version 22.02.2018 01:00:00) was downloaded from the data.gv.at - Open Data Österreich data portal. The DEM is based on Airborne Laser scans acquired in 2017. The horizontal and vertical accuracy is ± 20 cm and ± 10 cm, respectively (https://www.data.gv.at/katalog/dataset/land-tirol_tirol-gelnde).

	SARSimHT-NG – Simulation of Hydroterra SAR System Performance in the Mediterranean and the Alps Based on Experimental Airborne SAR Data	Doc.: DLR-HR-TR-SARSimHT-NG-01
	D1: Data Acquisition Report of SWE Experiment	Issue: 2.0 Date: 25.11.2021 Page: 17 of 110

3.6 Field measurements

Observations of snow depth were carried out along transects where each measurement point is identified by an ID. T2-5 stands for the 5th measurement in transect 2. The accumulated fresh snow is measured along existing transects. In this case TN2-5 stands for the repeated observation of the 5th point in transect 2. Snow pit observations follow the same naming convention.

3.6.1 Field campaign 02.03.2021

Observations: Snow depth measurements along T1, T4 and T5. Snow pit P-1 with stratigraphy, density and temperature observations at Obere Böden. Photographic documentation.

General remarks: Dry snow state along transects and in valley, Snow surface melting at S and E slopes.

Snow pit P-1 02-03-2021						
Personnel			Date		Time	
H. Rott, S. Scheiblauer			02.03.2021		13:30 CET	
Code	Site	(GPS N)	(GPS E)	GPS No	Altitude m	Slope °
P-1	Wörgetal	47.215	10.9641		2330	1
Clouds/8	Type	Meteo				
0/8		Sun, SSW 1				

Temperature	
Air	N/A
160	-6.2
155	-8.5
150	-8.3
140	-8.1
130	-7.1
120	-6.3
110	-5.6
100	-5.0
90	-4.4
80	-4.0
70	-3.4
60	-3.0
50	-2.6
40	-2.2
30	-1.8
20	-1.5
10	-1.1
5	-0.8
0	-0.6
Ground	Frozen

Vertical profile				
cm top	Rho [kg/m ³]	Delta z cm	SWE [mm]	comment
166	241.28	19	45.84	
147	299.29	8	23.94	
139	324.81	8	25.98	
131	338.73	8	27.10	
123	357.29	6	21.44	
117	352.65	8	28.21	
109	357.29	7	25.01	
102	394.41	8	31.55	
94	403.69	9	36.33	
85	306.25	9	27.56	
76	401.37	8	32.11	
68	399.05	9	35.91	
59	401.37	8	32.11	
51	403.69	8	32.29	
43	401.37	8	32.11	
35	310.89	8	24.87	
27	317.85	8	25.43	
19	408.33	8	32.67	
11	303.93	11	33.43	
0				
mean	345.73	166	573.91	sum

	SARSimHT-NG – Simulation of Hydroterra SAR System Performance in the Mediterranean and the Alps Based on Experimental Airborne SAR Data	Doc.: DLR-HR-TR-SARSimHT-NG-01
	D1: Data Acquisition Report of SWE Experiment	Issue: 2.0 Date: 25.11.2021 Page: 18 of 110

Stratigraphy				
Snow surface	Ø [mm]	Type	Hardness	Comment
166-150	0.50	dFdc	R1	
150-141	0.50	dFdc	R2	
141-104	0.70	RGlR	R3	
104-89	0.80	FCxr	R4	@ 100 cm: FC_20210302_WOEpit1_100cm.JPG
89-73	1.50	FCxr	R2	
73-44	1.50	FCxr	R3	
44-39	1.80	FCxr	R4	
39-17	2.00	FCxr	R2	@ 35 cm: FC_20210302_WOEpit1_35cm.JPG
17-9	2.00	FCxr	R5	
9-0	2.50	FCso & DHpr	R2	@ 5 cm: FC_20210302_WOEpit1_5cm.JPG

Total Snow Depth Transect 02-03-2021		
Personnel		
T1, T4, T5: H. Rott, S. Scheiblauer, 02-03-2021		
Clouds/8	Type	Meteo
"0/8		SSW1
Snow state: dry along transects and in valley, Snow surface melting at S and E slopes		

Point	SD 1	SD 2	SD 3	SD 4	SD 5	mean [cm]	Note	GPS Nr.
T1-1	116	117	145	165	139	136.4		35
T1-2	121	111	123	107	109	114.2		36
T1-3	130	141	131	133	128	132.6		37
T1-4	143	141	149	144	145	144.4		38
T1-5	145	139	157	143	139	144.6		39
T1-6	200	206	209	196	201	202.4		40
T1-7	163	163	167	168	124	157.0		41
T1-8	158	154	158	153	156	155.8		42
T1-9	141	149	153	159	160	152.4		43
T1-10	71	140	133	132	125	120.2		44
T1-11	104	103	111	108	96	104.4		45
T1-12	87	91	100	112	117	101.4	near ski tracks	46
T1-13	153	164	163	170	162	162.4	near ski tracks	47
T1-14	173	164	181	167	163	169.6		48
T1-15	138	136	137	139	143	138.6	pond	49
						142.4	mean	

Point	SD 1	SD 2	SD 3	SD 4	SD 5	mean [cm]	GPS Nr.
T4-1	135	224	207	108	141	163.0	26
T4-2	202	201	202	191	201	199.4	27
T4-3	201	188	191	202	184	193.2	29
T4-4	128	145	134	130	118	131.0	30
T4-5	139	142	133	122	139	135.0	31
T4-6	112	111	105	101	102	106.2	32

T4-7	67	66	62	57	50	60.4	33
T4-8	102	103	93	100	94	98.4	34
						138.5	mean
Point	SD 1	SD 2	SD 3	SD 4	SD 5	mean [cm]	GPS Nr.
T5-1	184	180	130	168	159	164.2	15
T5-2	100	91	110	94	112	101.4	16
T5-3	82	90	97	89	88	89.2	17
T5-4	109	108	104	107	110	107.6	18
T5-5	184	157	161	166	175	168.6	19
T5-6	163	132	122	103	174	138.8	20
T5-7	83	74	71	76	90	78.8	21
T5-8	67	71	66	62	65	66.2	22
T5-9	183	167	157	174	172	170.6	23
T5-10	83	89	94	90	93	89.8	24
T5-11	103	106	101	102	101	102.6	25
						118.0	mean

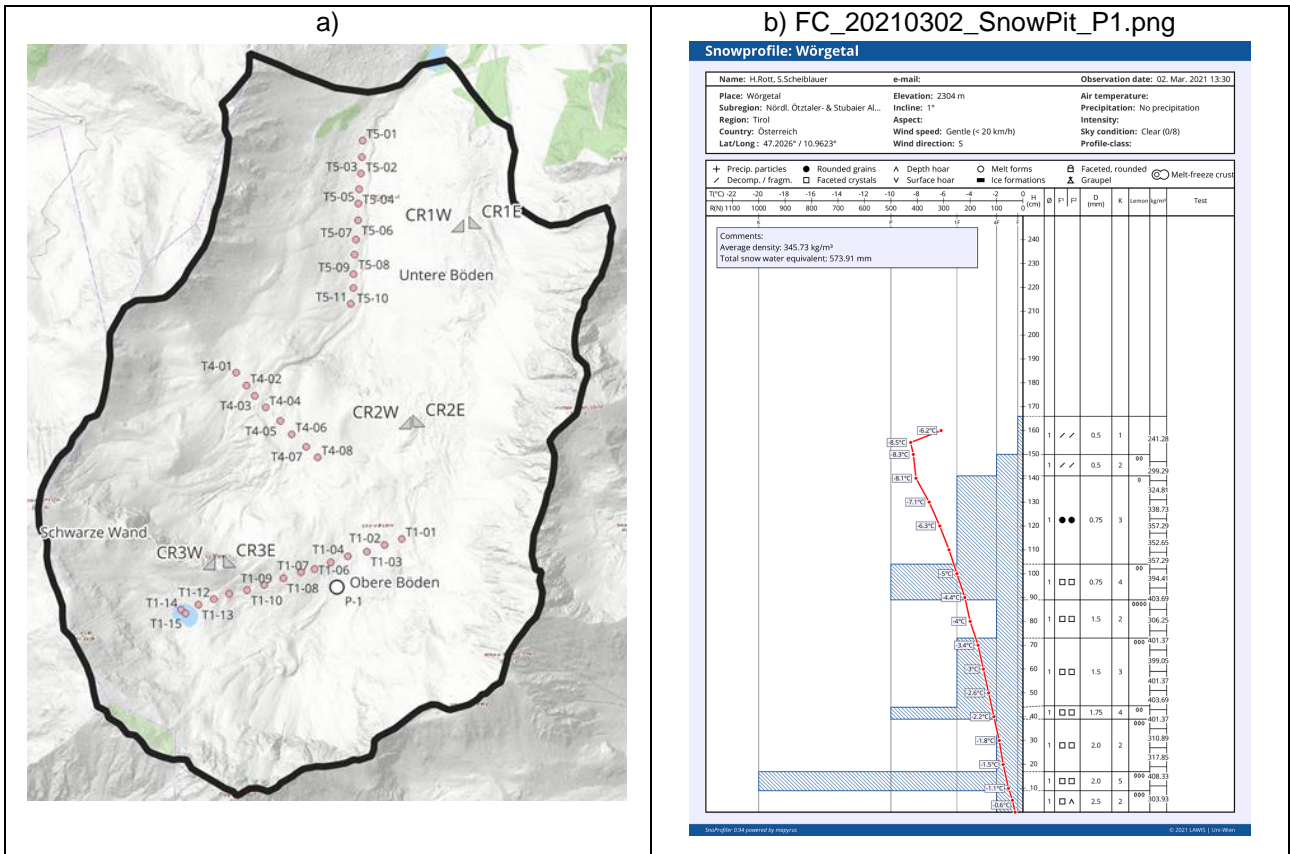


Figure 3-4: a) Snow depth measured along Transects T1, T4 and T5 on 02.03.2021. Location of snow pit is marked with P-1. b) Snow pit P-1 at Obere Böden (2304m) [filename: FC_20210302_SnowPit_P1.png].

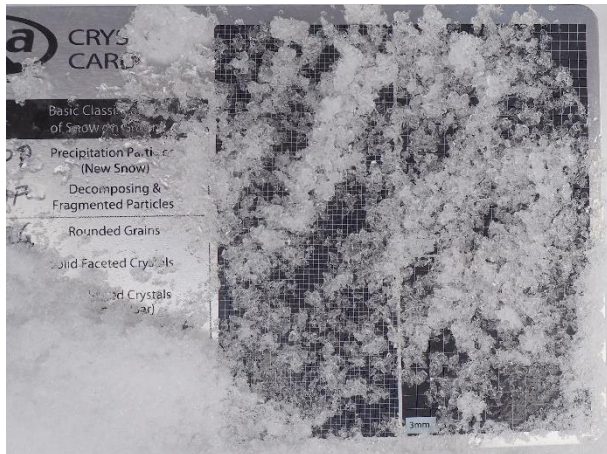
a) FC_20210302_WOEpit1SC1.JPG



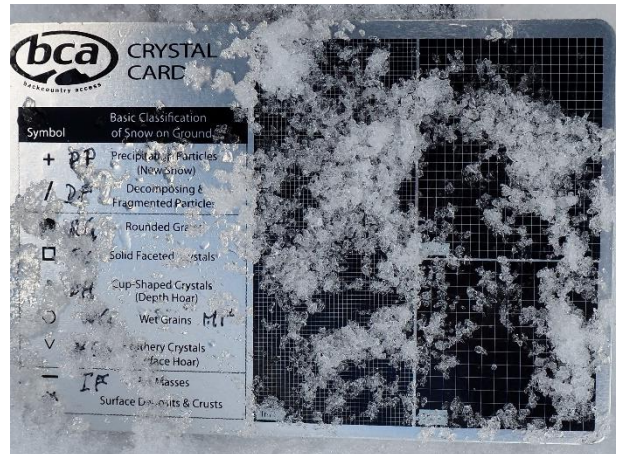
b) FC_20210302_WOEpit1SC2.JPG



c) FC_20210302_WOEpit1_5cm.JPG



d) FC_20210302_WOEpit1_35cm.JPG



e) FC_20210302_WOEpit1_100cm.JPG

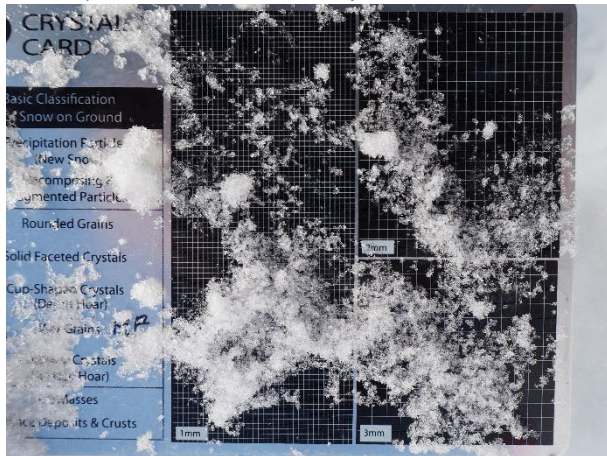


Figure 3-5: a), b) Snow pit 1 setting and tracks (soft surface layer) PF 15 cm, PS 7-10 cm c) Snow crystals at 5 cm, d) Snow crystals at 35 cm, e) Snow crystals at 100 cm.

	SARSimHT-NG – Simulation of Hydroterra SAR System Performance in the Mediterranean and the Alps Based on Experimental Airborne SAR Data	Doc.: DLR-HR-TR-SARSimHT-NG-01 Issue: 2.0 Date: 25.11.2021 Page: 21 of 110
	D1: Data Acquisition Report of SWE Experiment	

3.6.2 Field campaign 03.03.2021

Observations: Snow depth measurements along T2 and T3. Two snow pits P-2 and P-3 with stratigraphy, density and temperature observations at Untere Böden and one in the vicinity of CR2. Photographic documentation.

General remarks: Dry snow state.

Snow pit P-2 03-03-2021						
Personnel H. Rott, N. Mölg			Date 03.03.2021		Time 12:00 CET	
Code	Site	(GPS N)	(GPS E)	GPS No	Altitude m	Slope °
P-2	Wörgetal	47,20694	10,96414	149	2257	1
Clouds/8	Type	Meteo				
8/8	As trans					

Temperature	
Air	N/A
102	-3.8
95	-5.2
90	-5.4
80	-4.6
70	-3.9
60	-3.1
50	-2.4
40	-1.8
30	-1.2
20	-1.0
10	-0.6
5	-0.5
0	-0.3
Ground	frozen

Vertical profile				
cm top	Rho [kg/m³]	Delta z cm	SWE [mm]	comment
108	201.84	19	38.35	
89	322.49	8	25.80	
81	324.81	9	29.23	
72	368.89	8	29.51	
64	387.45	8	31.00	
56	317.85	9	28.61	
47	308.57	10	30.86	
37	359.61	8	28.77	
29	341.05	8	27.28	
21	396.73	21	83.31	
0				
mean	326.59	108	352.72	sum

Stratigraphy				
Snow surface	Ø [mm]	Type	Hardness	Comment
108-106	1.00	MFcr	R3	
106-91	0.70	dFdc	R1	
91-86	1.00	RGlR	R2	
86-82	1.00	RGlR	R3	
82-75	1.00	RGlR	R2	
75-57	1.00	FCxr	R3	
57-52	2.50	MFcr	R3	with clusters
52-27	2.00	FCxr	R2	
27-0	2.50	FCxr & DHpr	R3	

	SARSimHT-NG – Simulation of Hydroterra SAR System Performance in the Mediterranean and the Alps Based on Experimental Airborne SAR Data	Doc.: DLR-HR-TR-SARSimHT-NG-01 Issue: 2.0 Date: 25.11.2021 Page: 22 of 110
	D1: Data Acquisition Report of SWE Experiment	

Snow pit P-3 03-03-2021						
Personnel			Date		Time	
H.Rott, N. Mölg			03.03.2021		13:30 CET	
Code	Site	(GPS N)	(GPS E)	GPS No	Altitude m	Slope °
P-3	Wörgetal	47,21504	10,96408	150	2063	3
Clouds/8	Type	Meteo				
8/8	As trans					

Temperature	
Air	N/A
100	-2.1
90	-4.4
80	-4.3
70	-3.6
60	-3.0
50	-2.2
40	-1.7
30	-1.2
20	-0.8
10	-0.3
0	-0.1
Ground	not frozen
-3	+0,3

Vertical profile				
cm top	Rho [kg/m ³]	Delta z cm	SWE [mm]	comment
105	308.57	19	58.63	
86	354.97	8	28.40	
78	350.33	9	31.53	
69	382.81	9	34.45	
60	406.01	9	36.54	
51	410.65	10	41.06	
41	364.25	9	32.78	
32	378.17	9	34.04	
23	396.73	7	27.77	
16	269.70	16	43.15	
0				
mean	350.81	105	368.35	sum

Stratigraphy

Snow surface	Ø [mm]	Type	Hardness	Comment
105-103	1.50	MFcr	R3	
103-94	1.00	RGl	R2	
94-59	1.00	FCxr	R3	
59-53	1.50	MFcr	R4	with cluster
53-48	1.50	FCxr	R3	
48-27	2.00	FCxr & DHpr	R2	
27-5	2.50	FCxr & DHpr	R3	
5-0	2.50	FCxr & DHpr	R2	

Total Snow Depth Transect 03-03-2021		
Personnel		
T2, T3: H. Rott, N. Mölg		
Clouds/8	Type	Meteo
"8/8	As trans	SSW1-2
Snow state: dry		

Point	SD 1	SD 2	SD 3	SD 4	SD 5	mean [cm]	Note	GPS Nr.
T2-1	95	94	63	75	92	83.8		145
T2-2	83	84	106	115	112	100.0		

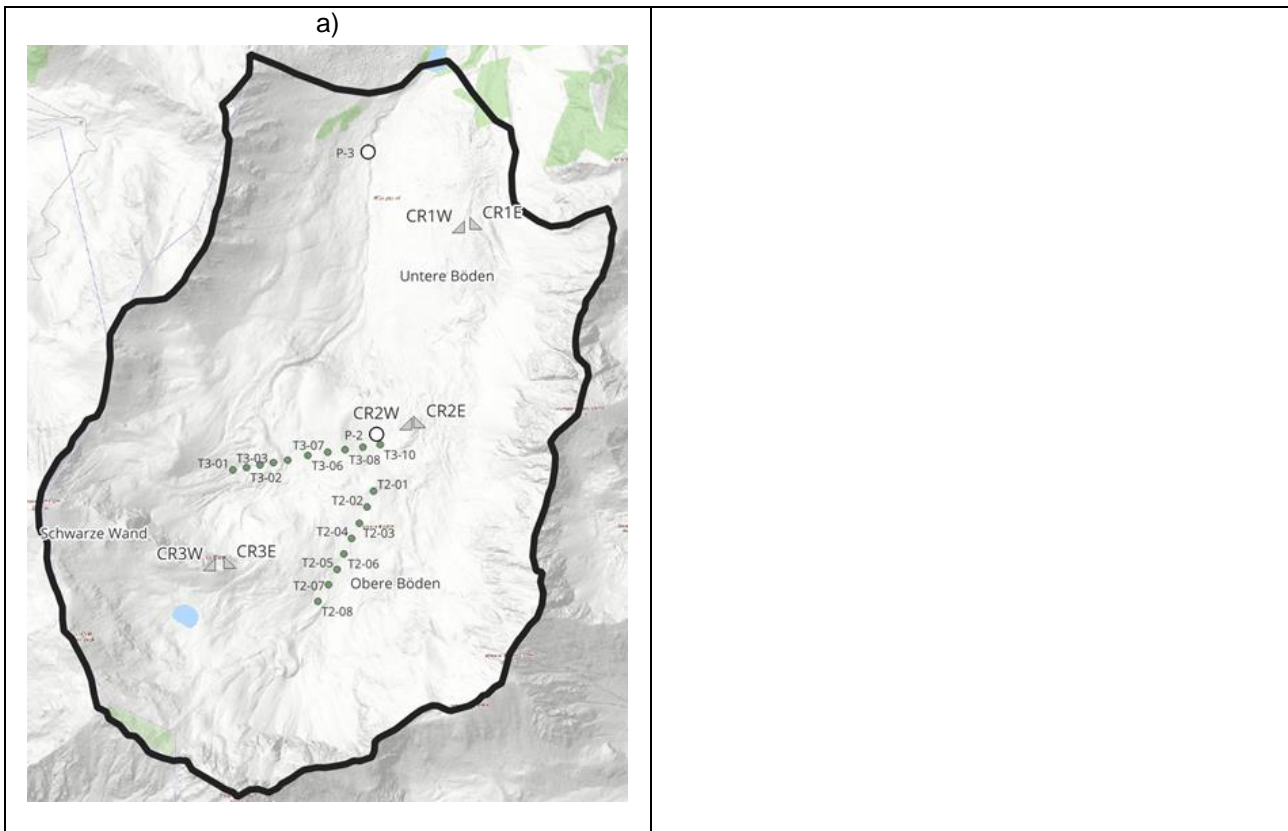


SARSimHT-NG – Simulation of Hydroterra SAR System Performance in the Mediterranean and the Alps Based on Experimental Airborne SAR Data

D1: Data Acquisition Report of SWE Experiment

Doc.: DLR-HR-TR-SARSimHT-NG-01
 Issue: 2.0
 Date: 25.11.2021
 Page: 23 of 110

T2-3	151	153	146	150	181	156.2		
T2-4	137	148	143	147	142	143.4		146
T2-5	134	136	128	148	130	135.2		
T2-6	192	171	186	177	170	179.2		
T2-7	107	115	126	121	121	118.0		147
T2-8	164	183	202	189	190	185.6		148
						137.7	mean	
Point	SD 1	SD 2	SD 3	SD 4	SD 5	mean [cm]	Note	GPS Nr.
T3-1	151	144	193	178	188	170.8		141
T3-2	118	65	58	66	80	77.4		
T3-3	98	92	89	93	82	90.8		
T3-4	92	70	101	82	75	84.0		
T3-5	162	155	154	139	152	152.4		142
T3-6	113	127	124	122	122	121.6		
T3-7	167	155	168	161	170	164.2		
T3-8	158	157	150	156	150	154.2		
T3-9	85	95	93	94	86	90.6		143
T3-10	101	111	104	101	100	103.4		144
						127.7	mean	



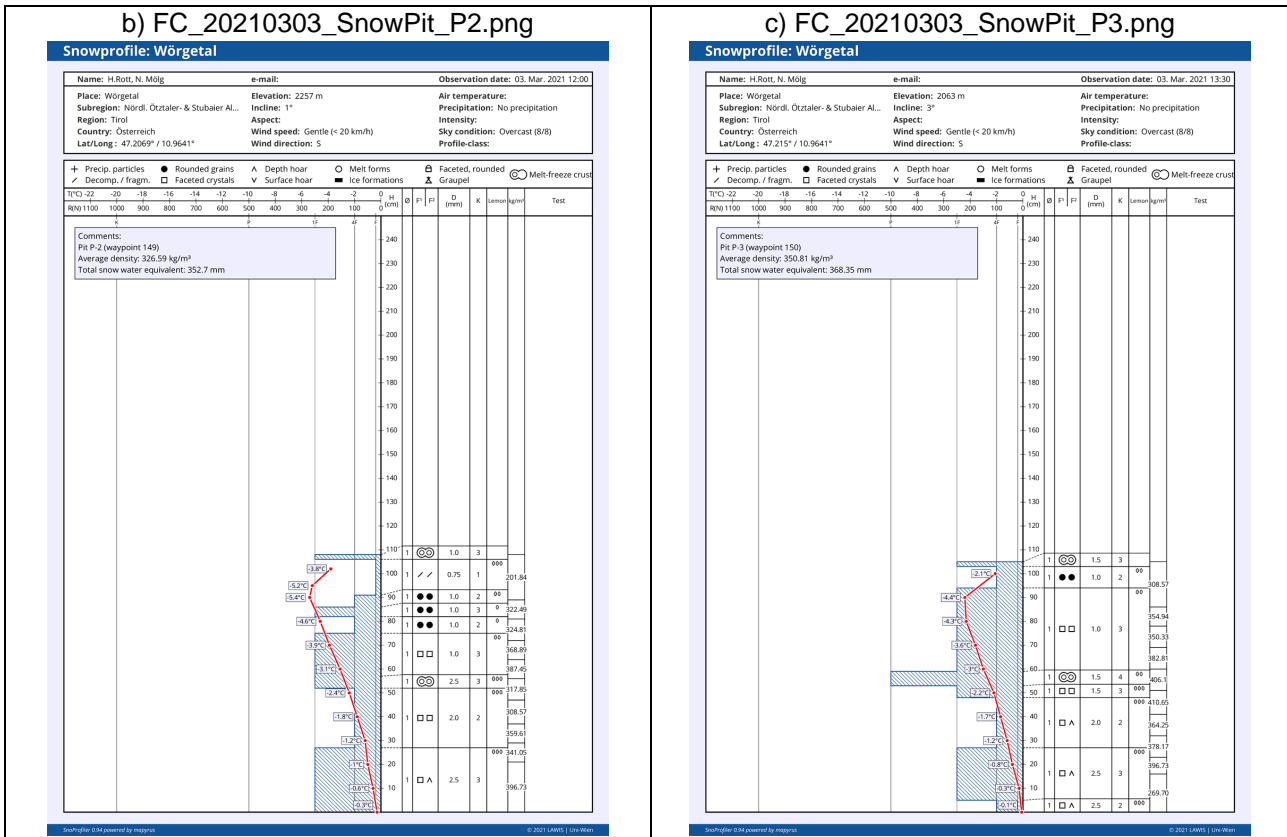


Figure 3-6: Snow depth measured along Transects T2 and T3 on 03.03.2021. Locations of snow pits are marked with P-2 and P-3, Snow pit P-2 between Untere and Obere Böden (2257 m) [FC_20210303_SnowPit_P2.png], Snow pit P-3 at Untere Böden (2063 m) [FC_20210303_SnowPit_P3.png].

3.6.3 Field campaign 06.03.2021

Observations: CR check, Observation of fresh snow along T1, T2, T4 and T5. Four density measurements of the homogeneous fresh snow. Repeated observations at PN-1 and PN-3a. Photographic documentation.

General remarks: Dry snow state along transects and in valley; surface melt (thin layer) on E- and S-facing slopes. Fresh snow type: Stellar dendrites.

Fresh Snow Sampling, 06-03-2021		
Personnel		
H. Rott		
Clouds/8	Type	Meteo
0/8		sun, calm & SSW1
Snow state: dry along transects and in valley; surface melt (thin layer) on E- and S-facing slopes		
Fresh snow type: Stellar dendrites		

Code	Time	Lat	Lon	SD (fresh)	Measurement	rho [kg/m ³]	SWE [mm]
PN-3a	10:00 CET	47.21534	10.96389	10.00	1	81.2	8.12
				10.00	2	85.26	8.53
				10.00	3	89.32	8.93
					mean	85.26	

	SARSimHT-NG – Simulation of Hydroterra SAR System Performance in the Mediterranean and the Alps Based on Experimental Airborne SAR Data			Doc.: DLR-HR-TR-SARSimHT-NG-01 Issue: 2.0 Date: 25.11.2021 Page: 25 of 110		
	D1: Data Acquisition Report of SWE Experiment					

PN-A	10:45 CET	47.20878	10.95832	12.00	1	94.74	11.37
				12.50	2	94.19	11.77
				12.50	3	94.19	11.77
				mean		94.37	
PN-B	11:10 CET	47.20629	10.96166	10.50	1	96.67	10.15
				10.50	2	92.8	9.74
				mean		94.74	
PN-1	11:50 CET	47.20219	10.9615	15.00	1	86.61	12.99
				15.00	2	94.74	14.21
				15.00	3	94.74	14.21
				mean		92.03	

Fresh Snow Depth Transects, 06-03-2021			
Personnel			
H. Rott			
Clouds/8	Type	Meteo	
0/8		sun, calm & SSW1	
Snow state: dry along transects and in valley; surface melt (thin layer) on E- and S-facing slopes			
Fresh snow type: Stellar dendrites			

Point	Fresh SD 1	Fresh SD 2	Fresh SD 3	Fresh SD 4	Fresh SD 5	mean [cm]	Note	GPS Nr.
N1-1						15	Depression	
N1-2						16		
N1-3						12		
N1-4						18		
N1-5						18		
N1-6						15	Frozen Pond	
N1-7						16		
N1-8						17		
						15.88	mean	
N2-1						12	Depression	
N2-2						16		
N2-3						17		
N2-4						12.5		
N2-5						17		
N2-6						17		
						15.25	mean	
N4-1						12.5	Depression	
N4-2						12		



N4-3	18	
N4-4	13	
N4-5	13	
N4-6	11	
	13.25	mean
<hr/>		
N5-1	11	Gentle NE slope
N5-2	12.5	
N5-3	13.5	
N5-4	11	
N5-5	12	Gentle NE slope
N5-6	12	Depression
N5-7	14	
	12.29	mean

a) FC_20210306_CR3W_viewdownthevalley.JPG



b) FC_20210306_WOE_crystals-A.JPG



c) FC_20210306_WOE_crystals-B.JPG



d) FC_20210306_WOE_lower-valley.JPG



e) WOE_snow-state_N-slope_2021-03-06.JPG



f) FC_20210306_WOE_view_up-valley.JPG

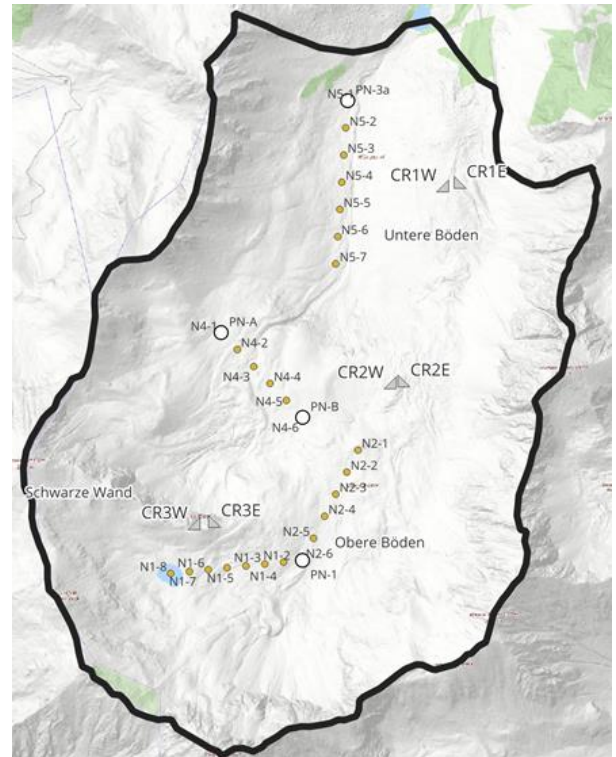


Figure 3-7: Snow state on 06.03.2021.

3.6.4 Field campaign 19.03.2021

Observations: Cleaning of CR, observation of fresh snow along T1, T4 and T5. Two density measurements of the homogeneous fresh snow at PN-2 and PN3b were made. Photographic documentation of weather and snow conditions.

General remarks: Dry snow state, roughly 40 cm of fresh snow.

	SARSimHT-NG – Simulation of Hydroterra SAR System Performance in the Mediterranean and the Alps Based on Experimental Airborne SAR Data	Doc.: DLR-HR-TR-SARSimHT-NG-01 Issue: 2.0 Date: 25.11.2021 Page: 28 of 110
	D1: Data Acquisition Report of SWE Experiment	

Fresh Snow Sampling PN-2 19-03-2021						
Personnel			Date		Time	
T. Nagler, N. Mölg			19.03.2021		10:45 CET	
Code	Site	(GPS N)	(GPS E)	GPS No	Altitude m	Slope °
PN-2	Wörgetal	47,207	10,96415	186	2254	1
Clouds/8	Type	Meteo				
0/8	As trans					

Temperature	
Air	-9.50
38	-6.2
30	-7.5
20	-6.7
10	-5.1
0	-4.2

Vertical profile				
cm top	Rho [kg/m³]	Delta z cm	SWE [mm]	comment
43	85.84	19	16.31	
24	169.57	17	28.83	
7	214.60	7	15.02	
0				
mean	139.90	43	60.16	sum

Stratigraphy				
Snow surface	Ø [mm]	Type	Hardness	Comment
43-38	0.50	PPsd	1	
38-37.5	1.00	MFcr	3	Cluster
37.5-12	0.50	DFdc	1	
12-0	0.50	DFdc	3	

Fresh Snow Sampling PN-3b 19-03-2021						
Personnel			Date		Time	
T. Nagler, N. Mölg			19.03.2021		13:30 CET	
Code	Site	(GPS N)	(GPS E)	GPS No	Altitude m	Slope °
PN-3b	Wörgetal	47,21401	10,96412	161	2107	3
Clouds/8	Type	Meteo				
0/8	As trans					

Temperature	
Air	N/A
38	-10.4
30	-9.0
20	-6.0
10	-4.6
0	-3.7

Vertical profile				
cm top	Rho [kg/m³]	Delta z cm	SWE [mm]	comment
44	128.97	17	21.92	
27	155.24	17	26.39	
10	174.58	10	17.46	
0				
mean	149.48	44	65.77	sum

Stratigraphy				
Snow surface	Ø [mm]	Type	Hardness	Comment
43-28	0.50	PPsd	1	
28-0	0.50	DFdc	2	

 	SARSimHT-NG – Simulation of Hydroterra SAR System Performance in the Mediterranean and the Alps Based on Experimental Airborne SAR Data	Doc.: DLR-HR-TR-SARSimHT-NG-01 Issue: 2.0 Date: 25.11.2021 Page: 29 of 110
	D1: Data Acquisition Report of SWE Experiment	

Fresh Snow Depth Transect 19-03-2021		
Personnel		
N1 S. Scheiblauer		
Clouds/8	Type	Meteo
0/8		
Snow state: dry, roughly 40 cm of fresh snow		

Point	Fresh SD 1	Fresh SD 2	Fresh SD 3	SD 4	SD 5	mean [cm]	Note	GPS Nr.
N1-01	40	42	46	42	45	43		9
N1-02	45	44	44	44	40	43.4		10
N1-03	37	41	42	40	42	40.4		11
N1-04	40	40	42	38	36	39.2		12
N1-05	39	40	40	39	40	39.6		13
N1-06	42	45	41	41	42	42.2		14
N1-07	41	44	43	45	43	43.2		15
N1-08	43	45	46	47	45	45.2		16
N1-09	45	47	46	45	44	45.4		17
N1-10	44	47	46	45	45	45.4		18
N1-11	45	46	48	43	47	45.8		19
N1-12	45	46	47	44	46	45.6		20
N1-13	42	44	42	43	47	43.6		21
						43.2	mean	

Fresh Snow Depth Transect 19-03-2021		
Personnel		
N4, N5 T. Nagler, N. Mölg		
Clouds/8	Type	Meteo
0/8		
Snow state: dry		

Point	SD 1	SD 2	SD 3	SD 4	SD 5	mean [cm]	Note	GPS Nr.
N5-01	38	38	39			38.3		162
N5-02	42	42	41			41.7		163
N5-03	37	37	35			36.3		164
N5-04	40	40	40			40		165
N5-05	42	42	44	42	43	42.6		166
N5-06	55	55	55	55		55		167
N5-07	43	42	41	42		42		168
N5-08	31	29	31	31	32	30.8		169
N5-09	51	52	51	48	52	50.8		170
N5-10	42	42	44	44	43	43		171
N5-11	56	60	58	57	56	57.4		172
N5-12	56	58	60	63	57	58.8		173

 	SARSimHT-NG – Simulation of Hydroterra SAR System Performance in the Mediterranean and the Alps Based on Experimental Airborne SAR Data	Doc.: DLR-HR-TR-SARSimHT-NG-01 Issue: 2.0 Date: 25.11.2021 Page: 30 of 110
D1: Data Acquisition Report of SWE Experiment		

N5-13	66	70	67	65	65	66.6		174
N5-14	49	50	47	50	50	49.2		175
N5-15	50	49	49	48	50	49.2		176
N5-16	50	51	50	52	50	50.6		177
						44.7	<i>mean</i>	

Point	SD 1	SD 2	SD 3	SD 4	SD 5	mean [cm]	Note	GPS Nr.
N4-01	53	44	52	52	56	53		178
N4-02	48	37	41	46	46	45		179
N4-03	36		39	38	40	38		180
N4-04	51	48	49	50	48	49.2		181
N4-05	48	48	47	48	48	47.8		182
N4-06	58	57	56	59	52	56.4		183
N4-07	40	40	40	40	40	40		184
N4-08	48	48	48	49	49	48.4		185
						47.2	<i>mean</i>	

Point	SD 1	SD 2	SD 3	SD 4	SD 5	mean [cm]	Note	GPS Nr.
N6-01	50	51	54	58	49	52.4		188
N6-02	46	45	46	41	40	43.6		189
N6-03	37	36	38	36	36	36.6		190
N6-04	47	49	50	48	50	48.8		191
N6-05	42	45	40	38	38	40.6		192
N6-06	48	46	44	43	45	45.2		193
N6-07	42	43	42	42	44	42.6		194
N6-08	39	36	35	38	39	37.4		195
N6-09	39	37	39	45	37	39.4		196
N6-10	38	37	37	37	36	36		197
						42.2	<i>mean</i>	

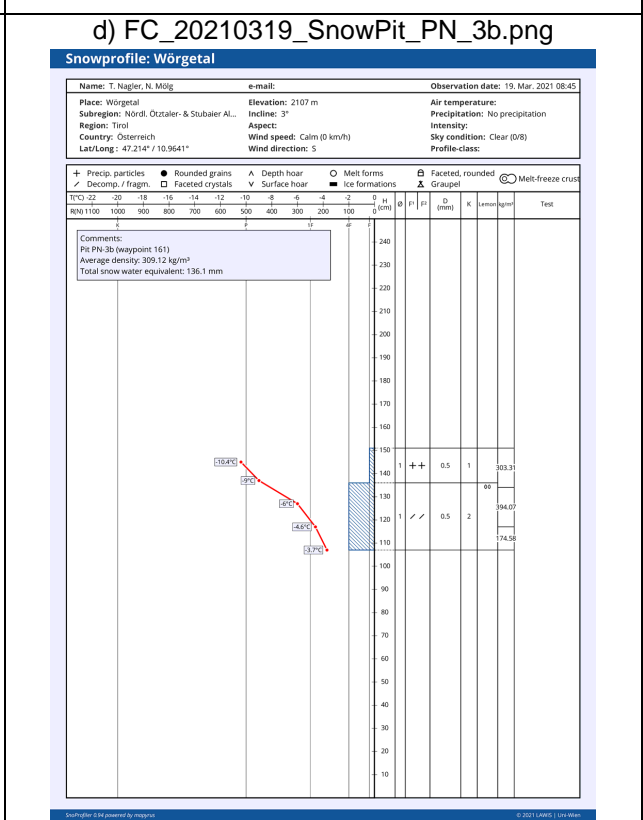
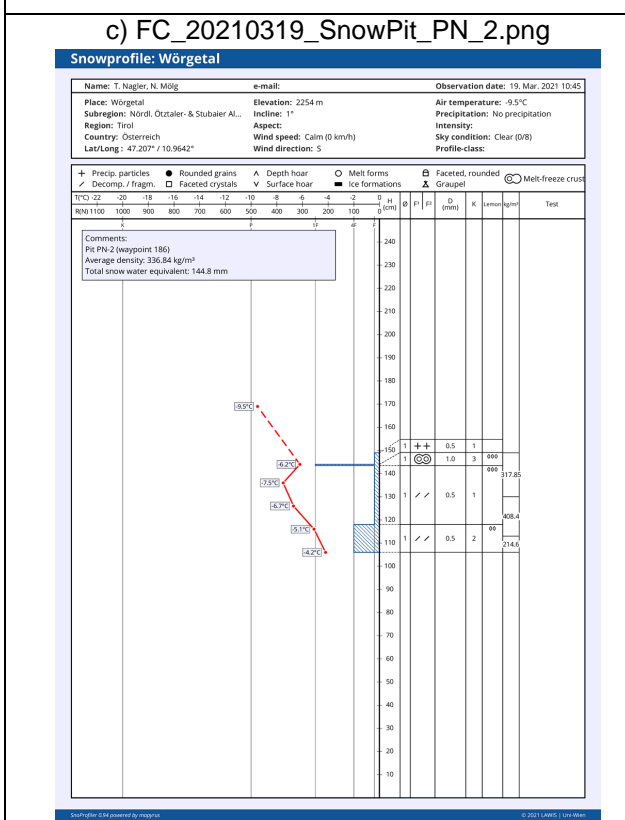
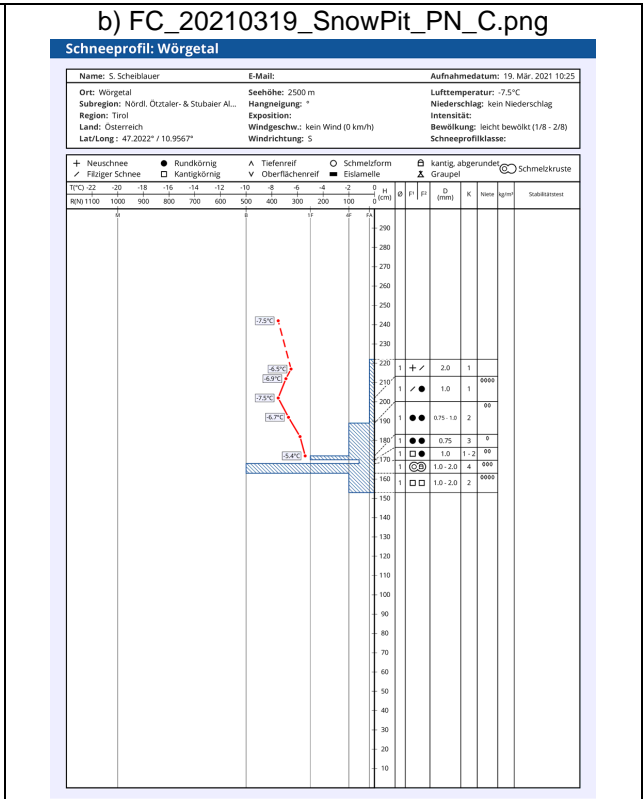
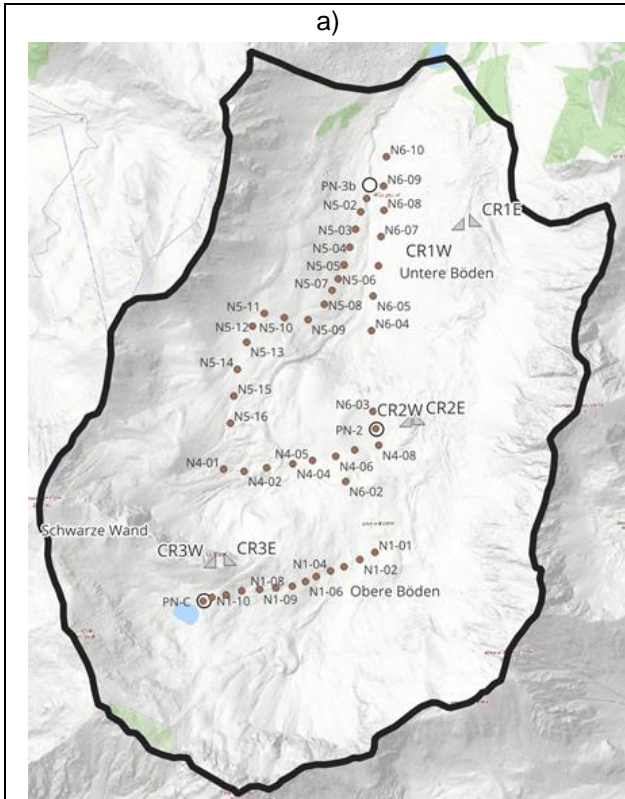


Figure 3-8: The snow deposited between 13. -19. 03.2021 was measured along the previously observed transects. Stratification of the fresh fallen snow layer deposited between 13. and 19.03.2021. Snow pits PN-A, PN-2 & PN-3.

a) FC_20210319_CR1E.jpg



b) FC_20210319_CR2E.jpg



c) FC_20210319_CR3E.jpg



d) FC_20210319_freshsnowpack.jpg



e) FC_20210319_CR2_viewdownthevalley

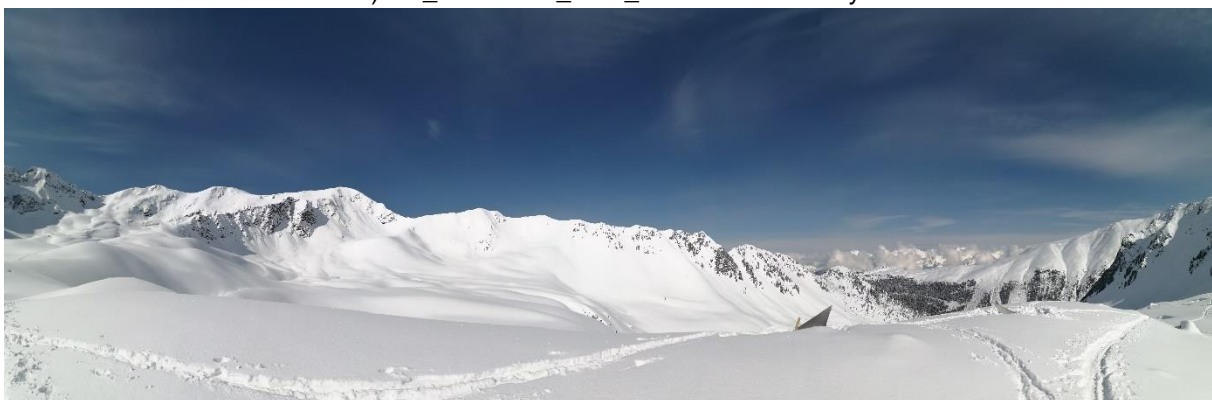


Figure 3-9: a) Corner reflector CR1E in the morning, b) CR2E c) CR2W d) roughly 30 cm of fresh snow, fallen between 13. - 19.03.2021, e) view down the valley (northwest) from CR2. *Note:* All reflectors were cleaned and wiped dry before the SAR flights.

	<p>SARSimHT-NG – Simulation of Hydroterra SAR System Performance in the Mediterranean and the Alps Based on Experimental Airborne SAR Data</p> <p>D1: Data Acquisition Report of SWE Experiment</p>	<p>Doc.: DLR-HR-TR-SARSimHT-NG-01 Issue: 2.0 Date: 25.11.2021 Page: 33 of 110</p>
---	---	--

3.6.5 FC Dates Wörgetal

Date	Task	Personnel
18.2. + 23.2. 2021	Exploration of test area, selection of location of CR, snow pits and transects,	H. Rott
1. 3. 2021	Setup of CR	N. Mölg, T. Nagler, H. Rott, S. Scheiblauer
2. 3. 2021	Check of CR, and completion, Field measurements	H. Rott, S. Scheiblauer
3. 3. 2021	CR check, Snow measurements	N. Mölg, H. Rott
6. 3. 2021	CR check, Snow measurements	T. Nagler, H. Rott
9. 3. 2021	CR check	H. Rott
13. 3. 2021	Geodetic GPS measurements of CR (phase centre)	T. Nagler
19. 3. 2021	CR check, Snow measurements	N. Mölg, T. Nagler, S. Scheiblauer
30. 3. 2021	Cleaning of Test area	N. Mölg, T. Nagler, S. Scheiblauer

3.7 Meteorological datasets

Close to the test site the University of Innsbruck operates the automatic weather station 'Gossenkölle' (2427 m a.s.l.). The station is located in the Kühtai region.

The station provides measurements of the following parameters:

- Precipitation in mm
- Air temperature in °C
- Snow depth in cm

3.8 Database description

The collected datasets are stored according to the folder structure shown in Figure 3-10. Under the root directory the content is:

- **CornerReflector**: documentation of corner reflectors
- **DEM**: 5m DEM of test site, version v20180222

- **FC_20210302** to **FC_20210330**: geospatial data of transects and snow pits, measurements in separate tables as well as photographic documentation of snow conditions, measurements
- **meteo**: meteorological data from nearby automatic weather station Gossenkölle (Kühtai)
- **qgis**: qgis project to display and map geospatial data sets

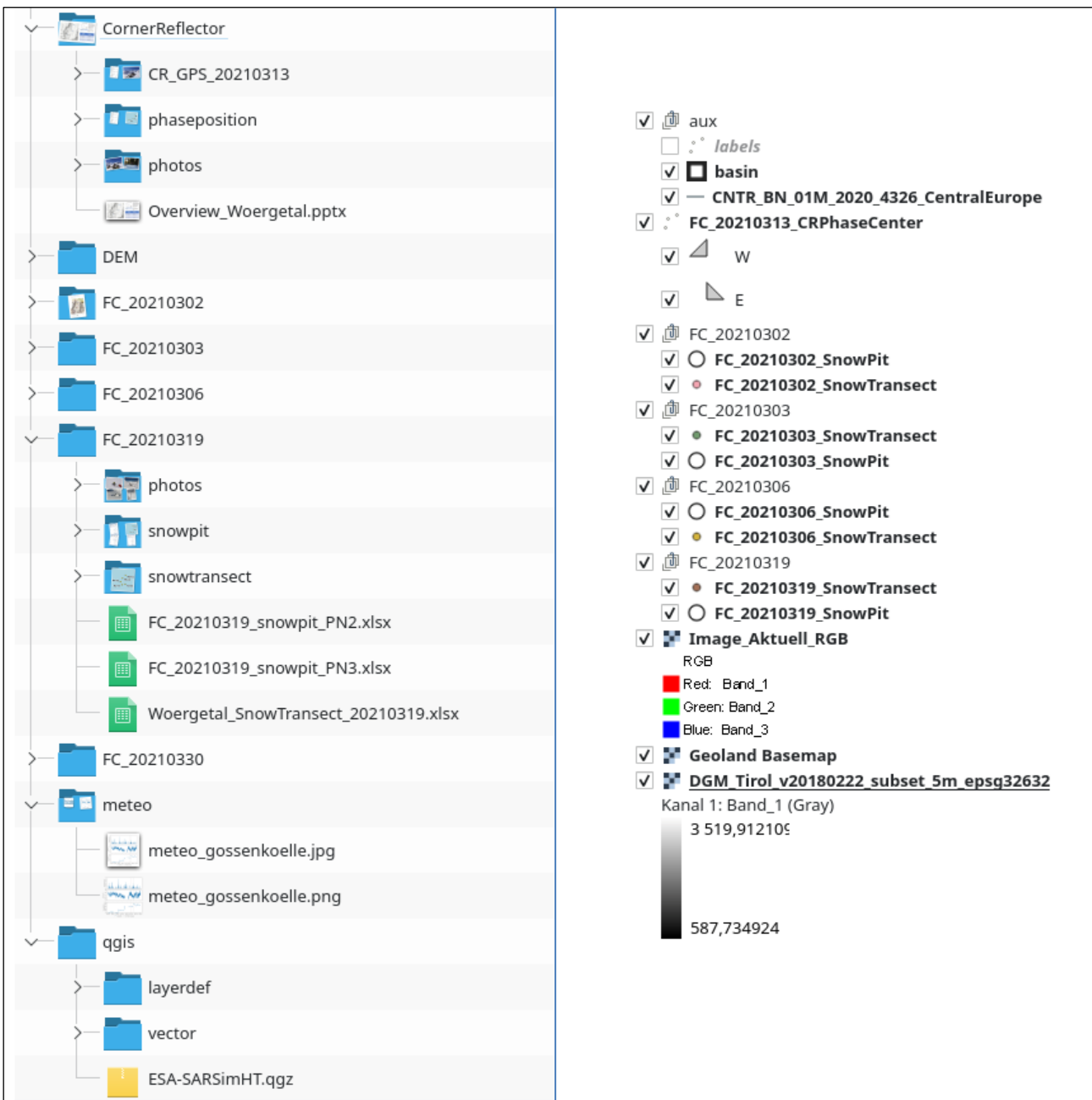


Figure 3-10: Structure of the database; directories and files (left) and QGIS (right).

4 Processing Strategy and Inventory

4.1 Preparations

Several auxiliary information data sets need to be prepared in order to process acquired airborne SAR data. They include the Digital Elevation Model (DEM), corner reflector positions (tie points), airplane motion data (IGI), antenna mounts and antenna properties, mission planning information and replica assignments, i.e., the waveform sent out by the radar system. DEM preparation, tie points and a squint angle analysis deserve to be described in more detail.

4.1.1 Digital Elevation Model and Tie Points

A laser-scanned Digital Elevation Model (DEM) has been provided by our project partner ENVEO. Its total coverage is depicted in Figure 4-1 and the red frame marks the test site Wörgetal (Figure 4-2).

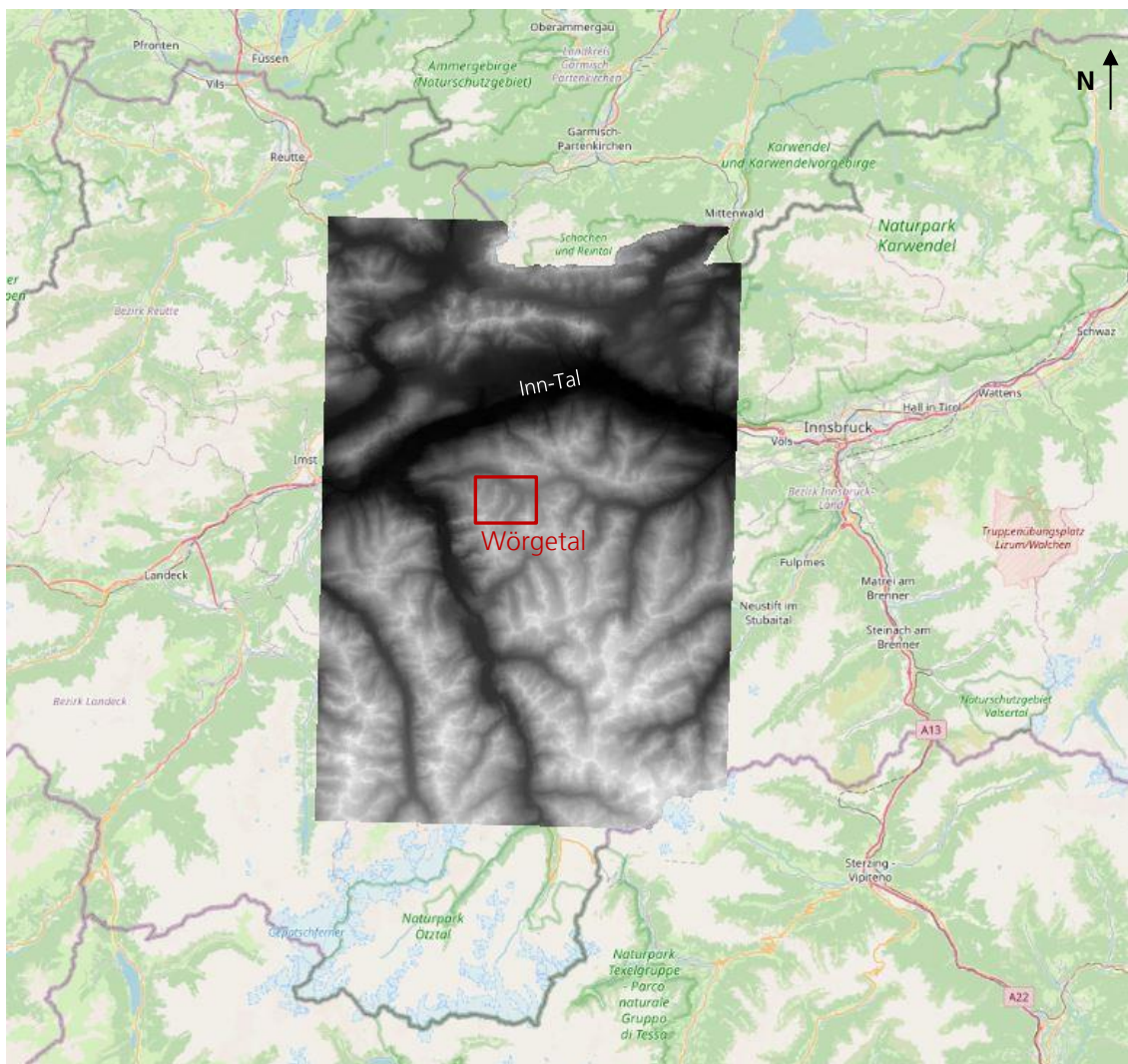


Figure 4-1: Coverage of the Digital Elevation Model (DEM) used for precise SAR processing.

An initially delivered version of this DEM had some artefacts (chessboard pattern). After noticing interferometric phase artefacts, the DEM has been exchanged and all processing has been repeated. All data delivered and all processing results are based on the correct DEM. A visualization of the DEM at test site

Wörgetal including the corner reflector positions (CR1, CR2, CR3) marked as red dots is shown in Figure 4-2.

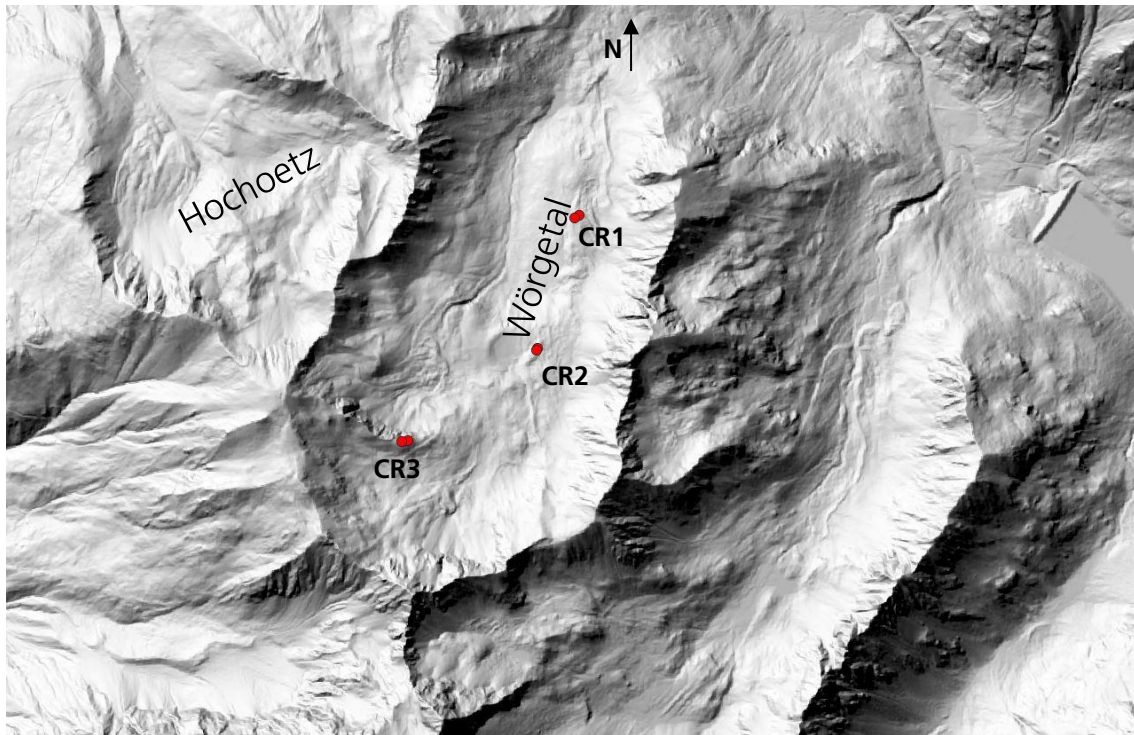


Figure 4-2: DEM coverage at test site Wörgetal, with shading applied for visualization purposes.

The DEM key indicators are listed in Table 4-1.

Table 4-1: Digital Elevation Model (DEM) key indicators

Coordinate Reference System (CRS)	EPSG:32632 - WGS 84 / UTM zone 32N - projected	
Extension	633400.00 / 5199700.00 : 671500.00 / 5255500.00	
Unit	Meter	
X-Dimension	7620	
Y-Dimension	11160	
Data	Float32 - 32-Bit floating-point number	
Format	GeoTIFF	
Region	Tirol, Austria	
Area or Point	Area	
Dimensions	X: 7620; Y: 11160; Channels: 1	
Origin	N 633400 / E 5255500	
Pixel Size [m]	+5, -5	
Accuracy [m]	+ / - 0.2 (horizontal)	+ / - 0.1 (vertical)
Undulation [m]	50.69	

	<p>SARSimHT-NG – Simulation of Hydroterra SAR System Performance in the Mediterranean and the Alps Based on Experimental Airborne SAR Data</p> <p>D1: Data Acquisition Report of SWE Experiment</p>	<p>Doc.: DLR-HR-TR-SARSimHT-NG-01 Issue: 2.0 Date: 25.11.2021 Page: 37 of 110</p>
---	---	--

Furthermore, corner reflectors allow us checking the *radiometric*, *polarimetric* and *interferometric* calibration as well as the *geolocation* of the acquired SAR data after mapping them to the selected georeference system, being UTM projection (zone 32N) with respect to the WGS 84 ellipsoid (EPSG 3857) here.

Six foldable corner reflectors were put up, each sized 95 cm in edge length. For C-band, this edge length is sufficient. For L-band, however, it showed to be too small. An edge length of at least 1.50 m would have been required for L-band. However, it was not possible to put up larger corner reflectors which would have provided a better radar cross section. Three corner reflectors sites were selected, called CR1, CR2 and CR3 and two corner reflectors (pointing E=East and W=West) were put up at each site. Their coordinates and orientation are listed in Table 4-2.

Table 4-2: Corner reflectors at test site Wörgetal.

Name	Site	Size [cm]	Longitude [°]	Latitude [°]	h_wgs [m]	Pointing [°]	Elevation [°]
CR1E	Wörgetal	95	10.96827298	47.21274508	2224.10	90	31
CR1W	Wörgetal	95	10.96804210	47.21264808	2224.88	270	18
CR2E	Wörgetal	95	10.96569560	47.20709547	2338.64	90	28
CR2W	Wörgetal	95	10.96562117	47.20703839	2339.39	270	19
CR3E	Wörgetal	95	10.95758372	47.20320258	2467.51	90	19
CR3W	Wörgetal	95	10.95722408	47.20314324	2473.17	270	26

The exact position of all corner reflectors put up at the site has been measured with high-precision GPS equipment. It is therefore interesting to check the heights found in the used laser DEM with those measured at the site with GPS equipment. This comparison can be found in Table 4-3.

Table 4-3: Comparison CR-heights (GPS) versus DEM-heights (Laser).

Name	CR h_wgs [m]	DEM h_wgs [m]	Difference [m]
CR1E	2224.10	2223.24	0.86
CR1W	2224.88	2224.24	0.64
CR2E	2338.64	2337.78	0.86
CR2W	2339.39	2338.12	1.27
CR3E	2467.51	2467.64	-0.13
CR3W	2473.17	2472.80	0.37

The deviations found in Table 4-3 are mainly ascribed to the limited resolution of the laser DEM. A pixel size of 5 m x 5 m is too coarse to map topographic details especially in regions like the Wörgetal. The GPS measurements are assumed to be accurate.

4.1.2 Ideal Track Assignment

An initialization process runs prior to standard SAR processing. It prepares auxiliary data which will be needed in subsequent processing. Amongst others, it converts the laser DEM into radar slant range geometry and determines respective ideal tracks for SAR processing.

Table 4-4: Image geometries and interferometric groups.

Image Geometry	Track	Band	Flight Direction	Illumination
1	10	L-Band	towards south	towards west
2	10	C-Band	towards south	towards west
3	11	L-Band	towards north	towards east
4	11	C-Band	towards north	towards east

For simulated Hydro-Terra image synthesis it is required to process all data onto a *common ideal straight-line* reference track in order to allow seamless combination of Doppler bands within each interferometric group. In total, we have **four image geometries** for the 2021 Wörgetal experiment, one from each side (West and East) and one for each band (L-band and C-band), see Table 4-4. The two image geometries, valid for both L- and C-band, are depicted in Figure 4-3, respectively.

Thus, the initialization process of the processing has been started such that one common optimal ideal straight-line track will be assigned to all passes belonging to the same interferometric group.

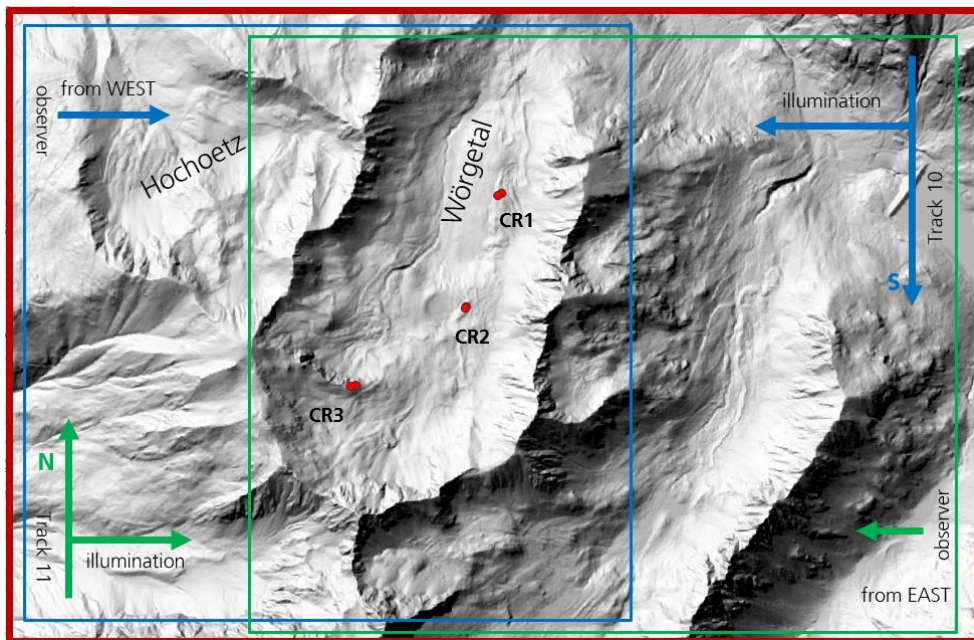


Figure 4-3: Wörgetal, two image geometries, one from East, one from West

4.1.3 Squint Angle Analysis

Another parameter that influences the final image geometry is the squint angle resulting from prevailing wind conditions during SAR data acquisition. The stronger the wind, the stronger the aircraft has to be turned against the wind, that is, the aircraft nose is not pointing into flight direction anymore (yaw angle is non-zero). As a result, the acquired SAR image is squinted, i.e. not rectangular shaped but parallelogram shaped and the stronger the wind was, the stronger the image is squinted. Examples are given in Figure 4-4.

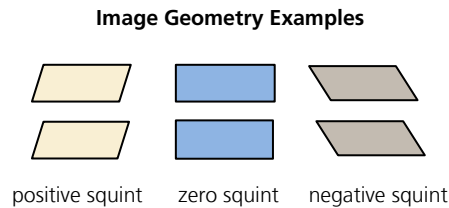


Figure 4-4: Image geometries due to wind conditions.

SAR processing can compensate different wind conditions up to some degree, depending on the width of the antenna main lobe in flight direction, which is smaller the smaller the wavelength is. It is, however, recommended to select the Doppler centroid as close as possible to the actual squint angle because forcing another squint angle means to mis-align the processed azimuth bandwidth from the optimum high-gain main-lobe area of the antenna. The image noise level would increase the further the scene is processed from its actual squint angle.

We therefore did a squint angle analysis and found that two flights each have similar averaged squint angles, shown in Table 4-5. Common squint angles in each track (column) are marked with the same colour. In other words, it is recommended to form *pairs of flights* which will be processed such that they are forced to their own *common squint* angle, as listed in Table 4-6.

Table 4-5: Average squint angles in acquired data.

Name	Track 10	Track 11
FL01	2.4	0.31
FL02	-0.23	2.26
FL03	-3.69	6.41
FL04	-3.78	7.33
FL05	2.81	0.23
FL06	-2.46	4.39
FL07	-2.04	5.45
FL08	-0.26	2.96

Table 4-6: Interferometric groups and forced squint angles.

#	Interferometric Group	Time Lag	Track 10	Track 11	Try
01	FL01-FL05	4 days	2.6	0.25	T01
02	FL02-FL08	16 days	-0.24	2.6	T02
03	FL03-FL04	0.5 day	-3.75	6.7	T03
04	FL06-FL07	1 day	-2.25	5.7	T04
08	FL01-FL08	1, 2, 2.5, 4, 6, 7, 17 days	0.00	0.00	T08

We thus form four groups of two flights each with their own common squint angle and additionally, for the purpose of being able to compare all data arbitrarily, we form another group, which contains master passes only, where we force the squint angle to zero in order to be able to assess all flights

	<p>SARSimHT-NG – Simulation of Hydroterra SAR System Performance in the Mediterranean and the Alps Based on Experimental Airborne SAR Data</p> <p>D1: Data Acquisition Report of SWE Experiment</p>	<p>Doc.: DLR-HR-TR-SARSimHT-NG-01 Issue: 2.0 Date: 25.11.2021 Page: 40 of 110</p>
---	---	--

within the same geometry and the loss of individual image quality as a result of the forced squint angles. The first four interferometric groups will therefore yield an optimum image quality and the last group will allow us to assess possible losses in image quality if all data were processed in the same group forced with zero squint angle.

4.1.4 Processing Strategy

We process all data in five different groups, listed in Table 4-6. We have four groups (T01 – T04) in which two flights are grouped together and one group (T08) in which master passes of all flights are grouped together.

This will allow us to simulate **eight** Hydroterra image products and **four** Hydroterra interferograms for each look direction:

- FL01 versus FL05, time-lag = 4 days
- FL02 versus FL08, time lag = 16 days
- FL03 versus FL04, time lag = half a day
- FL06 versus FL07, time lag = one day.

Furthermore, group T08 allows to assess changes (e.g. due to snow fall) between arbitrary flights and arbitrary time lags, although not with simulated Hydroterra data but in full F-SAR quality.

4.2 Processing Results

4.2.1 Processing Parameters

This campaign is processed with standard processing parameters. They are summarized in Table 4-7.

Table 4-7: Processing Parameters.

Processor	STEP	STEP
Kernel Type	Extended Omega-K	Extended Omega-K
Software Version	6203	6203
Band	L	C
Centre Frequency [GHz]	1.325	5.300
PRF [Hz]	905.79	1811.59
Chirp Duration (μ s)	10.016	10.016
Range Delay (μ s)	22.399	22.399
Range Sampling [MHz]	250	500
Platform velocity [m/s]	93.2	93.2
Wavelength [cm]	22.62	5.65
Sensor Altitude [m]	5700	5700
Average Terrain Height [m]	2213	2213
Chirp Bandwidth [MHz]	150	384
Processed Azimuth Bandwidth [Hz]	199	239

Weighting Factor Azimuth	0.54	0.54
Weighting Factor Range	0.54	0.54
Resolution Azimuth [cm]	60	50
Resolution Range [cm]	130	50
Pixel Size Azimuth [cm]	40	20
Pixel Size Range [cm]	60	30

The pixel sizes decrease by a factor of two from L-band to C-band such that image sizes increase by a factor of four from L-band to C-band.

4.2.2 Overview and Image Geometries

The following two images (Figure 4-5 and Figure 4-6) represent two different image geometries, illuminated from the east and west, respectively. They show the entire scene from two sides in L-band. All other images in L-band look roughly the same except for changes which can merely be detected in interferograms. Another two image geometries arise in C-band such that, in total, we have four image geometries at the Wörgetal test site.

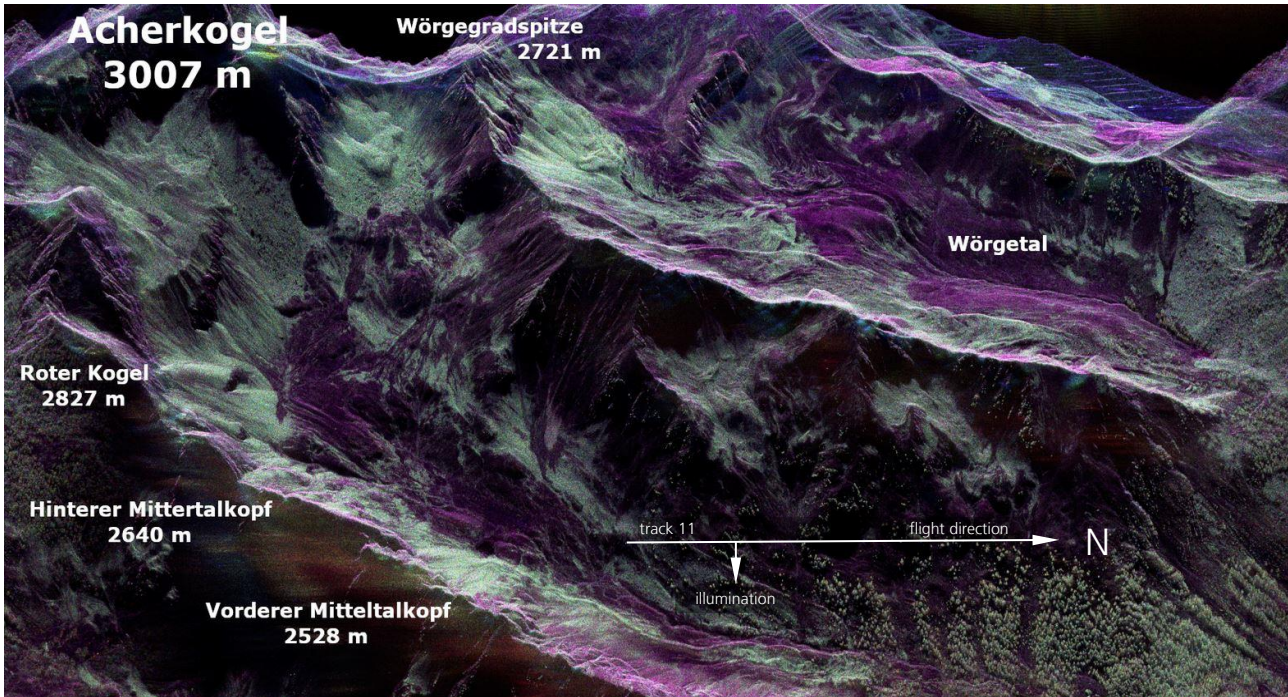


Figure 4-5: Wörgetal (top) from the East, ground truth has been taken at Wörgetal (L-band).

In order to give some orientation, we provide the names of several mountains surrounding the test site Wörgetal. Furthermore, to give an idea of the achieved image resolution we show a detail of Figure 4-6, the Hochoetz skiing area, in Figure 4-7.

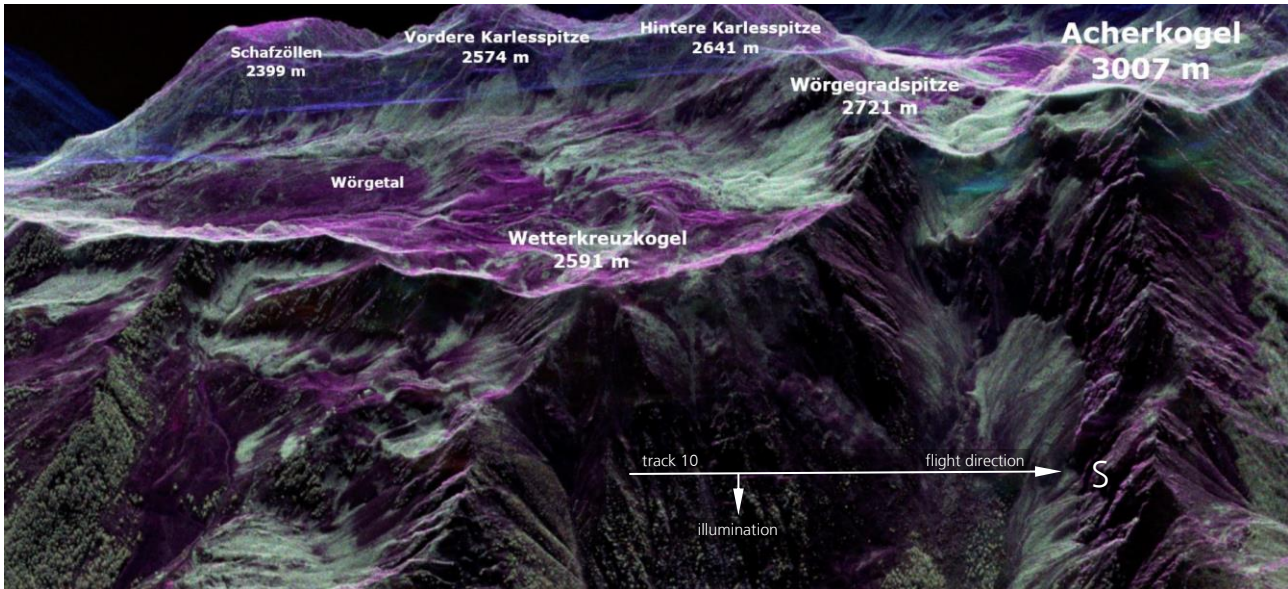


Figure 4-6: Wörgetal (top) from the WEST, Wetterkreuzkogel (2591 m), Hochoetz skiing area (L-Band).

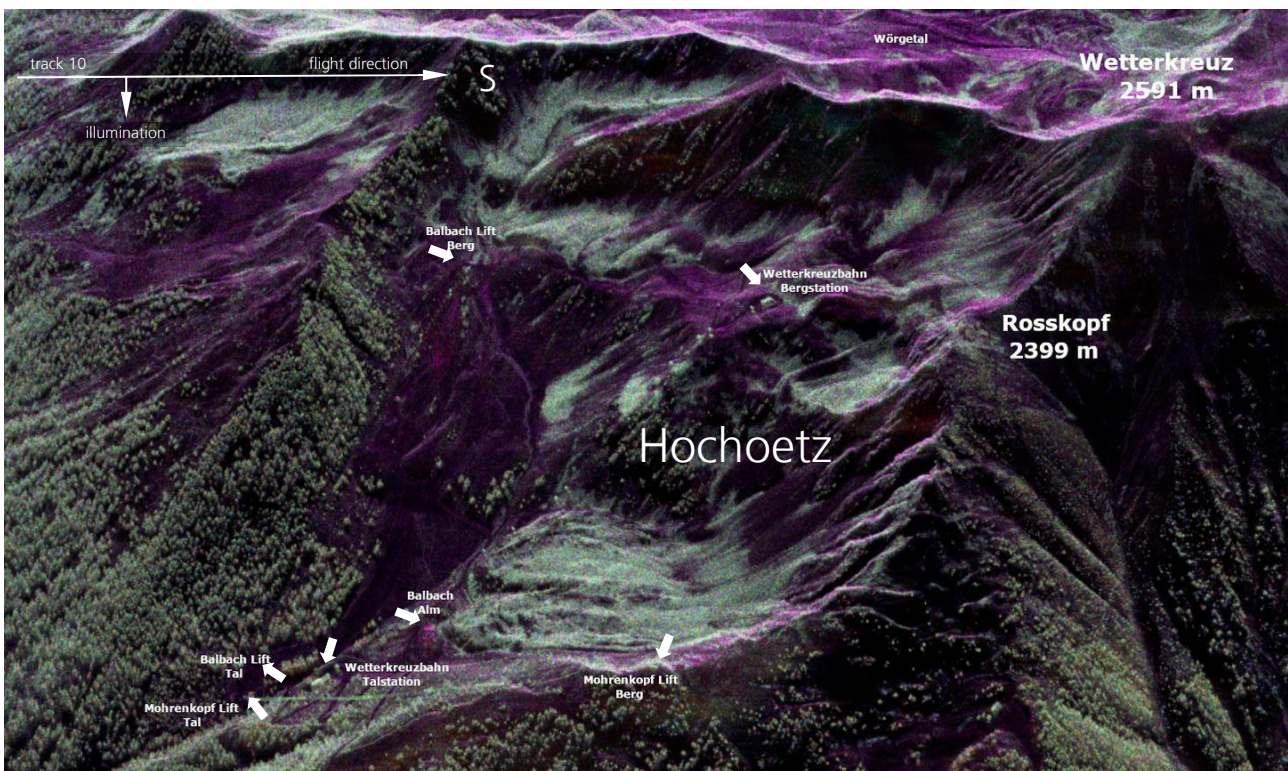


Figure 4-7: Wörgetal (top), west flank detail image, Hochoetz skiing area.

Several buildings can be recognized in Figure 4-7, one is Wetterkreuzbahn Station up on the mountain and down in the valley (green colour), another one is Balbach Alm (violet colour). Furthermore, ski lift pillars at the Balbach Lift and a lift rope of Mohrenkopf Lift can be recognized, for example.

4.2.3 Corner Reflectors in RGI Data

The corner reflectors in L-band can barely be seen because they are actually too small (0.95 m edge length). A size of at least 1.50 m edge length would have been needed.

In order to give an overview, we have a look at the corner reflector sites in Radar Geometry Images (RGI) from both sides, East (Figure 4-8, Figure 4-9) and West (Figure 4-10, Figure 4-11).

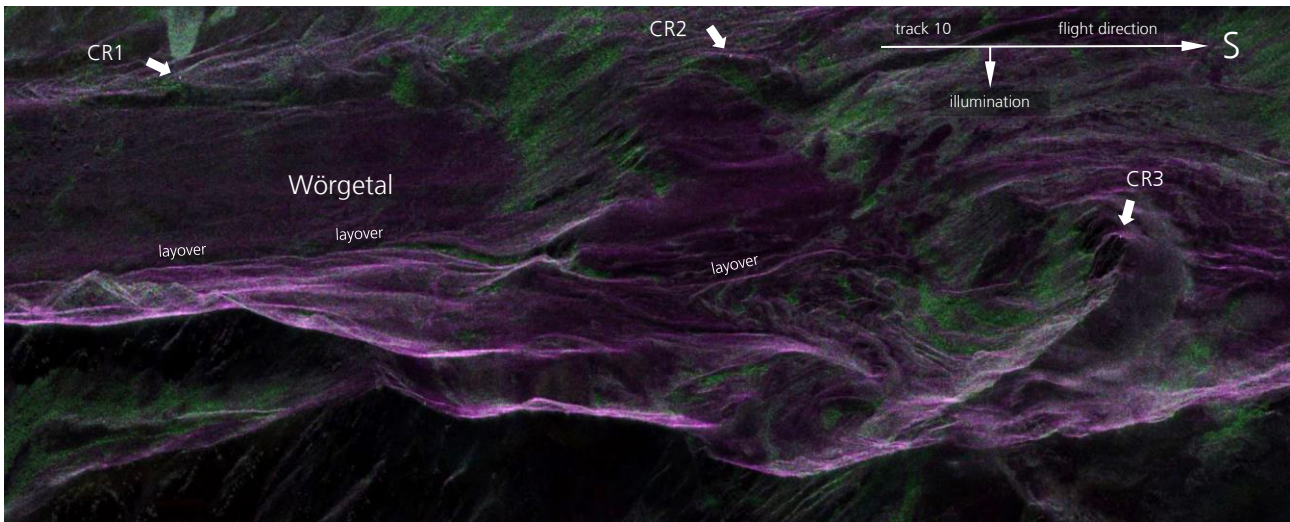


Figure 4-8: Wörgetal illuminated from the east; corner reflectors (visible); 21hterra0110, C-band.

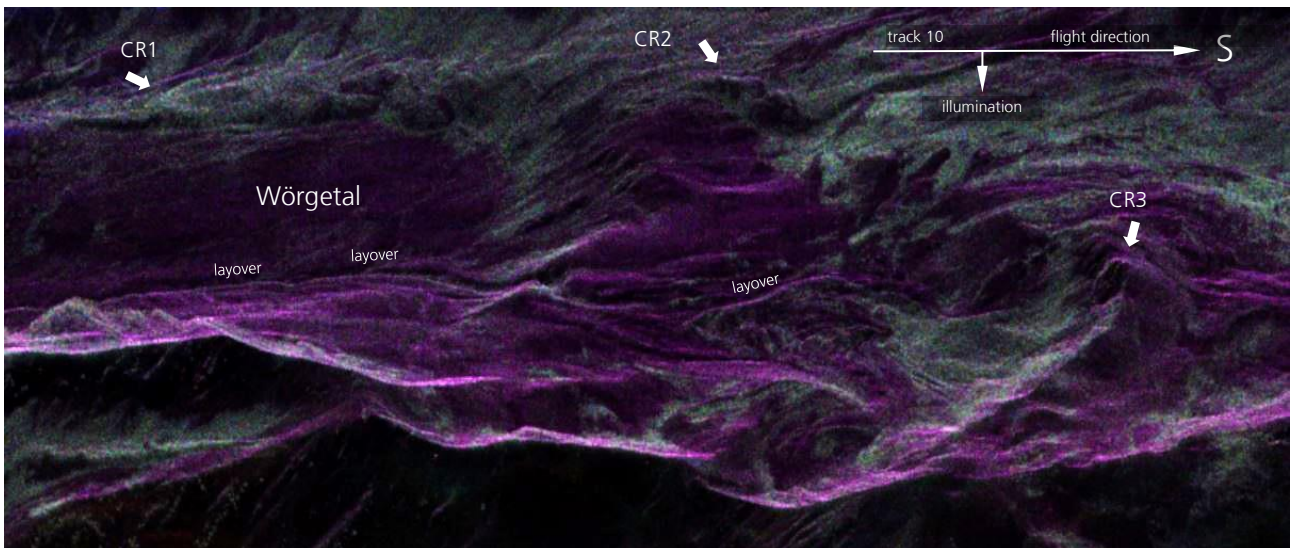


Figure 4-9: Wörgetal illuminated from the east; corner reflectors (barely visible); 21hterra0110, L-band.

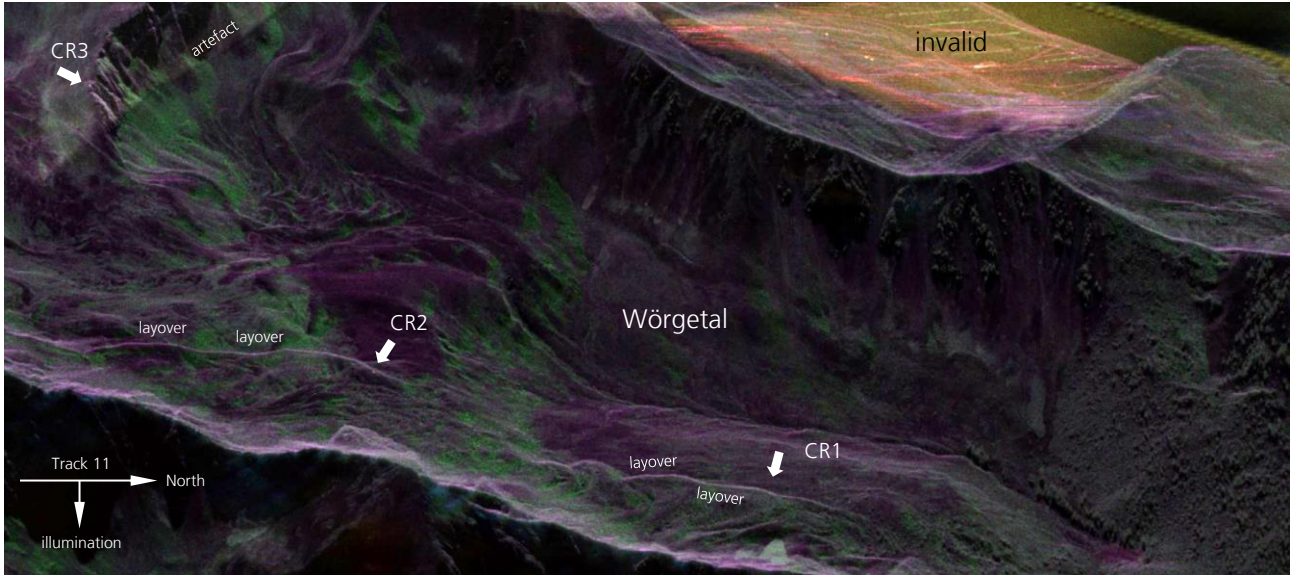


Figure 4-10: Wörgetal illuminated from the west; corner reflectors (visible); 21hterra0109, C-band.

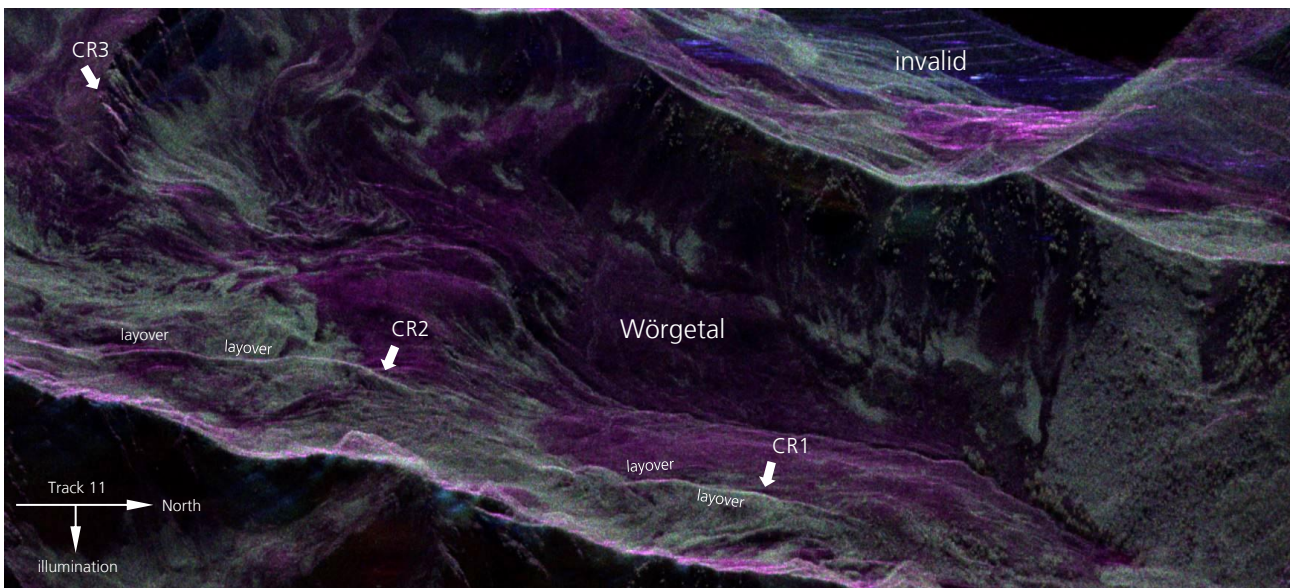


Figure 4-11: Wörgetal illuminated from the west; corner reflectors (barely visible); 21hterra0109, L-band.

The following cut-outs give an overview over all corner reflectors in C-band (purple dots).



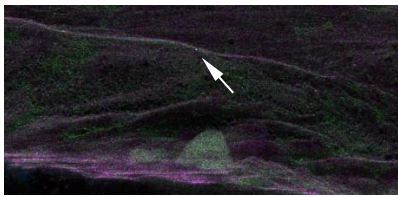
CR1E in 0102_C



CR2E in 0102_C



CR3E in 0102_C



CR1W in 0111_C



CR2W in 0111_C



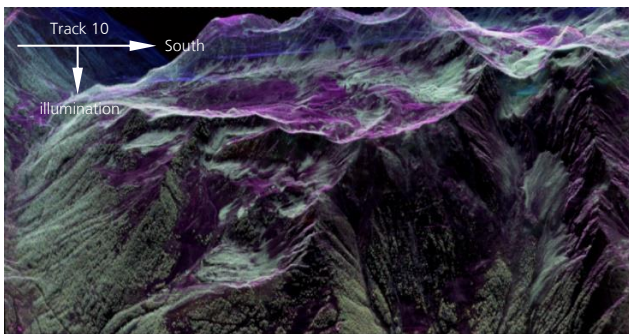
CR3W in 0111_C

One may recall, at each site there are two corner reflectors with opposite pointing directions. Letters E (east) and W (west) indicate the individual pointing of a CR.

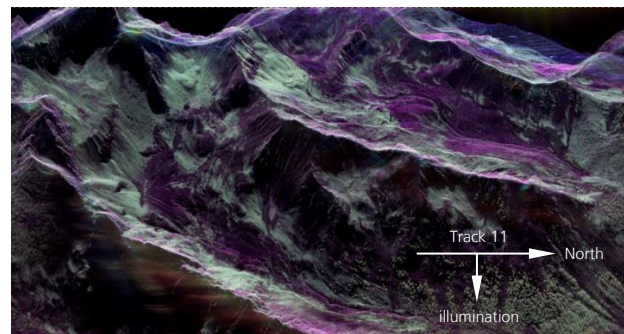
4.2.4 Radar Geometry Image (RGI) Product Generation

We have processed 4 x 2 interferometric groups where we combine 2 flights in each group, 8 flights in total yield 4 groups. Additionally, each group exists twice: two different radar looking directions, from east (track 10) and from west (track 11).

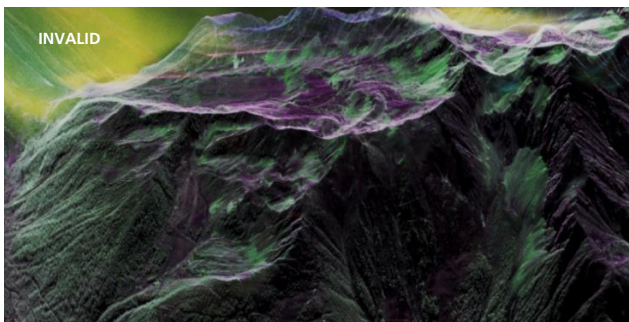
Exemplarily we show one image each from the west and the east in L- and C-band. In our products, we have generated both, lexicographic (RGB=HH,HV,VV) and Pauli (RGB=HH-VV,2*HV,HH+VV) decompositions. The following four images shown here are lexicographic colour composites, only.



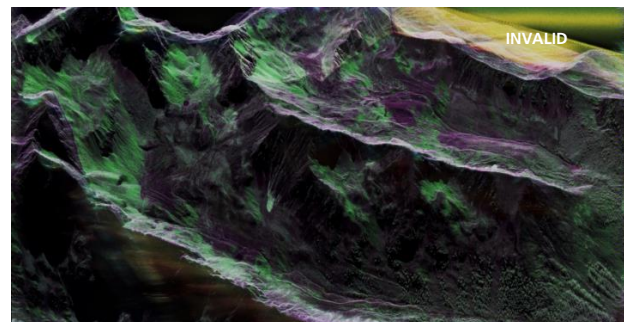
RGI, 21hterra0102_L, track 10, from East



RGI, 21hterra0103_L, track 11, from West



RGI, 21hterra0102_C, track 10, from East



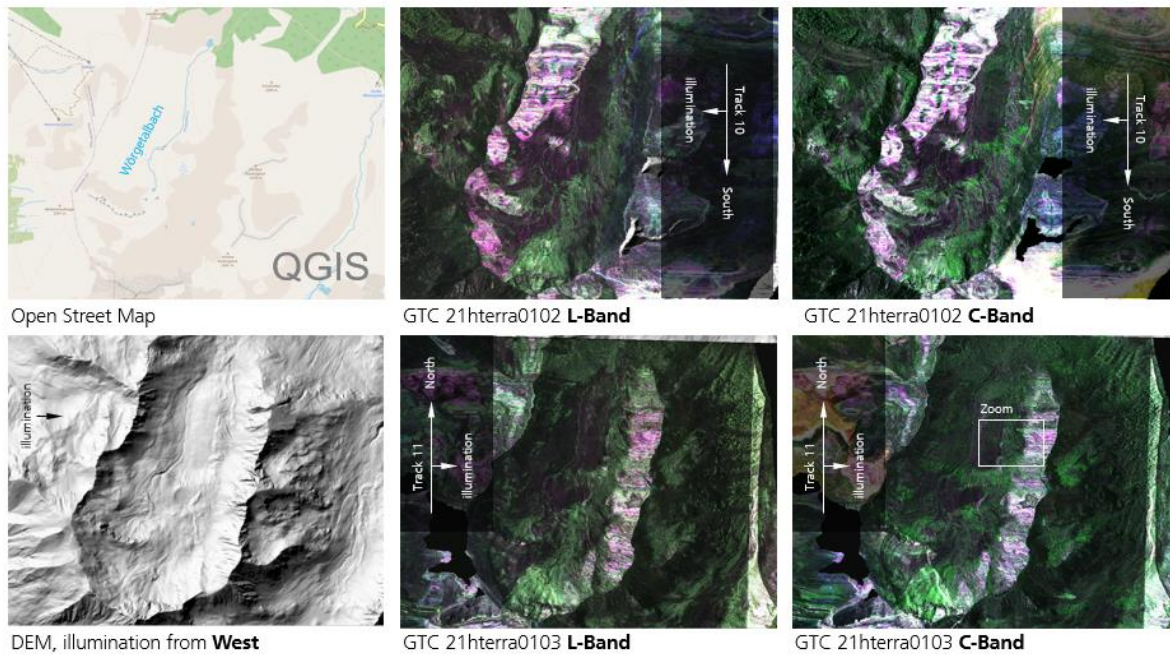
RGI, 21hterra0103_C, track 11, from West

Due to high mountain ridges at the test site with steep slopes on either side, we have severe effects by a special kind of layover in these scenes. Areas in near range are affected by a superposition, a range ambiguity, where backscatter from both sides of a ridge is detected by the radar at the same time.

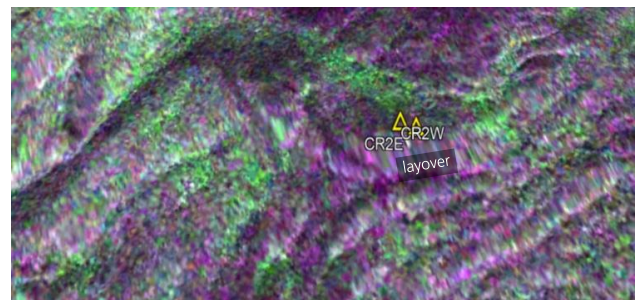
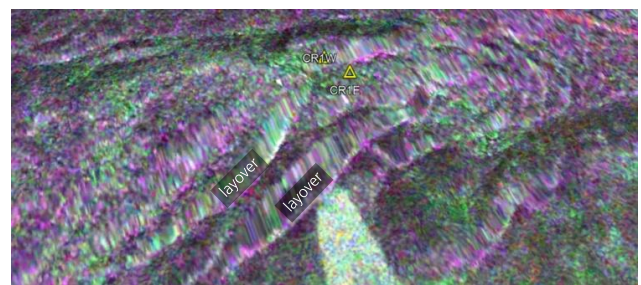
4.2.5 Geocoded and Terrain Corrected (GTC) Product Generation

We have geocoded primary (master) passes, only. Secondary (slave) passes may be converted into geocoded image geometries by using the respective lookup tables (LUT) in the GTC product of the primary pass.

Geocoded and Terrain Corrected (GTC) Products

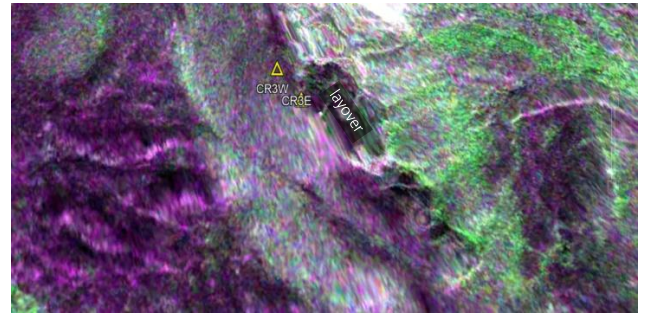


Following are details in the geocoded image geometry at all three corner reflector sites:





Site CR3, Google Earth



Site CR3, polgeo_21hterra0102_C_t01

4.2.6 Interferometric Image Product (INF) Product Generation

An Interferometric product (INF) is a Radar Geometry Image (RGI) converted to the image geometry of a given master pass. The step between RGI and INF is, hence, a **co-registration step** in which samples of the slave image are re-sampled to the master image geometry.

An important step, in order to achieve this, is to estimate pixel by pixel the offset between master and slave image at a subpixel precision for all image pixels. For airborne platforms, here the Do-228 aircraft, this amounts to estimate the difference between master and slave flight paths at a very high accuracy. We use the so-called **multi-squint algorithm** to estimate and compensate residual motion errors.

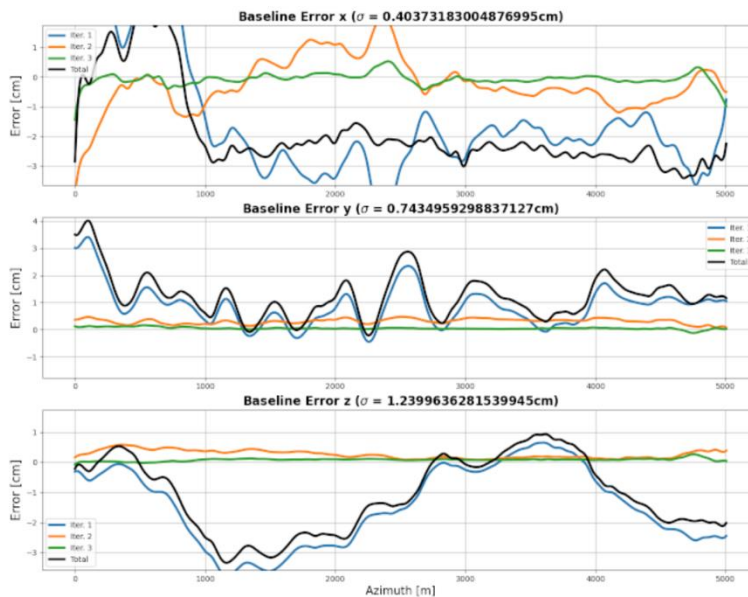


Figure 4-12: Baseline error estimation, master 0102, slave 0104.

A sufficient accuracy is usually achieved after three iterations (blue, yellow, green) as shown in Figure 4-12 where the baseline between master 0102 and slave 0104 is estimated. The black line indicates the final result used for pixel co-registration and phase compensation.

The overall **quality of convergence** between the master and its slave scenes in Interferometric Group 01 is depicted in Figure 4-13. The black frame in the first column marks an example shown in detail below (C-hh: Figure 4-18 and Figure 4-19, as colour composite in Figure 4-20 and Figure 4-21).

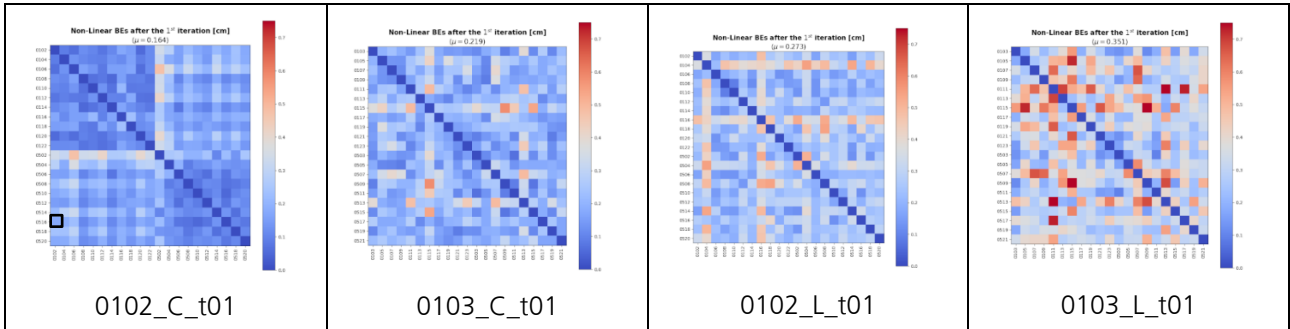


Figure 4-13: Performance of interferometric Group 01 (Flight 01 + Flight 05).

Correspondingly, we summarize here the convergence quality in all interferometric groups in order to have an idea of the co-registration quality in all INF products.

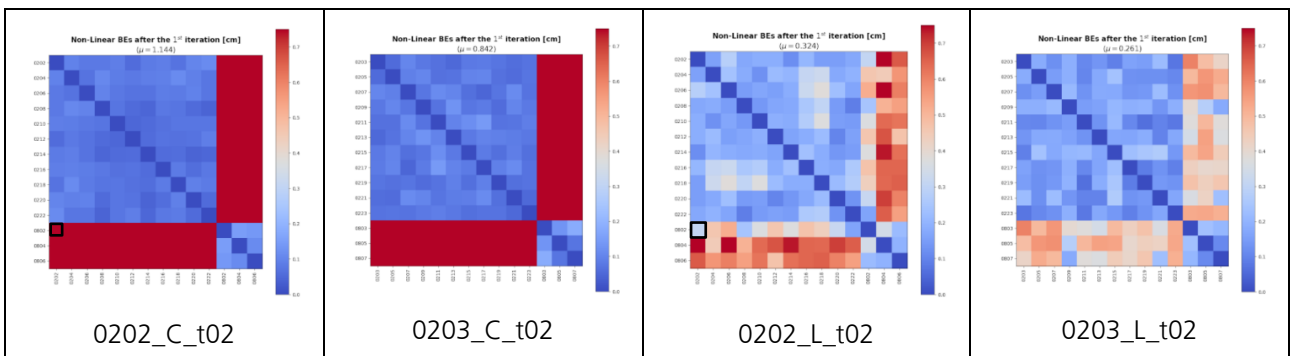


Figure 4-14: Performance of interferometric Group 02 (Flight 02 + Flight 08).

Dark red colours in Figure 4-14 indicate loss in coherence in C-band due to heavy snow fall between flights FL02 and FL08. This effect is less severe in L-band due to the longer wavelength. Two black frames in Figure 4-14 mark examples shown in detail below. Even at C-band there is still useful information (L-band: Figure 4-24 and Figure 4-25; C-band: Figure 4-26 and Figure 4-27).

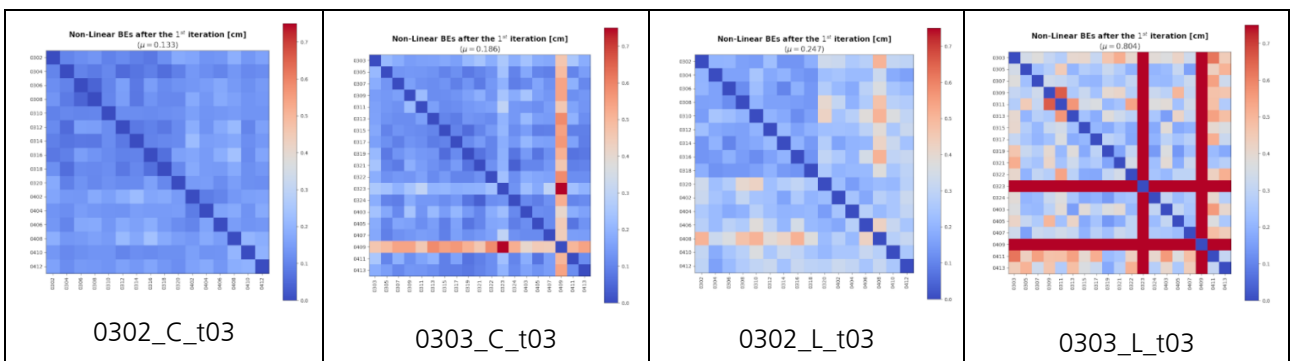


Figure 4-15: Performance of interferometric Group 03 (Flight 03 + Flight 04).

The red indicators (rows and columns) in Figure 4-15 mark passes with larger deviations from the nominal flight path (pass 0323 and pass 0409). See also the yellow lines in the product lists below. Pass 0323 was aborted during flight; pass 0409 had deviations from the nominal track larger than 16 m. By mistake they were included in the first processing run which caused a poor product quality. This has been

corrected for by re-processing the stacks (Group 03, WEST) in L- and C-band without the passes 0323 and 0409. The re-processed data sets can be found as 'stack11Cnew7' and 'stack11Lnewhh' in the delivered data.

Note that 'stack11Cnew7' is not re-processed in **tomographic** mode (as is the default) but in **interferometric** mode which means that (an INF product for the master pass 0303 including a baseline error and other plots is not created and) only interferometric pairs are formed instead of comparing each member with each member in this group. This was then required after satisfying results could not be obtained in tomographic mode. A simple phase offset calibration has been applied using the corner reflectors.

The respective L-band data set 'stack11Lnewhh', in contrast, is re-processed in tomographic mode but a special feature here is that we used the **HH channel** as the master channel (instead of using VV as is the default) because this approach showed better tomographic calibration results in this case.

However, we decided to deliver both the standard 'stack11C' and 'stack11L' as well as the re-processed 'stack11Cnew7' and 'stack11Lnewhh' data sets such that the data analyst can freely decide to use the one or the other results.

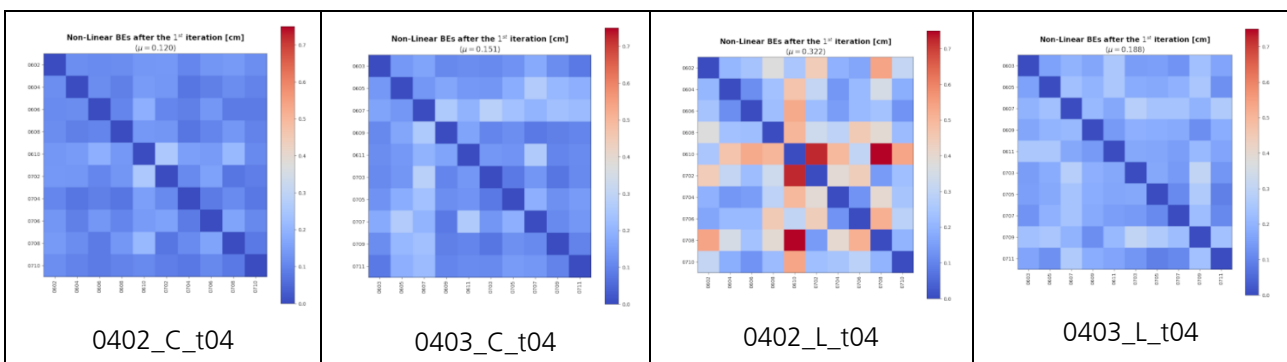


Figure 4-16: Performance of interferometric Group 04 (Flight 06 + Flight 07).

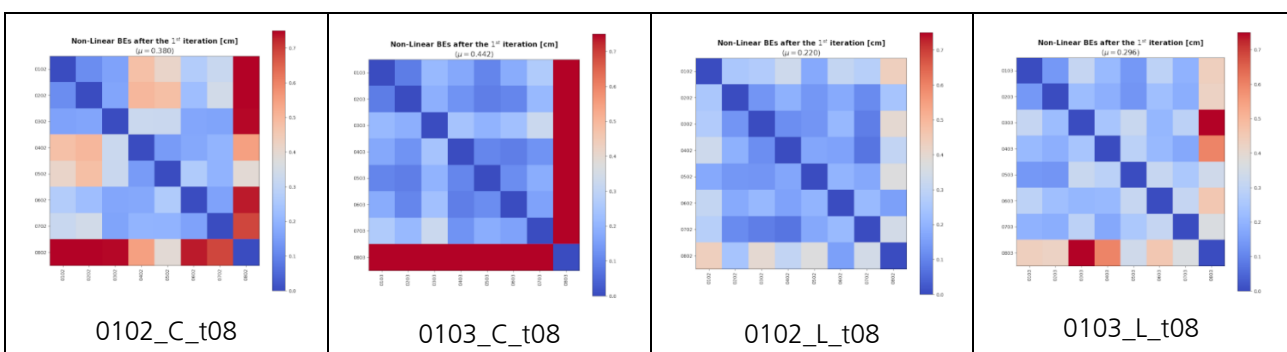


Figure 4-17: Performance of interferometric Group 08 (Flight 01 until Flight 08, only master passes).

In Figure 4-17 (FL01, FL02, ..., FL08) on the far left (column 01), we see the same effect as in Figure 4-14 (FL02+FL08): drop in coherence due to snow fall. There is a degradation from FL04 to FL05 and a severe drop from FL07 to FL08, the latter due to the large time gap (ten days) and snow.

Let us have a look at several examples of interferometric products. In Figure 4-18 and Figure 4-19 we see the C-band HH channel interferometric coherence and phase, respectively. The combination of HH-HV-VV in coherence and phase is further depicted in Figure 4-20 and Figure 4-21, respectively. Finally, an example in L-band is shown in Figure 4-22 and Figure 4-23.



Figure 4-18: Interferometric coherence, C-band, coh_21hterra0102_21hterra0516_Chh_t01.png.

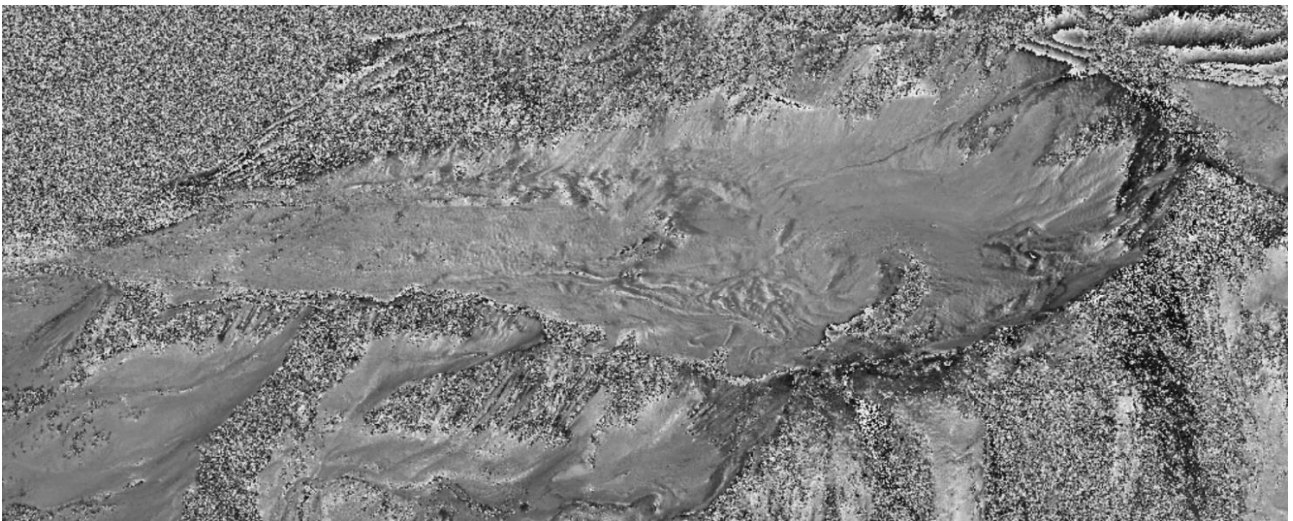


Figure 4-19: Interferometric phase, C-band, pha_21hterra0102_21hterra0516_Chh_t01.png.

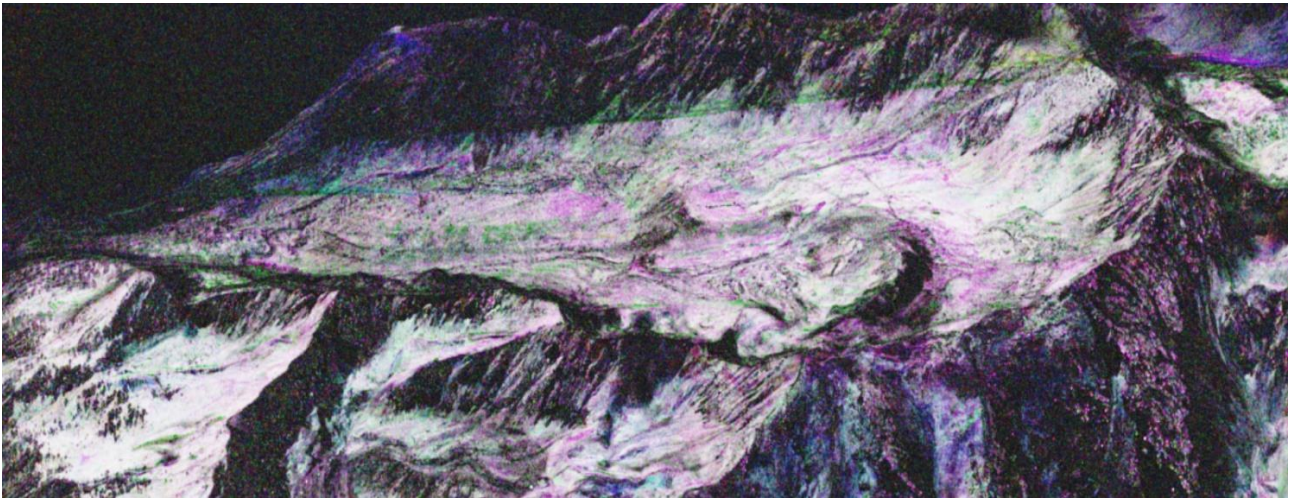


Figure 4-20: Interferometric coherence, C-band, coh_21hterra0102_21hterra0516_Chh-hv-w_t01.png.

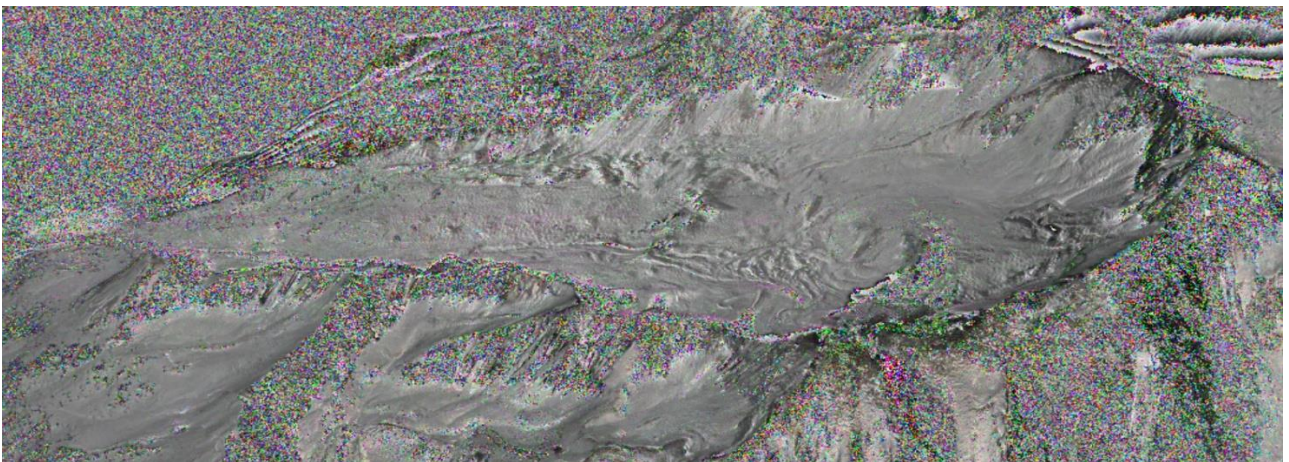


Figure 4-21: Interferometric phase, C-band, phy_21hterra0102_21hterra0516_Chh-hv-w_t01.png.

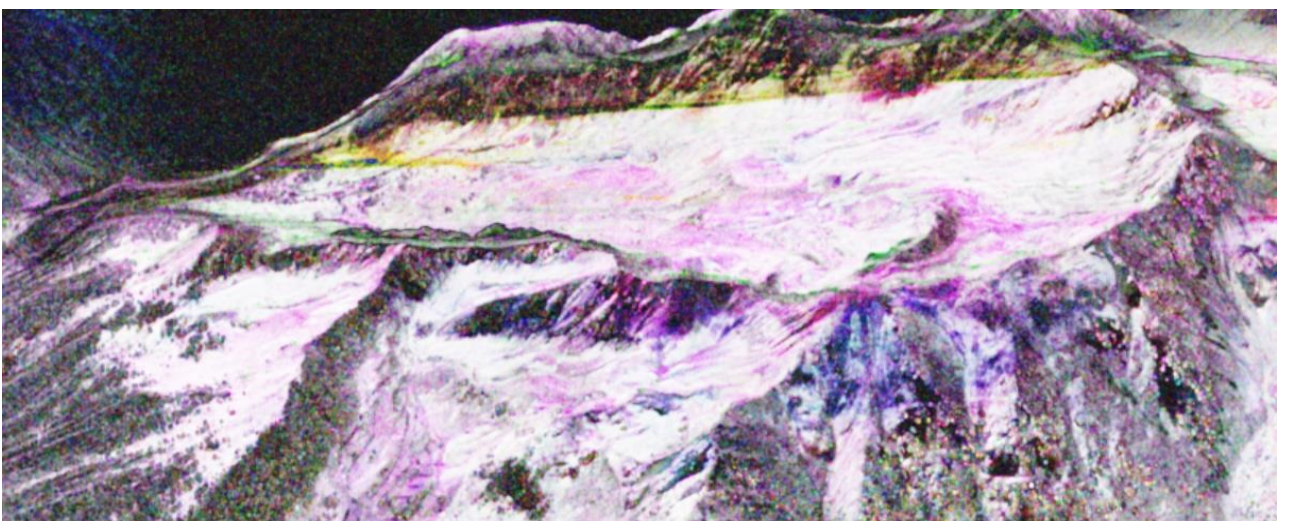


Figure 4-22: Interferometric coherence, L-band, coh_21hterra0102_21hterra0516_Lhh-hv-vv_t01.png.

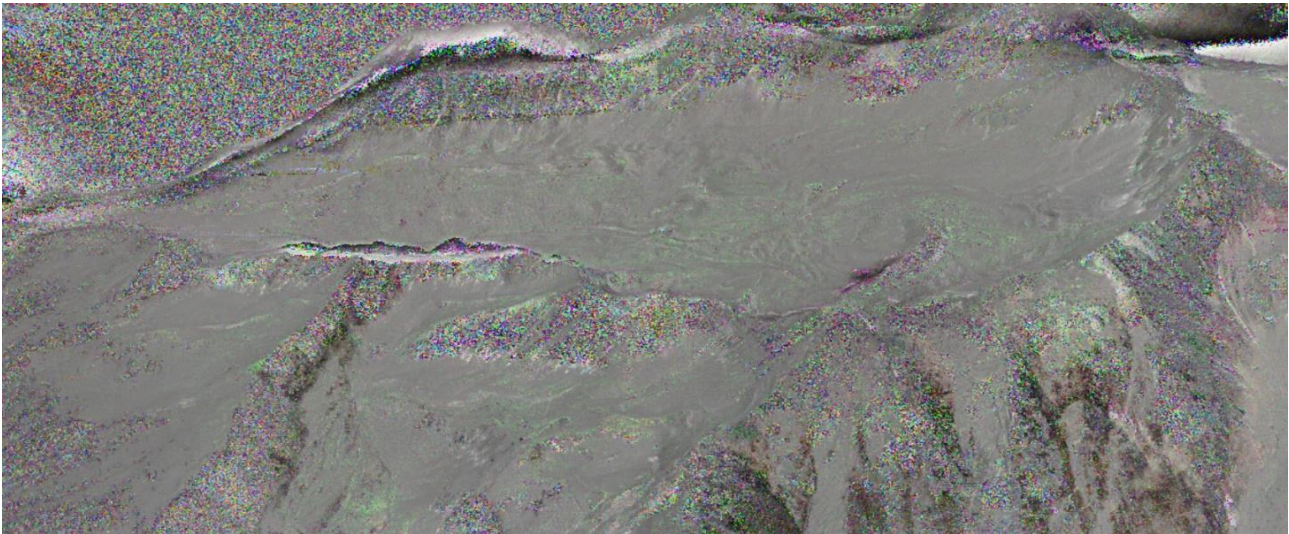


Figure 4-23: Interferometric phase, L-band, pha_21hterra0102_21hterra0516_Lhh-hv-vv_t01.png.

Next, we show a **best**-case (L-band, Figure 4-24 and Figure 4-25) and a **worst**-case (C-band, Figure 4-26 and Figure 4-27) scenario taken from interferometric Group 02 (comparing FL02 – FL08) (see the two black boxes in Figure 4-14).



Figure 4-24: Interferometric coherence, coh_21hterra0202_21hterra0802_Lhh_t02.png.

	<p>SARSimHT-NG – Simulation of Hydroterra SAR System Performance in the Mediterranean and the Alps Based on Experimental Airborne SAR Data</p> <p>D1: Data Acquisition Report of SWE Experiment</p>	<p>Doc.: DLR-HR-TR-SARSimHT-NG-01 Issue: 2.0 Date: 25.11.2021 Page: 53 of 110</p>
---	---	--

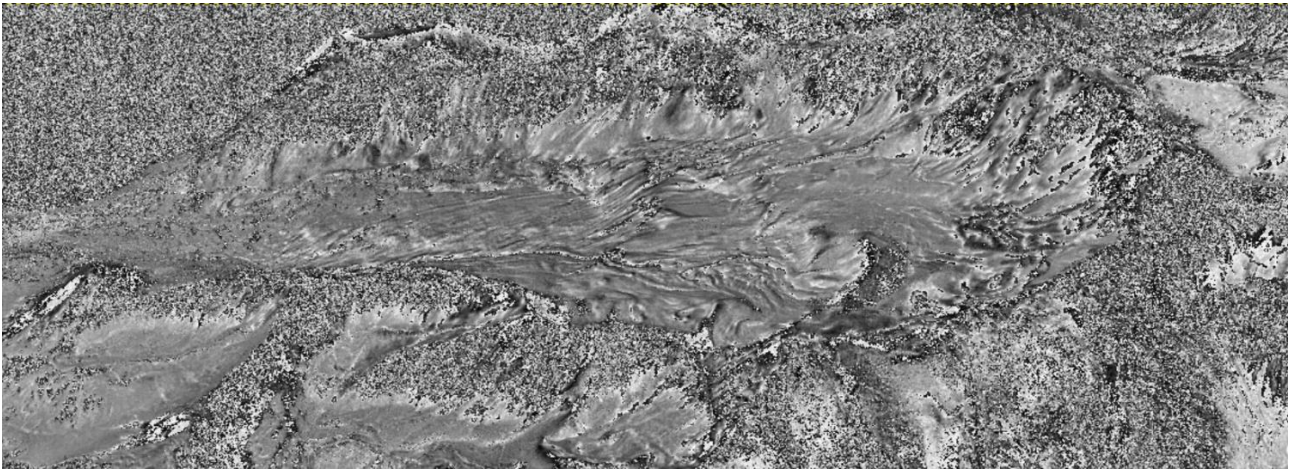


Figure 4-25: Interferometric phase, pha_21hterra0202_21hterra0802_Lhh_t02.png.

In contrast (worst case), a low coherence (C-band) example is shown next. The low coherence is associated with heavy snow fall prior to flight 08 and the large time gap (ten days) between FL07 and FL08. Yet, there is obviously still some information left both in coherence (Figure 4-26) and phase (Figure 4-27).

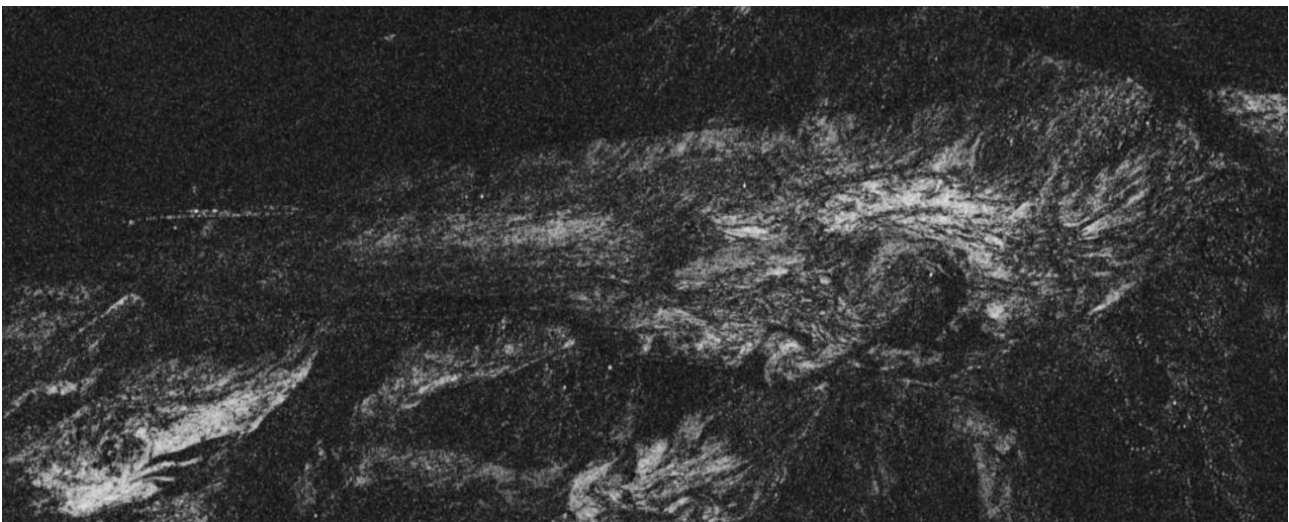


Figure 4-26: Interferometric coherence, coh_21hterra0202_21hterra0802_Chh_t02.png.

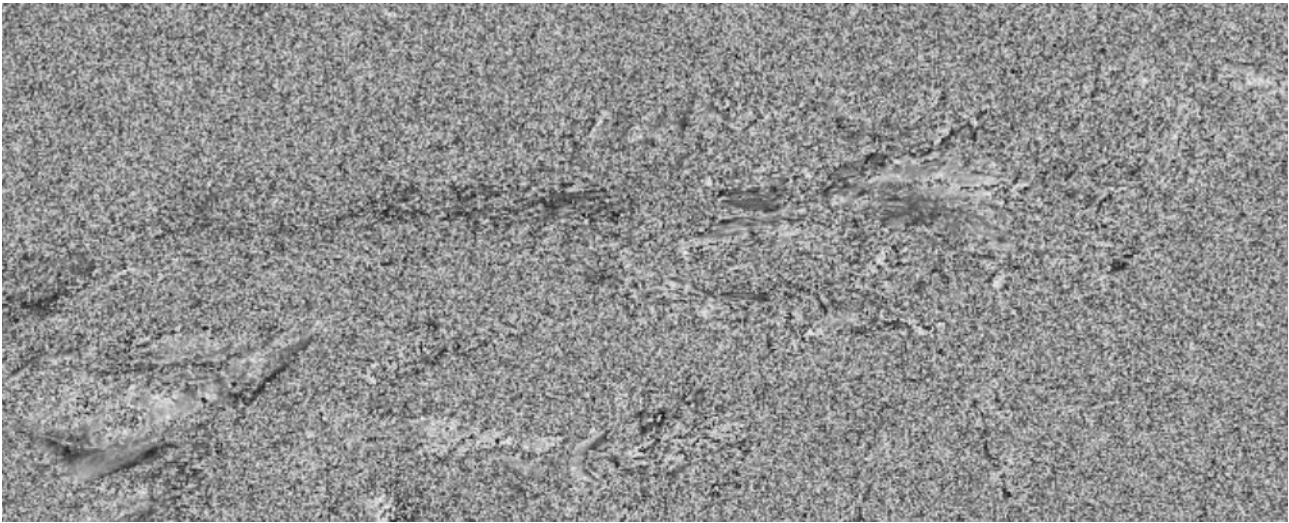


Figure 4-27: Interferometric phase, pha_21hterra0202_21hterra0802_Chh_t02.png.

Figure 4-28 shows the sequence of flights (coloured circles) and indicates snow fall events between flights. The colour depicts similar squint angle, that is, the same interferometric group is indicated in the same colour. The largest difference is between FL02 and FL08, hence, the largest coherence drop can be found in interferometric Group 02.



Figure 4-28: Snow fall events between FL04 and FL05 as well as between FL07 and FL08.

An overview of the change of coherence from flight to flight is given in Figure 4-29. A change can be observed from FL04 to FL05, another from FL07 to FL08.



Figure 4-29: Change of coherence over time in L-band (upper row) and C-band (lower row), HH channels.

The correlation between snow fall / time delay on one hand and change in coherence on the other hand is impressively demonstrated in Figure 4-29. The effect is stronger the shorter the wavelength. It is well visible in L-band (upper row) and more severe in C-band (lower row).

4.3 Calibration Check

We used the corner reflectors put up at the test site for a verification of the calibration of the SAR instrument. This calibration check must be taken with caution, for several reasons:

- The corner reflector edge length is 0.95 m which is too small for L-band. The edge length of corner reflectors for calibration checks in L-band should be larger than 1.50 m.
- The corner reflectors put up at the test site had to be foldable. Due to the impassable terrain in the mountainous region it was not possible to put up large corner reflectors.
- Corner reflector signals may lie in regions of layover.
- The corner reflectors at the test site are subject to respective wind and weather conditions.

Hence, in the following figures and tables the results of the calibration check are presented for **C-band** only.

Corner reflector CR3W located in the upper part of Wörgetal and with orientation for Track 11 has been excluded from the analysis (see Table 4-2) because of unreliable RCS and co-polar phase estimates (see diagrams below). Very likely the backscatter of the local terrain superimposes with the signal from the CR.

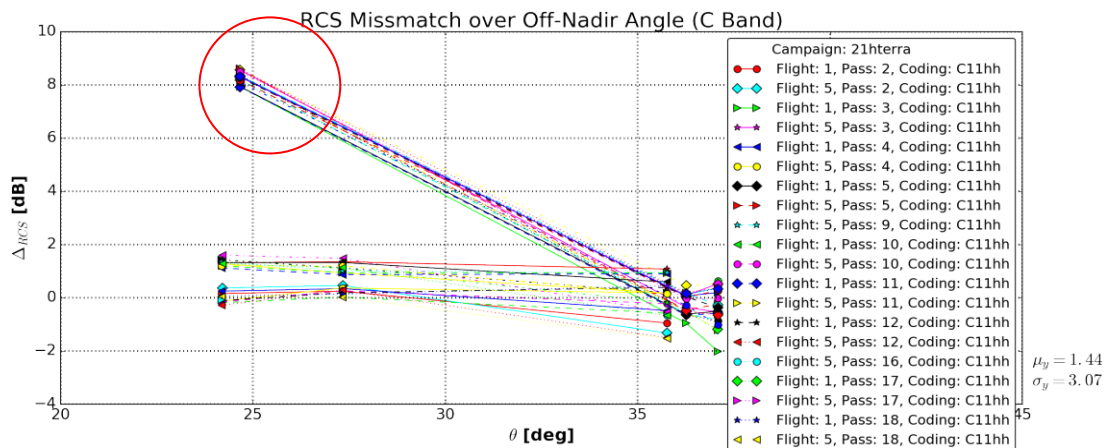


Figure 4-30: Radar Cross Section (RCS) deviations from nominal (zero), outliers produced by CR3W (red).

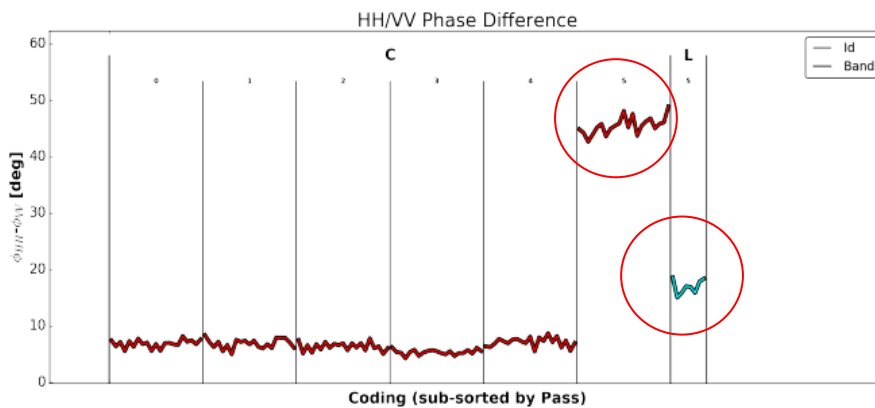


Figure 4-31: HH-VV phase difference deviations from nominal (zero), outliers produced by CR3W (red).

After exclusion of corner reflector CR3W, the corner reflector check yields to following diagrams in RCS values and phase differences between HH and VV polarization (see diagrams below). The typical noise floor of phase differences between HH and VV is at 5-7 degrees.

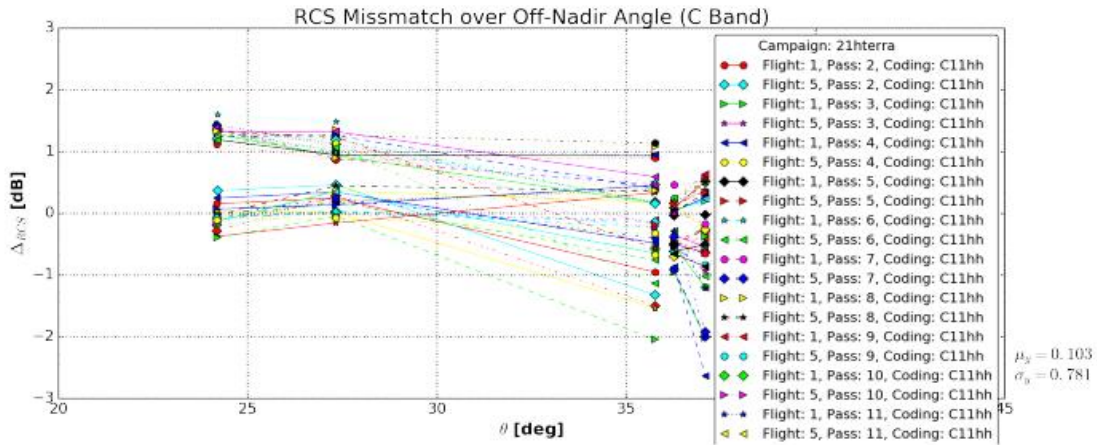


Figure 4-32: Radar Cross Section (RCS), C-band, mean value is 0.1 dB.

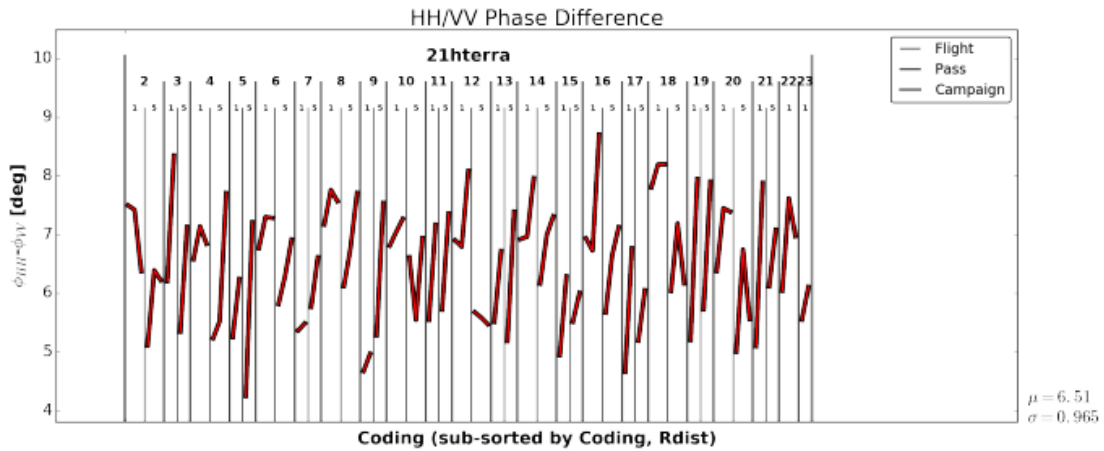


Figure 4-33: HH-VV phase difference, mean value is 6.5 degrees.

RCS mismatch (real RCS to theoretical RCS) should not appear higher than +/- 1 dB. We measure a mismatch which is a little bit higher than this tolerance. We assume it is caused by interactions with the local terrain.

Diagrams reporting the achieved azimuth and range position errors, as well as the achieved azimuth and range resolution are shown below.

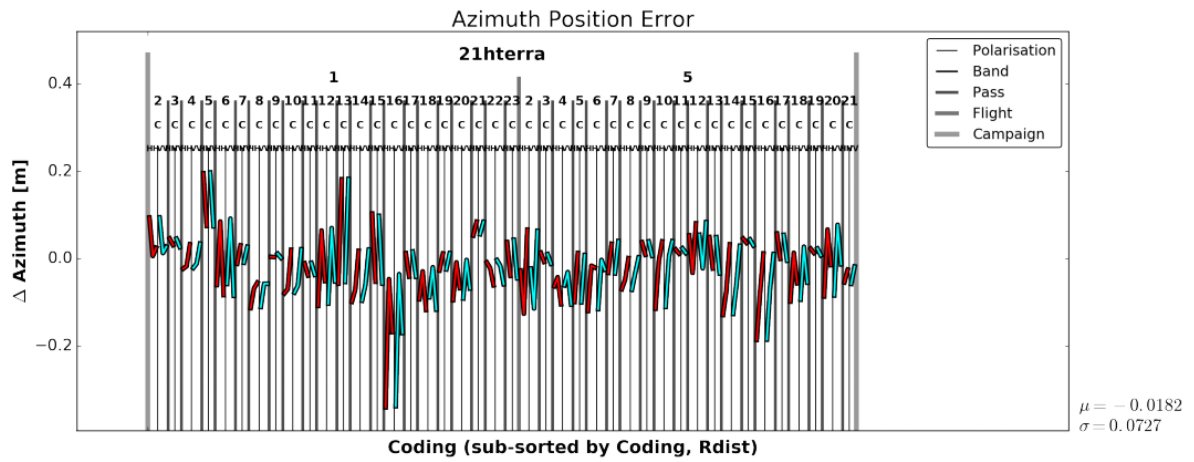


Figure 4-34: Azimuth position error, mean value is 0 m.

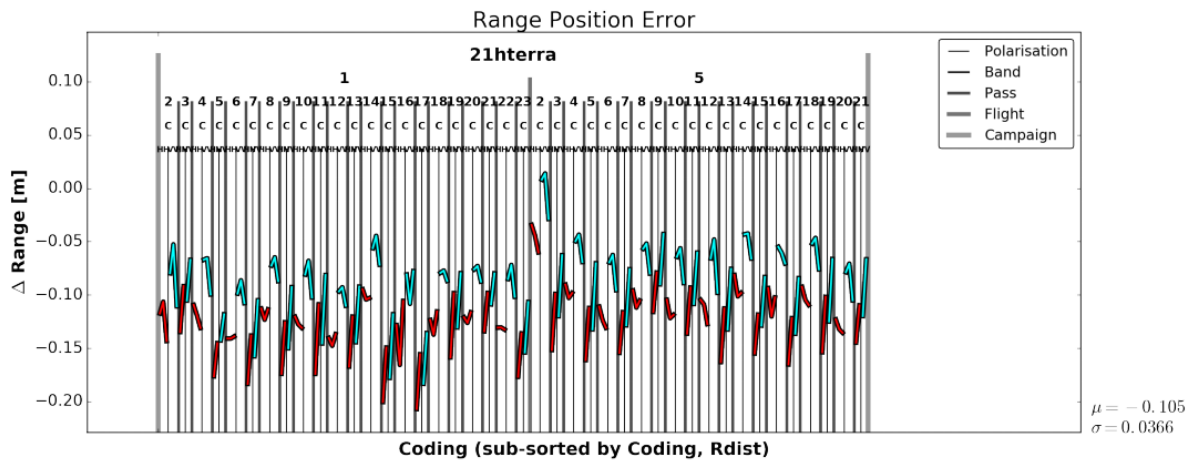


Figure 4-35: Range Position Error, minor differences between HH (red) and VV (blue).

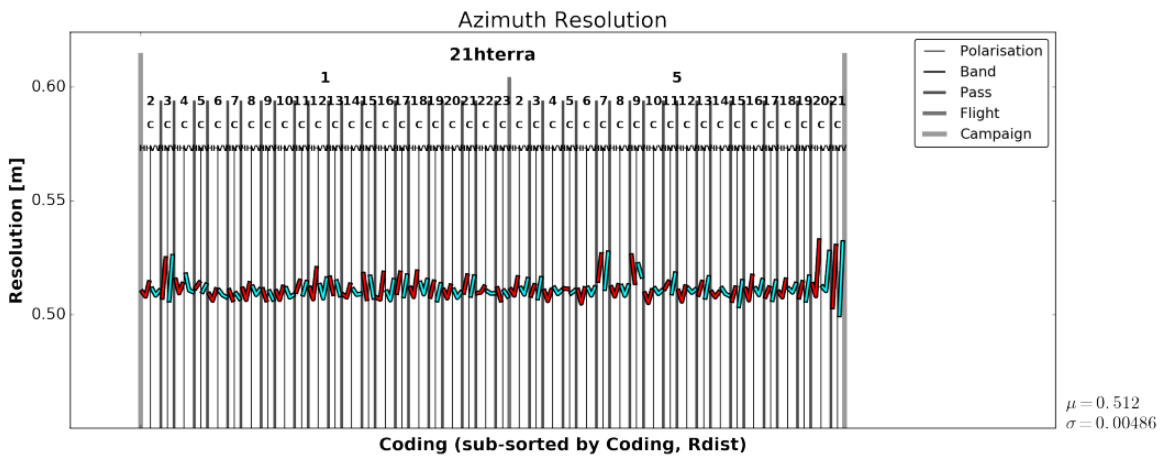


Figure 4-36: Azimuth resolution, mean value is 51.2 cm.

	<p>SARSimHT-NG – Simulation of Hydroterra SAR System Performance in the Mediterranean and the Alps Based on Experimental Airborne SAR Data</p> <p>D1: Data Acquisition Report of SWE Experiment</p>	<p>Doc.: DLR-HR-TR-SARSimHT-NG-01 Issue: 2.0 Date: 25.11.2021 Page: 59 of 110</p>
---	---	--

4.4 Inventory of Data Products

Below all RGI, GTC and INF products are listed according to their interferometric group membership (refer to Table 4-6). The **try number** indicates the membership to a group, the same number is part of the filename: T01, T02, T03, T04 and T08. We have **four groups** (T01-T04) and one group to combine all **eight flights** (T08) considering master passes only to keep the amount of resulting data manageable.

The following **rules** apply:

- RGI products (L- and C-band) are those of master passes,
- GTC products (L- and C-band) are created only for master passes,
- INF products are created with respect to master passes, L- and C-band separately.

4.4.1 Radar Geometry Image (RGI) Products

The following RGI products (master passes) are delivered.

No.	RGI Product	Group	Track	Band	Size
1	/mnt/HydroTerra/fsar_data/21HTERRA/FL01/PS02/T01/RGI	1	10	C, L	12G
2	/mnt/HydroTerra/fsar_data/21HTERRA/FL01/PS03/T01/RGI	1	11	C, L	12G
3	/mnt/HydroTerra/fsar_data/21HTERRA/FL02/PS02/T02/RGI	2	10	C, L	9.7G
4	/mnt/HydroTerra/fsar_data/21HTERRA/FL02/PS03/T02/RGI	2	11	C, L	9.6G
5	/mnt/HydroTerra/fsar_data/21HTERRA/FL03/PS02/T03/RGI	3	10	C, L	12G
6	/mnt/HydroTerra/fsar_data/21HTERRA/FL03/PS03/T03/RGI	3	11	C, L	9.6G
7	/mnt/HydroTerra/fsar_data/21HTERRA/FL06/PS02/T04/RGI	4	10	C, L	12G
8	/mnt/HydroTerra/fsar_data/21HTERRA/FL06/PS03/T04/RGI	4	11	C, L	9.6G
9	/mnt/HydroTerra/fsar_data/21HTERRA/FL01/PS02/T08/RGI	8	10	C, L	12G
10	/mnt/HydroTerra/fsar_data/21HTERRA/FL01/PS03/T08/RGI	8	11	C, L	9.6G

RGI products of slave passes are not delivered because they are in their own image geometry. Instead, they are resampled to the respective master image geometry resulting in the delivered INF products.

4.4.2 Geocoded and Terrain Corrected (GTC) Products

The following GTC products are delivered.

No.	GTC Product	Group	Track	Band	Size
1	/mnt/HydroTerra/fsar_data/21HTERRA/FL01/PS02/T01/GTC	1	10	C, L	4.1G
2	/mnt/HydroTerra/fsar_data/21HTERRA/FL01/PS03/T01/GTC	1	11	C, L	3.2G
3	/mnt/HydroTerra/fsar_data/21HTERRA/FL02/PS02/T02/GTC	2	10	C, L	3.1G
4	/mnt/HydroTerra/fsar_data/21HTERRA/FL02/PS03/T02/GTC	2	11	C, L	2.5G
5	/mnt/HydroTerra/fsar_data/21HTERRA/FL03/PS02/T03/GTC	3	10	C, L	3.2G
6	/mnt/HydroTerra/fsar_data/21HTERRA/FL03/PS03/T03/GTC	3	11	C, L	2.6G
7	/mnt/HydroTerra/fsar_data/21HTERRA/FL06/PS02/T04/GTC	4	10	C, L	3.2G
8	/mnt/HydroTerra/fsar_data/21HTERRA/FL06/PS03/T04/GTC	4	11	C, L	2.6G

	SARSimHT-NG – Simulation of Hydroterra SAR System Performance in the Mediterranean and the Alps Based on Experimental Airborne SAR Data	Doc.: DLR-HR-TR-SARSimHT-NG-01 Issue: 2.0 Date: 25.11.2021 Page: 60 of 110
	D1: Data Acquisition Report of SWE Experiment	

9	/mnt/HydroTerra/fsar_data/21HTERRA/FL01/PS02/T08/GTC	8	10	C, L	3.2G
10	/mnt/HydroTerra/fsar_data/21HTERRA/FL01/PS03/T08/GTC	8	11	C, L	2.6G

Only master passes are geocoded because slave passes have the same image geometry as master passes. The GTC products of master passes include a GTC-LUT component. **Look-up tables (LUT)**, which may be used to convert slave passes into geocoded geometry or, vice versa, to convert geocoded ground truth data into slant range geometry.

4.4.3 Interferometric (INF) Products

The following INF products are delivered.

No.	INF Product - Group 01, Flight 01	Group	Track	Band	Size
1	/mnt/HydroTerra/fsar_data/21HTERRA/FL01/PS02/T01/INF_stack10C	1	10	C	211M
2	/mnt/HydroTerra/fsar_data/21HTERRA/FL01/PS02/T01/INF_stack10L	1	10	L	208M
3	/mnt/HydroTerra/fsar_data/21HTERRA/FL01/PS03/T01/INF_stack11C	1	11	C	177M
4	/mnt/HydroTerra/fsar_data/21HTERRA/FL01/PS03/T01/INF_stack11L	1	11	L	169M
5	/mnt/HydroTerra/fsar_data/21HTERRA/FL01/PS04/T01/INF_stack10C	1	10	C	16G
6	/mnt/HydroTerra/fsar_data/21HTERRA/FL01/PS04/T01/INF_stack10L	1	10	L	3.8G
7	/mnt/HydroTerra/fsar_data/21HTERRA/FL01/PS05/T01/INF_stack11C	1	11	C	13G
8	/mnt/HydroTerra/fsar_data/21HTERRA/FL01/PS05/T01/INF_stack11L	1	11	L	3.1G
9	/mnt/HydroTerra/fsar_data/21HTERRA/FL01/PS06/T01/INF_stack10C	1	10	C	16G
10	/mnt/HydroTerra/fsar_data/21HTERRA/FL01/PS06/T01/INF_stack10L	1	10	L	3.8G
11	/mnt/HydroTerra/fsar_data/21HTERRA/FL01/PS07/T01/INF_stack11C	1	11	C	13G
12	/mnt/HydroTerra/fsar_data/21HTERRA/FL01/PS07/T01/INF_stack11L	1	11	L	3.1G
13	/mnt/HydroTerra/fsar_data/21HTERRA/FL01/PS08/T01/INF_stack10C	1	10	C	16G
14	/mnt/HydroTerra/fsar_data/21HTERRA/FL01/PS08/T01/INF_stack10L	1	10	L	3.8G
15	/mnt/HydroTerra/fsar_data/21HTERRA/FL01/PS09/T01/INF_stack11C	1	11	C	13G
16	/mnt/HydroTerra/fsar_data/21HTERRA/FL01/PS09/T01/INF_stack11L	1	11	L	3.2G
17	/mnt/HydroTerra/fsar_data/21HTERRA/FL01/PS10/T01/INF_stack10C	1	10	C	16G
18	/mnt/HydroTerra/fsar_data/21HTERRA/FL01/PS10/T01/INF_stack10L	1	10	L	3.8G
19	/mnt/HydroTerra/fsar_data/21HTERRA/FL01/PS11/T01/INF_stack11C	1	11	C	13G
20	/mnt/HydroTerra/fsar_data/21HTERRA/FL01/PS11/T01/INF_stack11L	1	11	L	3.2G
21	/mnt/HydroTerra/fsar_data/21HTERRA/FL01/PS12/T01/INF_stack10C	1	10	C	16G
22	/mnt/HydroTerra/fsar_data/21HTERRA/FL01/PS12/T01/INF_stack10L	1	10	L	3.8G
23	/mnt/HydroTerra/fsar_data/21HTERRA/FL01/PS13/T01/INF_stack11C	1	11	C	13G
24	/mnt/HydroTerra/fsar_data/21HTERRA/FL01/PS13/T01/INF_stack11L	1	11	L	3.1G
25	/mnt/HydroTerra/fsar_data/21HTERRA/FL01/PS14/T01/INF_stack10C	1	10	C	16G
26	/mnt/HydroTerra/fsar_data/21HTERRA/FL01/PS14/T01/INF_stack10L	1	10	L	3.8G
27	/mnt/HydroTerra/fsar_data/21HTERRA/FL01/PS15/T01/INF_stack11C	1	11	C	13G
28	/mnt/HydroTerra/fsar_data/21HTERRA/FL01/PS15/T01/INF_stack11L	1	11	L	3.2G

	<p>SARSimHT-NG – Simulation of Hydroterra SAR System Performance in the Mediterranean and the Alps Based on Experimental Airborne SAR Data</p> <p>D1: Data Acquisition Report of SWE Experiment</p>	<p>Doc.: DLR-HR-TR-SARSimHT-NG-01 Issue: 2.0 Date: 25.11.2021 Page: 61 of 110</p>
---	---	--

29	/mnt/HydroTerra/fsar_data/21HTERRA/FL01/PS16/T01/INF_stack10C	1	10	C	16G
30	/mnt/HydroTerra/fsar_data/21HTERRA/FL01/PS16/T01/INF_stack10L	1	10	L	3.8G
31	/mnt/HydroTerra/fsar_data/21HTERRA/FL01/PS17/T01/INF_stack11C	1	11	C	13G
32	/mnt/HydroTerra/fsar_data/21HTERRA/FL01/PS17/T01/INF_stack11L	1	11	L	3.1G
33	/mnt/HydroTerra/fsar_data/21HTERRA/FL01/PS18/T01/INF_stack10C	1	10	C	16G
34	/mnt/HydroTerra/fsar_data/21HTERRA/FL01/PS18/T01/INF_stack10L	1	10	L	3.8G
35	/mnt/HydroTerra/fsar_data/21HTERRA/FL01/PS19/T01/INF_stack11C	1	11	C	13G
36	/mnt/HydroTerra/fsar_data/21HTERRA/FL01/PS19/T01/INF_stack11L	1	11	L	3.1G
37	/mnt/HydroTerra/fsar_data/21HTERRA/FL01/PS20/T01/INF_stack10C	1	10	C	16G
38	/mnt/HydroTerra/fsar_data/21HTERRA/FL01/PS20/T01/INF_stack10L	1	10	L	3.8G
39	/mnt/HydroTerra/fsar_data/21HTERRA/FL01/PS21/T01/INF_stack11C	1	11	C	13G
40	/mnt/HydroTerra/fsar_data/21HTERRA/FL01/PS21/T01/INF_stack11L	1	11	L	3.1G
41	/mnt/HydroTerra/fsar_data/21HTERRA/FL01/PS22/T01/INF_stack10C	1	10	C	16G
42	/mnt/HydroTerra/fsar_data/21HTERRA/FL01/PS22/T01/INF_stack10L	1	10	L	3.8G
43	/mnt/HydroTerra/fsar_data/21HTERRA/FL01/PS23/T01/INF_stack11C	1	11	C	13G
44	/mnt/HydroTerra/fsar_data/21HTERRA/FL01/PS23/T01/INF_stack11L	1	11	L	3.2G

No.	INF Product - Group 01, Flight 05	Group	Track	Band	Size
1	/mnt/HydroTerra/fsar_data/21HTERRA/FL05/PS02/T01/INF_stack10C	1	10	C	16G
2	/mnt/HydroTerra/fsar_data/21HTERRA/FL05/PS02/T01/INF_stack10L	1	10	L	3.8G
3	/mnt/HydroTerra/fsar_data/21HTERRA/FL05/PS03/T01/INF_stack11C	1	11	C	13G
4	/mnt/HydroTerra/fsar_data/21HTERRA/FL05/PS03/T01/INF_stack11L	1	11	L	3.2G
5	/mnt/HydroTerra/fsar_data/21HTERRA/FL05/PS04/T01/INF_stack10C	1	10	C	16G
6	/mnt/HydroTerra/fsar_data/21HTERRA/FL05/PS04/T01/INF_stack10L	1	10	L	3.8G
7	/mnt/HydroTerra/fsar_data/21HTERRA/FL05/PS05/T01/INF_stack11C	1	11	C	13G
8	/mnt/HydroTerra/fsar_data/21HTERRA/FL05/PS05/T01/INF_stack11L	1	11	L	3.2G
9	/mnt/HydroTerra/fsar_data/21HTERRA/FL05/PS06/T01/INF_stack10C	1	10	C	16G
10	/mnt/HydroTerra/fsar_data/21HTERRA/FL05/PS06/T01/INF_stack10L	1	10	L	3.8G
11	/mnt/HydroTerra/fsar_data/21HTERRA/FL05/PS07/T01/INF_stack11C	1	11	C	13G
12	/mnt/HydroTerra/fsar_data/21HTERRA/FL05/PS07/T01/INF_stack11L	1	11	L	3.2G
13	/mnt/HydroTerra/fsar_data/21HTERRA/FL05/PS08/T01/INF_stack10C	1	10	C	16G
14	/mnt/HydroTerra/fsar_data/21HTERRA/FL05/PS08/T01/INF_stack10L	1	10	L	3.8G
15	/mnt/HydroTerra/fsar_data/21HTERRA/FL05/PS09/T01/INF_stack11C	1	11	C	13G
16	/mnt/HydroTerra/fsar_data/21HTERRA/FL05/PS09/T01/INF_stack11L	1	11	L	3.2G
17	/mnt/HydroTerra/fsar_data/21HTERRA/FL05/PS10/T01/INF_stack10C	1	10	C	16G
18	/mnt/HydroTerra/fsar_data/21HTERRA/FL05/PS10/T01/INF_stack10L	1	10	L	3.8G
19	/mnt/HydroTerra/fsar_data/21HTERRA/FL05/PS11/T01/INF_stack11C	1	11	C	13G
20	/mnt/HydroTerra/fsar_data/21HTERRA/FL05/PS11/T01/INF_stack11L	1	11	L	3.2G
21	/mnt/HydroTerra/fsar_data/21HTERRA/FL05/PS12/T01/INF_stack10C	1	10	C	16G
22	/mnt/HydroTerra/fsar_data/21HTERRA/FL05/PS12/T01/INF_stack10L	1	10	L	3.8G



SARSimHT-NG – Simulation of Hydroterra SAR System Performance in the Mediterranean and the Alps Based on Experimental Airborne SAR Data

D1: Data Acquisition Report of SWE Experiment

Doc.: DLR-HR-TR-SARSimHT-NG-01
 Issue: 2.0
 Date: 25.11.2021
 Page: 62 of 110

23	/mnt/HydroTerra/fsar_data/21HTERRA/FL05/PS13/T01/INF_stack11C	1	11	C	13G
24	/mnt/HydroTerra/fsar_data/21HTERRA/FL05/PS13/T01/INF_stack11L	1	11	L	3.2G
25	/mnt/HydroTerra/fsar_data/21HTERRA/FL05/PS14/T01/INF_stack10C	1	10	C	16G
26	/mnt/HydroTerra/fsar_data/21HTERRA/FL05/PS14/T01/INF_stack10L	1	10	L	3.8G
27	/mnt/HydroTerra/fsar_data/21HTERRA/FL05/PS15/T01/INF_stack11C	1	11	C	13G
28	/mnt/HydroTerra/fsar_data/21HTERRA/FL05/PS15/T01/INF_stack11L	1	11	L	3.2G
29	/mnt/HydroTerra/fsar_data/21HTERRA/FL05/PS16/T01/INF_stack10C	1	10	C	16G
30	/mnt/HydroTerra/fsar_data/21HTERRA/FL05/PS16/T01/INF_stack10L	1	10	L	3.8G
31	/mnt/HydroTerra/fsar_data/21HTERRA/FL05/PS17/T01/INF_stack11C	1	11	C	13G
32	/mnt/HydroTerra/fsar_data/21HTERRA/FL05/PS17/T01/INF_stack11L	1	11	L	3.2G
33	/mnt/HydroTerra/fsar_data/21HTERRA/FL05/PS18/T01/INF_stack10C	1	10	C	16G
34	/mnt/HydroTerra/fsar_data/21HTERRA/FL05/PS18/T01/INF_stack10L	1	10	L	3.8G
35	/mnt/HydroTerra/fsar_data/21HTERRA/FL05/PS19/T01/INF_stack11C	1	11	C	13G
36	/mnt/HydroTerra/fsar_data/21HTERRA/FL05/PS19/T01/INF_stack11L	1	11	L	3.2G
37	/mnt/HydroTerra/fsar_data/21HTERRA/FL05/PS20/T01/INF_stack10C	1	10	C	16G
38	/mnt/HydroTerra/fsar_data/21HTERRA/FL05/PS20/T01/INF_stack10L	1	10	L	3.8G
39	/mnt/HydroTerra/fsar_data/21HTERRA/FL05/PS21/T01/INF_stack11C	1	11	C	13G
40	/mnt/HydroTerra/fsar_data/21HTERRA/FL05/PS21/T01/INF_stack11L	1	11	L	3.2G

No.	INF Product - Group 02, Flight 02	Group	Track	Band	Size
1	/mnt/HydroTerra/fsar_data/21HTERRA/FL02/PS02/T02/INF_stack10C	2	10	C	211M
2	/mnt/HydroTerra/fsar_data/21HTERRA/FL02/PS02/T02/INF_stack10L	2	10	L	202M
3	/mnt/HydroTerra/fsar_data/21HTERRA/FL02/PS03/T02/INF_stack11C	2	11	C	176M
4	/mnt/HydroTerra/fsar_data/21HTERRA/FL02/PS03/T02/INF_stack11L	2	11	L	169M
5	/mnt/HydroTerra/fsar_data/21HTERRA/FL02/PS04/T02/INF_stack10C	2	10	C	16G
6	/mnt/HydroTerra/fsar_data/21HTERRA/FL02/PS04/T02/INF_stack10L	2	10	L	3.8G
7	/mnt/HydroTerra/fsar_data/21HTERRA/FL02/PS05/T02/INF_stack11C	2	11	C	13G
8	/mnt/HydroTerra/fsar_data/21HTERRA/FL02/PS05/T02/INF_stack11L	2	11	L	3.1G
9	/mnt/HydroTerra/fsar_data/21HTERRA/FL02/PS06/T02/INF_stack10C	2	10	C	16G
10	/mnt/HydroTerra/fsar_data/21HTERRA/FL02/PS06/T02/INF_stack10L	2	10	L	3.8G
11	/mnt/HydroTerra/fsar_data/21HTERRA/FL02/PS07/T02/INF_stack11C	2	11	C	13G
12	/mnt/HydroTerra/fsar_data/21HTERRA/FL02/PS07/T02/INF_stack11L	2	11	L	3.1G
13	/mnt/HydroTerra/fsar_data/21HTERRA/FL02/PS08/T02/INF_stack10C	2	10	C	16G
14	/mnt/HydroTerra/fsar_data/21HTERRA/FL02/PS08/T02/INF_stack10L	2	10	L	3.8G
15	/mnt/HydroTerra/fsar_data/21HTERRA/FL02/PS09/T02/INF_stack11C	2	11	C	13G
16	/mnt/HydroTerra/fsar_data/21HTERRA/FL02/PS09/T02/INF_stack11L	2	11	L	3.1G
17	/mnt/HydroTerra/fsar_data/21HTERRA/FL02/PS10/T02/INF_stack10C	2	10	C	16G
18	/mnt/HydroTerra/fsar_data/21HTERRA/FL02/PS10/T02/INF_stack10L	2	10	L	3.8G
19	/mnt/HydroTerra/fsar_data/21HTERRA/FL02/PS11/T02/INF_stack11C	2	11	C	13G
20	/mnt/HydroTerra/fsar_data/21HTERRA/FL02/PS11/T02/INF_stack11L	2	11	L	3.1G

	<p>SARSimHT-NG – Simulation of Hydroterra SAR System Performance in the Mediterranean and the Alps Based on Experimental Airborne SAR Data</p> <p>D1: Data Acquisition Report of SWE Experiment</p>	<p>Doc.: DLR-HR-TR-SARSimHT-NG-01 Issue: 2.0 Date: 25.11.2021 Page: 63 of 110</p>
---	---	--

21	/mnt/HydroTerra/fsar_data/21HTERRA/FL02/PS12/T02/INF_stack10C	2	10	C	16G
22	/mnt/HydroTerra/fsar_data/21HTERRA/FL02/PS12/T02/INF_stack10L	2	10	L	3.8G
23	/mnt/HydroTerra/fsar_data/21HTERRA/FL02/PS13/T02/INF_stack11C	2	11	C	13G
24	/mnt/HydroTerra/fsar_data/21HTERRA/FL02/PS13/T02/INF_stack11L	2	11	L	3.1G
25	/mnt/HydroTerra/fsar_data/21HTERRA/FL02/PS14/T02/INF_stack10C	2	10	C	16G
26	/mnt/HydroTerra/fsar_data/21HTERRA/FL02/PS14/T02/INF_stack10L	2	10	L	3.8G
27	/mnt/HydroTerra/fsar_data/21HTERRA/FL02/PS15/T02/INF_stack11C	2	11	C	13G
28	/mnt/HydroTerra/fsar_data/21HTERRA/FL02/PS15/T02/INF_stack11L	2	11	L	3.1G
29	/mnt/HydroTerra/fsar_data/21HTERRA/FL02/PS16/T02/INF_stack10C	2	10	C	16G
30	/mnt/HydroTerra/fsar_data/21HTERRA/FL02/PS16/T02/INF_stack10L	2	10	L	3.8G
31	/mnt/HydroTerra/fsar_data/21HTERRA/FL02/PS17/T02/INF_stack11C	2	11	C	13G
32	/mnt/HydroTerra/fsar_data/21HTERRA/FL02/PS17/T02/INF_stack11L	2	11	L	3.1G
33	/mnt/HydroTerra/fsar_data/21HTERRA/FL02/PS18/T02/INF_stack10C	2	10	C	16G
34	/mnt/HydroTerra/fsar_data/21HTERRA/FL02/PS18/T02/INF_stack10L	2	10	L	3.8G
35	/mnt/HydroTerra/fsar_data/21HTERRA/FL02/PS19/T02/INF_stack11C	2	11	C	13G
36	/mnt/HydroTerra/fsar_data/21HTERRA/FL02/PS19/T02/INF_stack11L	2	11	L	3.1G
37	/mnt/HydroTerra/fsar_data/21HTERRA/FL02/PS20/T02/INF_stack10C	2	10	C	16G
38	/mnt/HydroTerra/fsar_data/21HTERRA/FL02/PS20/T02/INF_stack10L	2	10	L	3.8G
39	/mnt/HydroTerra/fsar_data/21HTERRA/FL02/PS21/T02/INF_stack11C	2	11	C	13G
40	/mnt/HydroTerra/fsar_data/21HTERRA/FL02/PS21/T02/INF_stack11L	2	11	L	3.1G
41	/mnt/HydroTerra/fsar_data/21HTERRA/FL02/PS22/T02/INF_stack10C	2	10	C	16G
42	/mnt/HydroTerra/fsar_data/21HTERRA/FL02/PS22/T02/INF_stack10L	2	10	L	3.8G
43	/mnt/HydroTerra/fsar_data/21HTERRA/FL02/PS23/T02/INF_stack11C	2	11	C	13G
44	/mnt/HydroTerra/fsar_data/21HTERRA/FL02/PS23/T02/INF_stack11L	2	11	L	3.1G

No.	INF Product - Group 02, Flight 08	Group	Track	Band	Size
1	/mnt/HydroTerra/fsar_data/21HTERRA/FL08/PS02/T02/INF_stack10C	2	10	C	16G
2	/mnt/HydroTerra/fsar_data/21HTERRA/FL08/PS02/T02/INF_stack10L	2	10	L	3.8G
3	/mnt/HydroTerra/fsar_data/21HTERRA/FL08/PS03/T02/INF_stack11C	2	11	C	13G
4	/mnt/HydroTerra/fsar_data/21HTERRA/FL08/PS03/T02/INF_stack11L	2	11	L	3.2G
5	/mnt/HydroTerra/fsar_data/21HTERRA/FL08/PS04/T02/INF_stack10C	2	10	C	16G
6	/mnt/HydroTerra/fsar_data/21HTERRA/FL08/PS04/T02/INF_stack10L	2	10	L	3.8G
7	/mnt/HydroTerra/fsar_data/21HTERRA/FL08/PS05/T02/INF_stack11C	2	11	C	13G
8	/mnt/HydroTerra/fsar_data/21HTERRA/FL08/PS05/T02/INF_stack11L	2	11	L	3.2G
9	/mnt/HydroTerra/fsar_data/21HTERRA/FL08/PS06/T02/INF_stack10C	2	10	C	16G
10	/mnt/HydroTerra/fsar_data/21HTERRA/FL08/PS06/T02/INF_stack10L	2	10	L	3.8G
11	/mnt/HydroTerra/fsar_data/21HTERRA/FL08/PS07/T02/INF_stack11C	2	11	C	13G
12	/mnt/HydroTerra/fsar_data/21HTERRA/FL08/PS07/T02/INF_stack11L	2	11	L	3.2G

No.	INF Product - Group 03, Flight 03	Group	Track	Band	Size
-----	-----------------------------------	-------	-------	------	------



SARSimHT-NG – Simulation of Hydroterra SAR System Performance in the Mediterranean and the Alps Based on Experimental Airborne SAR Data

D1: Data Acquisition Report of SWE Experiment

Doc.: DLR-HR-TR-SARSimHT-NG-01
Issue: 2.0
Date: 25.11.2021
Page: 64 of 110

1	/mnt/HydroTerra/fsar_data/21HTERRA/FL03/PS02/T03/INF_stack10C	3	10	C	211M
2	/mnt/HydroTerra/fsar_data/21HTERRA/FL03/PS02/T03/INF_stack10L	3	10	L	202M
3	/mnt/HydroTerra/fsar_data/21HTERRA/FL03/PS03/T03/INF_stack11C	3	11	C	174M
4	/mnt/HydroTerra/fsar_data/21HTERRA/FL03/PS03/T03/INF_stack11L	3	11	L	167M
5	/mnt/HydroTerra/fsar_data/21HTERRA/FL03/PS04/T03/INF_stack10C	3	10	C	16G
6	/mnt/HydroTerra/fsar_data/21HTERRA/FL03/PS04/T03/INF_stack10L	3	10	L	3.8G
7	/mnt/HydroTerra/fsar_data/21HTERRA/FL03/PS05/T03/INF_stack11C	3	11	C	13G
8	/mnt/HydroTerra/fsar_data/21HTERRA/FL03/PS05/T03/INF_stack11L	3	11	L	3.2G
9	/mnt/HydroTerra/fsar_data/21HTERRA/FL03/PS06/T03/INF_stack10C	3	10	C	16G
10	/mnt/HydroTerra/fsar_data/21HTERRA/FL03/PS06/T03/INF_stack10L	3	10	L	3.8G
11	/mnt/HydroTerra/fsar_data/21HTERRA/FL03/PS07/T03/INF_stack11C	3	11	C	13G
12	/mnt/HydroTerra/fsar_data/21HTERRA/FL03/PS07/T03/INF_stack11L	3	11	L	3.2G
13	/mnt/HydroTerra/fsar_data/21HTERRA/FL03/PS08/T03/INF_stack10C	3	10	C	16G
14	/mnt/HydroTerra/fsar_data/21HTERRA/FL03/PS08/T03/INF_stack10L	3	10	L	3.8G
15	/mnt/HydroTerra/fsar_data/21HTERRA/FL03/PS09/T03/INF_stack11C	3	11	C	13G
16	/mnt/HydroTerra/fsar_data/21HTERRA/FL03/PS09/T03/INF_stack11L	3	11	L	3.2G
17	/mnt/HydroTerra/fsar_data/21HTERRA/FL03/PS10/T03/INF_stack10C	3	10	C	16G
18	/mnt/HydroTerra/fsar_data/21HTERRA/FL03/PS10/T03/INF_stack10L	3	10	L	3.8G
19	/mnt/HydroTerra/fsar_data/21HTERRA/FL03/PS11/T03/INF_stack11C	3	11	C	13G
20	/mnt/HydroTerra/fsar_data/21HTERRA/FL03/PS11/T03/INF_stack11L	3	11	L	3.1G
21	/mnt/HydroTerra/fsar_data/21HTERRA/FL03/PS12/T03/INF_stack10C	3	10	C	16G
22	/mnt/HydroTerra/fsar_data/21HTERRA/FL03/PS12/T03/INF_stack10L	3	10	L	3.8G
23	/mnt/HydroTerra/fsar_data/21HTERRA/FL03/PS13/T03/INF_stack11C	3	11	C	13G
24	/mnt/HydroTerra/fsar_data/21HTERRA/FL03/PS13/T03/INF_stack11L	3	11	L	3.2G
25	/mnt/HydroTerra/fsar_data/21HTERRA/FL03/PS14/T03/INF_stack10C	3	10	C	16G
26	/mnt/HydroTerra/fsar_data/21HTERRA/FL03/PS14/T03/INF_stack10L	3	10	L	3.8G
27	/mnt/HydroTerra/fsar_data/21HTERRA/FL03/PS15/T03/INF_stack11C	3	11	C	13G
28	/mnt/HydroTerra/fsar_data/21HTERRA/FL03/PS15/T03/INF_stack11L	3	11	L	3.2G
29	/mnt/HydroTerra/fsar_data/21HTERRA/FL03/PS16/T03/INF_stack10C	3	10	C	16G
30	/mnt/HydroTerra/fsar_data/21HTERRA/FL03/PS16/T03/INF_stack10L	3	10	L	3.8G
31	/mnt/HydroTerra/fsar_data/21HTERRA/FL03/PS17/T03/INF_stack11C	3	11	C	13G
32	/mnt/HydroTerra/fsar_data/21HTERRA/FL03/PS17/T03/INF_stack11L	3	11	L	3.2G
33	/mnt/HydroTerra/fsar_data/21HTERRA/FL03/PS18/T03/INF_stack10C	3	10	C	16G
34	/mnt/HydroTerra/fsar_data/21HTERRA/FL03/PS18/T03/INF_stack10L	3	10	L	3.8G
35	/mnt/HydroTerra/fsar_data/21HTERRA/FL03/PS19/T03/INF_stack11C	3	11	C	13G
36	/mnt/HydroTerra/fsar_data/21HTERRA/FL03/PS19/T03/INF_stack11L	3	11	L	3.2G
37	/mnt/HydroTerra/fsar_data/21HTERRA/FL03/PS20/T03/INF_stack10C	3	10	C	16G
38	/mnt/HydroTerra/fsar_data/21HTERRA/FL03/PS20/T03/INF_stack10L	3	10	L	3.8G
39	/mnt/HydroTerra/fsar_data/21HTERRA/FL03/PS21/T03/INF_stack11C	3	11	C	13G
40	/mnt/HydroTerra/fsar_data/21HTERRA/FL03/PS21/T03/INF_stack11L	3	11	L	3.1G

	SARSimHT-NG – Simulation of Hydroterra SAR System Performance in the Mediterranean and the Alps Based on Experimental Airborne SAR Data	Doc.: DLR-HR-TR-SARSimHT-NG-01 Issue: 2.0 Date: 25.11.2021 Page: 65 of 110
	D1: Data Acquisition Report of SWE Experiment	

41	/mnt/HydroTerra/fsar_data/21HTERRA/FL03/PS22/T03/INF_stack11C	3	11	C	13G
42	/mnt/HydroTerra/fsar_data/21HTERRA/FL03/PS22/T03/INF_stack11L	3	11	L	3.2G
43	/mnt/HydroTerra/fsar_data/21HTERRA/FL03/PS23/T03/INF_stack11C	3	11	C	13G
44	/mnt/HydroTerra/fsar_data/21HTERRA/FL03/PS23/T03/INF_stack11L	3	11	L	3.2G
45	/mnt/HydroTerra/fsar_data/21HTERRA/FL03/PS24/T03/INF_stack11C	3	11	C	13G
46	/mnt/HydroTerra/fsar_data/21HTERRA/FL03/PS24/T03/INF_stack11L	3	11	L	3.2G

Bold face numbers indicate an **irregularity** compared to rows before and after.

Pass **0323** is an aborted pass (row 43, 44), in the reprocessing below we have excluded this pass.

No.	INF Product - Group 03, Flight 04	Group	Track	Band	Size
1	/mnt/HydroTerra/fsar_data/21HTERRA/FL04/PS02/T03/INF_stack10C	3	10	C	31G
2	/mnt/HydroTerra/fsar_data/21HTERRA/FL04/PS02/T03/INF_stack10L	3	10	L	3.8G
3	/mnt/HydroTerra/fsar_data/21HTERRA/FL04/PS03/T03/INF_stack11C	3	11	C	13G
4	/mnt/HydroTerra/fsar_data/21HTERRA/FL04/PS03/T03/INF_stack11L	3	11	L	3.2G
5	/mnt/HydroTerra/fsar_data/21HTERRA/FL04/PS04/T03/INF_stack10C	3	10	C	16G
6	/mnt/HydroTerra/fsar_data/21HTERRA/FL04/PS04/T03/INF_stack10L	3	10	L	3.8G
7	/mnt/HydroTerra/fsar_data/21HTERRA/FL04/PS05/T03/INF_stack11C	3	11	C	13G
8	/mnt/HydroTerra/fsar_data/21HTERRA/FL04/PS05/T03/INF_stack11L	3	11	L	3.2G
9	/mnt/HydroTerra/fsar_data/21HTERRA/FL04/PS06/T03/INF_stack10C	3	10	C	16G
10	/mnt/HydroTerra/fsar_data/21HTERRA/FL04/PS06/T03/INF_stack10L	3	10	L	3.8G
11	/mnt/HydroTerra/fsar_data/21HTERRA/FL04/PS07/T03/INF_stack11C	3	11	C	13G
12	/mnt/HydroTerra/fsar_data/21HTERRA/FL04/PS07/T03/INF_stack11L	3	11	L	3.2G
13	/mnt/HydroTerra/fsar_data/21HTERRA/FL04/PS08/T03/INF_stack10C	3	10	C	16G
14	/mnt/HydroTerra/fsar_data/21HTERRA/FL04/PS08/T03/INF_stack10L	3	10	L	3.8G
15	/mnt/HydroTerra/fsar_data/21HTERRA/FL04/PS09/T03/INF_stack11C	3	11	C	13G
16	/mnt/HydroTerra/fsar_data/21HTERRA/FL04/PS09/T03/INF_stack11L	3	11	L	3.2G
17	/mnt/HydroTerra/fsar_data/21HTERRA/FL04/PS10/T03/INF_stack10C	3	10	C	16G
18	/mnt/HydroTerra/fsar_data/21HTERRA/FL04/PS10/T03/INF_stack10L	3	10	L	3.8G
19	/mnt/HydroTerra/fsar_data/21HTERRA/FL04/PS11/T03/INF_stack11C	3	11	C	13G
20	/mnt/HydroTerra/fsar_data/21HTERRA/FL04/PS11/T03/INF_stack11L	3	11	L	3.2G
21	/mnt/HydroTerra/fsar_data/21HTERRA/FL04/PS12/T03/INF_stack10C	3	10	C	16G
22	/mnt/HydroTerra/fsar_data/21HTERRA/FL04/PS12/T03/INF_stack10L	3	10	L	3.8G
23	/mnt/HydroTerra/fsar_data/21HTERRA/FL04/PS13/T03/INF_stack11C	3	11	C	13G
24	/mnt/HydroTerra/fsar_data/21HTERRA/FL04/PS13/T03/INF_stack11L	3	11	L	3.2G

Pass **0409** (rows 15, 16) showed bad performance, in the reprocessing below this pass is excluded.

No.	INF Product - Group 04, Flight 06	Group	Track	Band	Size
1	/mnt/HydroTerra/fsar_data/21HTERRA/FL06/PS02/T04/INF_stack10C	4	10	C	210M



SARSimHT-NG – Simulation of Hydroterra SAR System Performance in the Mediterranean and the Alps Based on Experimental Airborne SAR Data

D1: Data Acquisition Report of SWE Experiment

Doc.: DLR-HR-TR-SARSimHT-NG-01
 Issue: 2.0
 Date: 25.11.2021
 Page: 66 of 110

2	/mnt/HydroTerra/fsar_data/21HTERRA/FL06/PS02/T04/INF_stack10L	4	10	L	202M
3	/mnt/HydroTerra/fsar_data/21HTERRA/FL06/PS03/T04/INF_stack11C	4	11	C	176M
4	/mnt/HydroTerra/fsar_data/21HTERRA/FL06/PS03/T04/INF_stack11L	4	11	L	169M
5	/mnt/HydroTerra/fsar_data/21HTERRA/FL06/PS04/T04/INF_stack10C	4	10	C	16G
6	/mnt/HydroTerra/fsar_data/21HTERRA/FL06/PS04/T04/INF_stack10L	4	10	L	3.8G
7	/mnt/HydroTerra/fsar_data/21HTERRA/FL06/PS05/T04/INF_stack11C	4	11	C	13G
8	/mnt/HydroTerra/fsar_data/21HTERRA/FL06/PS05/T04/INF_stack11L	4	11	L	3.1G
9	/mnt/HydroTerra/fsar_data/21HTERRA/FL06/PS06/T04/INF_stack10C	4	10	C	16G
10	/mnt/HydroTerra/fsar_data/21HTERRA/FL06/PS06/T04/INF_stack10L	4	10	L	3.8G
11	/mnt/HydroTerra/fsar_data/21HTERRA/FL06/PS07/T04/INF_stack11C	4	11	C	13G
12	/mnt/HydroTerra/fsar_data/21HTERRA/FL06/PS07/T04/INF_stack11L	4	11	L	3.1G
13	/mnt/HydroTerra/fsar_data/21HTERRA/FL06/PS08/T04/INF_stack10C	4	10	C	16G
14	/mnt/HydroTerra/fsar_data/21HTERRA/FL06/PS08/T04/INF_stack10L	4	10	L	3.8G
15	/mnt/HydroTerra/fsar_data/21HTERRA/FL06/PS09/T04/INF_stack11C	4	11	C	13G
16	/mnt/HydroTerra/fsar_data/21HTERRA/FL06/PS09/T04/INF_stack11L	4	11	L	3.1G
17	/mnt/HydroTerra/fsar_data/21HTERRA/FL06/PS10/T04/INF_stack10C	4	10	C	16G
18	/mnt/HydroTerra/fsar_data/21HTERRA/FL06/PS10/T04/INF_stack10L	4	10	L	3.8G
19	/mnt/HydroTerra/fsar_data/21HTERRA/FL06/PS11/T04/INF_stack11C	4	11	C	13G
20	/mnt/HydroTerra/fsar_data/21HTERRA/FL06/PS11/T04/INF_stack11L	4	11	L	3.1G

No.	INF Product - Group 04, Flight 07	Group	Track	Band	Size
1	/mnt/HydroTerra/fsar_data/21HTERRA/FL07/PS02/T04/INF_stack10C	4	10	C	16G
2	/mnt/HydroTerra/fsar_data/21HTERRA/FL07/PS02/T04/INF_stack10L	4	10	L	3.8G
3	/mnt/HydroTerra/fsar_data/21HTERRA/FL07/PS03/T04/INF_stack11C	4	11	C	13G
4	/mnt/HydroTerra/fsar_data/21HTERRA/FL07/PS03/T04/INF_stack11L	4	11	L	3.2G
5	/mnt/HydroTerra/fsar_data/21HTERRA/FL07/PS04/T04/INF_stack10C	4	10	C	16G
6	/mnt/HydroTerra/fsar_data/21HTERRA/FL07/PS04/T04/INF_stack10L	4	10	L	3.8G
7	/mnt/HydroTerra/fsar_data/21HTERRA/FL07/PS05/T04/INF_stack11C	4	11	C	13G
8	/mnt/HydroTerra/fsar_data/21HTERRA/FL07/PS05/T04/INF_stack11L	4	11	L	3.2G
9	/mnt/HydroTerra/fsar_data/21HTERRA/FL07/PS06/T04/INF_stack10C	4	10	C	16G
10	/mnt/HydroTerra/fsar_data/21HTERRA/FL07/PS06/T04/INF_stack10L	4	10	L	3.8G
11	/mnt/HydroTerra/fsar_data/21HTERRA/FL07/PS07/T04/INF_stack11C	4	11	C	13G
12	/mnt/HydroTerra/fsar_data/21HTERRA/FL07/PS07/T04/INF_stack11L	4	11	L	3.2G
13	/mnt/HydroTerra/fsar_data/21HTERRA/FL07/PS08/T04/INF_stack10C	4	10	C	16G
14	/mnt/HydroTerra/fsar_data/21HTERRA/FL07/PS08/T04/INF_stack10L	4	10	L	3.8G
15	/mnt/HydroTerra/fsar_data/21HTERRA/FL07/PS09/T04/INF_stack11C	4	11	C	13G
16	/mnt/HydroTerra/fsar_data/21HTERRA/FL07/PS09/T04/INF_stack11L	4	11	L	3.2G
17	/mnt/HydroTerra/fsar_data/21HTERRA/FL07/PS10/T04/INF_stack10C	4	10	C	16G
18	/mnt/HydroTerra/fsar_data/21HTERRA/FL07/PS10/T04/INF_stack10L	4	10	L	3.8G
19	/mnt/HydroTerra/fsar_data/21HTERRA/FL07/PS11/T04/INF_stack11C	4	11	C	13G

	<p>SARSimHT-NG – Simulation of Hydroterra SAR System Performance in the Mediterranean and the Alps Based on Experimental Airborne SAR Data</p> <p>D1: Data Acquisition Report of SWE Experiment</p>	<p>Doc.: DLR-HR-TR-SARSimHT-NG-01 Issue: 2.0 Date: 25.11.2021 Page: 67 of 110</p>
---	---	--

20	/mnt/HydroTerra/fsar_data/21HTERRA/FL07/PS11/T04/INF_stack11L	4	11	L	3.2G
----	---	---	----	---	------

No.	INF Product - Group 08, all flights (masters only)	Group	Track	Band	Size
1	/mnt/HydroTerra/fsar_data/21HTERRA/FL01/PS02/T08/INF_stack10C	8	10	C	209M
2	/mnt/HydroTerra/fsar_data/21HTERRA/FL01/PS02/T08/INF_stack10L	8	10	L	404M
3	/mnt/HydroTerra/fsar_data/21HTERRA/FL01/PS03/T08/INF_stack11C	8	11	C	176M
4	/mnt/HydroTerra/fsar_data/21HTERRA/FL01/PS03/T08/INF_stack11L	8	11	L	169M
5	/mnt/HydroTerra/fsar_data/21HTERRA/FL02/PS02/T08/INF_stack10C	8	10	C	16G
6	/mnt/HydroTerra/fsar_data/21HTERRA/FL02/PS02/T08/INF_stack10L	8	10	L	3.8G
7	/mnt/HydroTerra/fsar_data/21HTERRA/FL02/PS03/T08/INF_stack11C	8	11	C	13G
8	/mnt/HydroTerra/fsar_data/21HTERRA/FL02/PS03/T08/INF_stack11L	8	11	L	3.2G
9	/mnt/HydroTerra/fsar_data/21HTERRA/FL03/PS02/T08/INF_stack10C	8	10	C	16G
10	/mnt/HydroTerra/fsar_data/21HTERRA/FL03/PS02/T08/INF_stack10L	8	10	L	3.8G
11	/mnt/HydroTerra/fsar_data/21HTERRA/FL03/PS03/T08/INF_stack11C	8	11	C	13G
12	/mnt/HydroTerra/fsar_data/21HTERRA/FL03/PS03/T08/INF_stack11L	8	11	L	3.2G
13	/mnt/HydroTerra/fsar_data/21HTERRA/FL04/PS02/T08/INF_stack10C	8	10	C	16G
14	/mnt/HydroTerra/fsar_data/21HTERRA/FL04/PS02/T08/INF_stack10L	8	10	L	3.8G
15	/mnt/HydroTerra/fsar_data/21HTERRA/FL04/PS03/T08/INF_stack11C	8	11	C	13G
16	/mnt/HydroTerra/fsar_data/21HTERRA/FL04/PS03/T08/INF_stack11L	8	11	L	3.2G
17	/mnt/HydroTerra/fsar_data/21HTERRA/FL05/PS02/T08/INF_stack10C	8	10	C	16G
18	/mnt/HydroTerra/fsar_data/21HTERRA/FL05/PS02/T08/INF_stack10L	8	10	L	3.8G
19	/mnt/HydroTerra/fsar_data/21HTERRA/FL05/PS03/T08/INF_stack11C	8	11	C	13G
20	/mnt/HydroTerra/fsar_data/21HTERRA/FL05/PS03/T08/INF_stack11L	8	11	L	3.2G
21	/mnt/HydroTerra/fsar_data/21HTERRA/FL06/PS02/T08/INF_stack10C	8	10	C	16G
22	/mnt/HydroTerra/fsar_data/21HTERRA/FL06/PS02/T08/INF_stack10L	8	10	L	3.8G
23	/mnt/HydroTerra/fsar_data/21HTERRA/FL06/PS03/T08/INF_stack11C	8	11	C	13G
24	/mnt/HydroTerra/fsar_data/21HTERRA/FL06/PS03/T08/INF_stack11L	8	11	L	3.2G
25	/mnt/HydroTerra/fsar_data/21HTERRA/FL07/PS02/T08/INF_stack10C	8	10	C	16G
26	/mnt/HydroTerra/fsar_data/21HTERRA/FL07/PS02/T08/INF_stack10L	8	10	L	3.8G
27	/mnt/HydroTerra/fsar_data/21HTERRA/FL07/PS03/T08/INF_stack11C	8	11	C	13G
28	/mnt/HydroTerra/fsar_data/21HTERRA/FL07/PS03/T08/INF_stack11L	8	11	L	3.2G
29	/mnt/HydroTerra/fsar_data/21HTERRA/FL08/PS02/T08/INF_stack10C	8	10	C	16G
30	/mnt/HydroTerra/fsar_data/21HTERRA/FL08/PS02/T08/INF_stack10L	8	10	L	3.8G
31	/mnt/HydroTerra/fsar_data/21HTERRA/FL08/PS03/T08/INF_stack11C	8	11	C	13G
32	/mnt/HydroTerra/fsar_data/21HTERRA/FL08/PS03/T08/INF_stack11L	8	11	L	3.2G



L- and C-band stacks of Group 03, flights 03 and 04, 'stack11Cnew7' and 'stack11Lnewhh' were re-processed with passes 0323 and 0409 being excluded. These new stacks are delivered additionally.

No.	INF Product - Group 03, Flight 03 - reprocessed	Group	Track	Band	Size
-	/mnt/HydroTerra/fsar_data/21HTERRA/FL03/PS03/T03/INF_stack11Cnew7	-	-	-	-
1	/mnt/HydroTerra/fsar_data/21HTERRA/FL03/PS03/T03/INF_stack11Lnewhh	3	11	L	169M
2	/mnt/HydroTerra/fsar_data/21HTERRA/FL03/PS05/T03/INF_stack11Cnew7	3	11	C	13G
3	/mnt/HydroTerra/fsar_data/21HTERRA/FL03/PS05/T03/INF_stack11Lnewhh	3	11	L	3.2G
4	/mnt/HydroTerra/fsar_data/21HTERRA/FL03/PS07/T03/INF_stack11Cnew7	3	11	C	13G
5	/mnt/HydroTerra/fsar_data/21HTERRA/FL03/PS07/T03/INF_stack11Lnewhh	3	11	L	3.2G
6	/mnt/HydroTerra/fsar_data/21HTERRA/FL03/PS09/T03/INF_stack11Cnew7	3	11	C	13G
7	/mnt/HydroTerra/fsar_data/21HTERRA/FL03/PS09/T03/INF_stack11Lnewhh	3	11	L	3.2G
8	/mnt/HydroTerra/fsar_data/21HTERRA/FL03/PS11/T03/INF_stack11Cnew7	3	11	C	13G
9	/mnt/HydroTerra/fsar_data/21HTERRA/FL03/PS11/T03/INF_stack11Lnewhh	3	11	L	3.1G
10	/mnt/HydroTerra/fsar_data/21HTERRA/FL03/PS13/T03/INF_stack11Cnew7	3	11	C	13G
11	/mnt/HydroTerra/fsar_data/21HTERRA/FL03/PS13/T03/INF_stack11Lnewhh	3	11	L	3.2G
12	/mnt/HydroTerra/fsar_data/21HTERRA/FL03/PS15/T03/INF_stack11Cnew7	3	11	C	13G
13	/mnt/HydroTerra/fsar_data/21HTERRA/FL03/PS15/T03/INF_stack11Lnewhh	3	11	L	3.2G
14	/mnt/HydroTerra/fsar_data/21HTERRA/FL03/PS17/T03/INF_stack11Cnew7	3	11	C	13G
15	/mnt/HydroTerra/fsar_data/21HTERRA/FL03/PS17/T03/INF_stack11Lnewhh	3	11	L	3.2G
16	/mnt/HydroTerra/fsar_data/21HTERRA/FL03/PS19/T03/INF_stack11Cnew7	3	11	C	13G
17	/mnt/HydroTerra/fsar_data/21HTERRA/FL03/PS19/T03/INF_stack11Lnewhh	3	11	L	3.2G
18	/mnt/HydroTerra/fsar_data/21HTERRA/FL03/PS21/T03/INF_stack11Cnew7	3	11	C	13G
19	/mnt/HydroTerra/fsar_data/21HTERRA/FL03/PS21/T03/INF_stack11Lnewhh	3	11	L	3.2G
20	/mnt/HydroTerra/fsar_data/21HTERRA/FL03/PS22/T03/INF_stack11Cnew7	3	11	C	13G
21	/mnt/HydroTerra/fsar_data/21HTERRA/FL03/PS22/T03/INF_stack11Lnewhh	3	11	L	3.2G
22	/mnt/HydroTerra/fsar_data/21HTERRA/FL03/PS24/T03/INF_stack11Cnew7	3	11	C	13G
23	/mnt/HydroTerra/fsar_data/21HTERRA/FL03/PS24/T03/INF_stack11Lnewhh	3	11	L	3.2G

An **irregularity** is that an INF product in pass 0303 has not been created (not in tomographic mode). Pass **0323** has been excluded from this stack.

No.	INF Product - Group 03, Flight 04 - reprocessed	Group	Track	Band	Size
1	/mnt/HydroTerra/fsar_data/21HTERRA/FL04/PS03/T03/INF_stack11Cnew7	3	11	C	13G
2	/mnt/HydroTerra/fsar_data/21HTERRA/FL04/PS03/T03/INF_stack11Lnewhh	3	11	L	3.2G
3	/mnt/HydroTerra/fsar_data/21HTERRA/FL04/PS05/T03/INF_stack11Cnew7	3	11	C	13G
4	/mnt/HydroTerra/fsar_data/21HTERRA/FL04/PS05/T03/INF_stack11Lnewhh	3	11	L	3.2G
5	/mnt/HydroTerra/fsar_data/21HTERRA/FL04/PS07/T03/INF_stack11Cnew7	3	11	C	13G
6	/mnt/HydroTerra/fsar_data/21HTERRA/FL04/PS07/T03/INF_stack11Lnewhh	3	11	L	3.2G
7	/mnt/HydroTerra/fsar_data/21HTERRA/FL04/PS11/T03/INF_stack11Cnew7	3	11	C	13G
8	/mnt/HydroTerra/fsar_data/21HTERRA/FL04/PS11/T03/INF_stack11Lnewhh	3	11	L	3.2G

	SARSimHT-NG – Simulation of Hydroterra SAR System Performance in the Mediterranean and the Alps Based on Experimental Airborne SAR Data		Doc.: DLR-HR-TR-SARSimHT-NG-01 Issue: 2.0 Date: 25.11.2021 Page: 69 of 110	
	D1: Data Acquisition Report of SWE Experiment			

9	/mnt/HydroTerra/fsar_data/21HTERRA/FL04/PS13/T03/INF_stack11Cnew7	3	11	C	13G
10	/mnt/HydroTerra/fsar_data/21HTERRA/FL04/PS13/T03/INF_stack11Lnewhh	3	11	L	3.2G

Pass **0409** has been excluded from this stack.

New HydroTerra and Geosynchronous SAR simulation products have been created using these re-processed stacks.

Note: The analysis regarding Group 03 performed in Chapter 5 bases on the earlier processed stacks with passes 0323 and 0409 included. This part of the work could not be repeated with the new data, unfortunately.

4.5 Summary of Data Products

In total, we delivered 368 products as listed in Table 4-8.

Table 4-8: Overview of delivered F-SAR data products.

Product	Group 01		Group 02		Group 03		Group 04		Group 08	Total
	FL01	FL05	FL02	FL08	FL03	FL04	FL06	FL07	FL01-FL08	
RGI	2		2		2		2		2	10
GTC	2		2		2		2		2	10
INF	44	40	44	12	46	24	20	20	32	315
INF-re					23	10				33
Total	48	40	48	12	73	34	24	20	36	368

The reason why RGI and GTC products appear as multiples of 2 is that views from the EAST and from the WEST (track 10, track11) are provided. The reason why INF products appear as multiples of 4 is that the views EAST and WEST are subdivided into C- and L-band, additionally.

An odd number of passes emerges in Group 03 where we have more track 11 passes than track 10 passes. In the re-processed stack, we have an odd number of passes because one INF product (master 0303 in C-band) does not exist. This stack is re-processed in interferometric mode (pairwise) instead of tomographic (anyone with anyone) mode which is the default.

5 Simulation of Hydroterra Products

5.1 Overview

As part of 'WP210 – Hydroterra Product Simulation and Analysis – SWE Experiment', DLR has simulated Hydroterra products in C-band, which will be delivered to ESA.

In Section 5.2 the simulation procedure of geosynchronous SAR and Hydroterra products is described. This procedure was used to simulate the products which are presented in Section 5.3 and in Section 5.4.

To investigate primarily the impact of the long integration time of geosynchronous SAR on SWE retrieval, products with the resolution and NESZ of the F-SAR system have been simulated. With such a high resolution it is easier to discriminate between different effects and compare geosynchronous SAR products to the ones of LEO SAR. These products are presented and preliminarily analysed in Section 5.3 and they are referred to as geosynchronous SAR products with F-SAR resolution.

In Section 5.4 Hydroterra products with the parameters of scenario 4 of the interferometric type (Glacier flow / Landslides) were simulated. The goal of these products is to perform an assessment of the potential to retrieve SWE from realistic Hydroterra data.

As described in Table 4-6, different interferometric groups have been processed. From these groups simulated interferometric Hydroterra products were computed:

- Flight 01 – Flight 05
- Flight 02 – Flight 08
- Flight 03 – Flight 04
- Flight 06 – Flight 07.

The interferometric products of the simulated geosynchronous SAR with F-SAR resolution and of the simulated Hydroterra products are shown in Sections 5.3 and 5.4.

During the different flights different number of passes were performed. This results in different possible maximum integration times for different flights. In this work the azimuth resolution was kept constant, while the integration time was varied. For both flights of one interferometric pair the same number of passes were chosen, which is here the maximum number of passes of the flight with the smallest number in one interferometric pair. Table 5-1 summarizes the different integration times of the different flights.

Table 5-1: Integration times of the different flights.

Flight	Integration Time	Number of Passes
Flight 1	106.63 min.	11
Flight 2	23.82 min.	3
Flight 3	66.52 min.	6
Flight 4	70.47 min.	6
Flight 5	110.50 min.	11
Flight 6	48.03 min.	5
Flight 7	48.82 min.	5
Flight 8	23.38 min.	3

5.2 Simulation Procedure

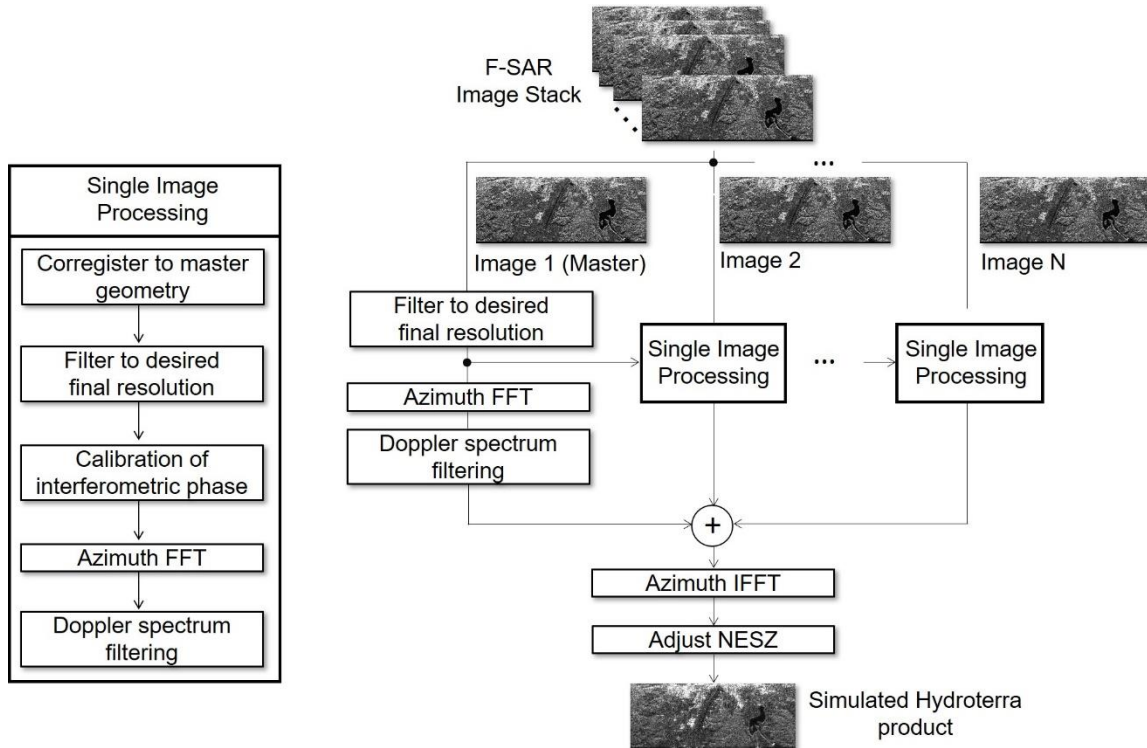


Figure 5-1: Simulation procedure to generate simulated Hydroterra SLC products.

The simulation procedure of Hydroterra image products is visualized in Figure 5-1. Each image from the stack is filtered to the desired resolution in azimuth and slant range and normalized in terms of energy [4]. One image is defined as master (here it was image 1) and the other images are co-registered to the master geometry. In the next step, an interferometric calibration is performed in order to coherently align the images in a proper way. This is performed for each slave image by subtracting the interferometric phase between this image and the master. After the phase calibration, each image is Fourier transformed to the azimuth frequency domain, where a different bandpass filter is applied to each image. This bandpass filter is needed to simulate the slow velocity of a satellite in a geosynchronous orbit.

The bandwidth and centre frequency of each band pass filter is calculated to ensure the desired final resolution of the Hydroterra product. An overlap of 50% between adjacent bands is performed by using a weighting function. An overlap is needed to eliminate phase jumps in the final product, which otherwise would degrade the final simulated Hydroterra product, something which is not occurring in a real Hydroterra product. Phase jumps occur because spectra from different images are combined; implying different phase offsets at the edges between the spectra might be present. A weighting function ensures a smooth transition between bands. After bandpass filtering, all images are coherently combined in the azimuth frequency domain. Afterwards, an inverse Fourier transform in the azimuth domain is performed and the noise equivalent sigma zero (NESZ) of the product is adjusted to the one of a Hydroterra product, as described in [4]. The result of this simulation is a simulated Hydroterra single-look complex (SLC) product. The simulation procedure is described in more detail in [5].

5.3 Simulated Geosynchronous SAR Products with F-SAR Resolution

5.3.1 Simulation and Analysis of Geosynchronous SAR Image Products

In Figure 5-2 and Figure 5-6 exemplarily the simulated geosynchronous SAR SLC images for the flights 2 and 5 for track 10 are presented and in Figure 5-4 and Figure 5-8 the ones for track 11 are visualized. These flights are chosen, because flight 5 has the longest integration time and flight 2 the shortest (after flight 8). In Figure 5-3, Figure 5-5, Figure 5-7 and Figure 5-9 the SLCs of the first pass of the respective flight and track are shown for comparison.

To analyse the differences between a geosynchronous SAR SLC and a conventional SAR image, in Figure 5-10, Figure 5-12, Figure 5-14 and Figure 5-16 the contrast of the geosynchronous SAR images and in Figure 5-11, Figure 5-13, Figure 5-15 and Figure 5-17 the contrast of conventional SAR images is analysed. The contrast can be calculated from [6]

$$C = \frac{Var\{I\}}{(E\{I\})^2}$$

Here I is the magnitude of the image, $Var\{\}$ denotes the variance and $E\{\}$ the expectation value. Higher contrast indicates better image quality if the same scene is analysed. The contrast was calculated from a sliding window with 16x16 pixels. Figures 5-11 to 5-17 show a higher contrast for conventional SAR images. Table 5-2 summarizes the difference of the mean contrast between geosynchronous SAR images and conventional SAR images for all flights, tracks and polarisations. The contrast of the conventional SAR images is always higher. The difference is the highest for the HV polarisation for all flights. To compare the contrast difference between different flights and integration times, further investigation is needed. The area, of which data was acquired, differed due to different squint angles and RF interferences were present during data acquisition.

Table 5-2: Difference of mean contrast between geosynchronous SAR image and conventional SAR image for different flights, tracks and polarisations.

	HH	HV	VV
Flight 1, track 10	0.041	0.050	0.039
Flight 1, track 11	0.045	0.052	0.044
Flight 2, track 10	0.031	0.035	0.028
Flight 2, track 11	0.029	0.034	0.028
Flight 3, track 10	0.038	0.043	0.034
Flight 3, track 11	0.045	0.050	0.043
Flight 4, track 10	0.049	0.056	0.047
Flight 4, track 11	0.055	0.061	0.053
Flight 5, track 10	0.049	0.059	0.046
Flight 5, track 11	0.050	0.057	0.047
Flight 6, track 10	0.049	0.057	0.046
Flight 6, track 11	0.044	0.050	0.040
Flight 7, track 10	0.040	0.047	0.037

	<p>SARSimHT-NG – Simulation of Hydroterra SAR System Performance in the Mediterranean and the Alps Based on Experimental Airborne SAR Data</p> <p>D1: Data Acquisition Report of SWE Experiment</p>	<p>Doc.: DLR-HR-TR-SARSimHT-NG-01 Issue: 2.0 Date: 25.11.2021 Page: 73 of 110</p>
---	---	--

Flight 7, track 11	0.042	0.048	0.040
Flight 8, track 10	0.035	0.039	0.031
Flight 8, track 11	0.033	0.036	0.031

The corner reflectors from the test site were utilized to validate the correct phase calibration. The idea is to evaluate the parameters of the azimuth impulse response function of simulated geosynchronous SAR products and compare them to the ones of single passes. If the phase was calibrated correctly, then the parameters should match. If, however, the phase was not calibrated correctly, then a degradation of the parameters should be visible for the simulated geosynchronous SAR products. In Figure 5-18 to Figure 5-25 this evaluation is performed.

Figure 5-18 shows the azimuth impulse response function parameters of corner reflectors inside the test scene of flight 2 for track 10 and the HH polarization. The azimuth impulse response function parameters of the same flight and track, but for the VV polarisation are demonstrated in Figure 5-19. The azimuth impulse response parameters of flight 2 and track 11 are shown in Figure 5-20 and Figure 5-21 for the polarisations HH and VV. The parameters of both tracks and both polarisation for flight 5 are visualized in Figure 5-22, Figure 5-23, Figure 5-24 and Figure 5-25.

For this analysis the azimuth resolution, peak-to-sidelobe ratio (PSLR) and integrated sidelobe ratio (ISLR) were evaluated. The yellow dot corresponds to each measured parameter of the simulated geosynchronous SAR product and the blue dot corresponds to the mean value of the relevant parameter of all passes of the relevant image stack and the error bar show the 3σ . Note that no spectral weighting was used.

The analysis of the corner reflectors confirms a correct phase calibration during the simulation of geosynchronous SAR products, since all parameters of the azimuth impulse response function are either within 3σ or the deviations are so small that they can be explained by the limited resolution due to zero padding.

CR3W located in the upper part of Wörgetal and with orientation for Track 11 has been excluded from the analysis because of unreliable RCS and co-polar phase estimates.

Table 5-3: CR number mapping used in Figures 5-18 to 5-25 ('not visible' refers to the CR's look direction).

CR	Track 10	Track 11
CR1E	0	not visible
CR1W	not visible	0
CR2E	1	not visible
CR2W	not visible	1
CR3E	2	not visible
CR3W	excluded	excluded



Figure 5-2: Simulated single-look complex (SLC) product of geosynchronous SAR (resolution: 0.5 m x 0.5 m; samples: 24320 x 7536) from F-SAR data of flight 2 with track 10 for different polarisations. From left to right: HH, HV, VV.



Figure 5-3: For comparison an F-SAR single pass, single-look complex (SLC) image (resolution: 0.5 m x 0.5 m; samples: 24320 x 7536) of flight 2 with track 10 for different polarisations. From left to right: HH, HV, VV.

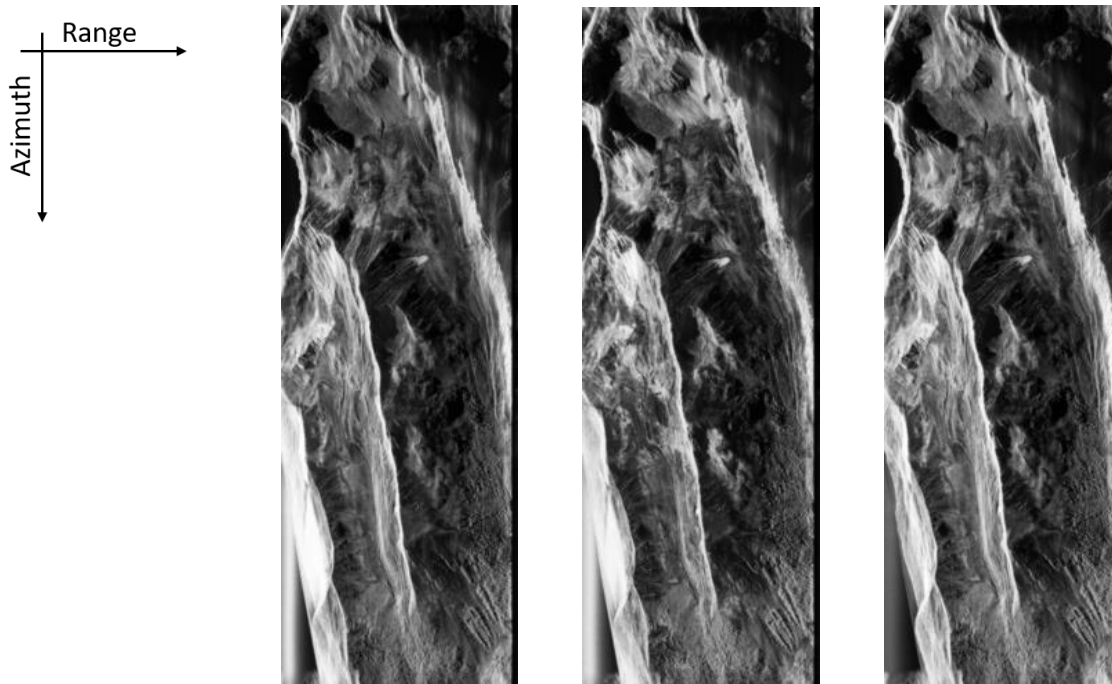


Figure 5-4: Simulated single-look complex (SLC) product of geosynchronous SAR (resolution: 0.5 m x 0.5 m; samples: 20224 x 7536) from F-SAR data of flight 2 with track 11 for different polarisations. From left to right: HH, HV, VV.

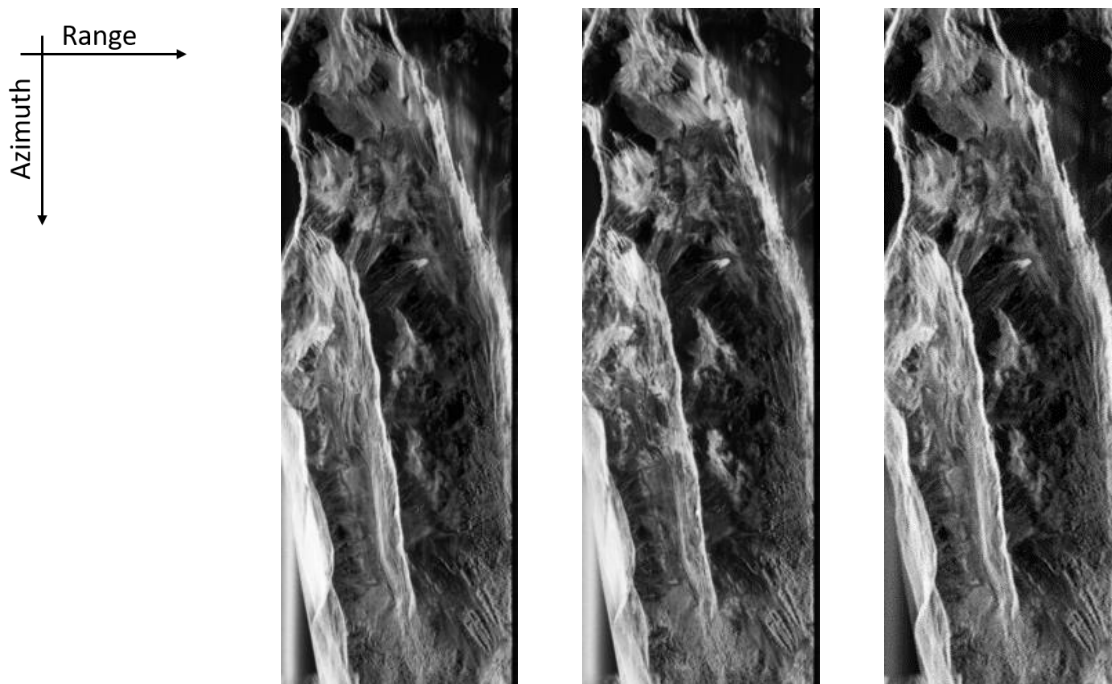


Figure 5-5: For comparison an F-SAR single pass, single-look complex (SLC) image (resolution: 0.5 m x 0.5 m; samples: 20224 x 7536) of flight 2 with track 11 for different polarisations. From left to right: HH, HV, VV.

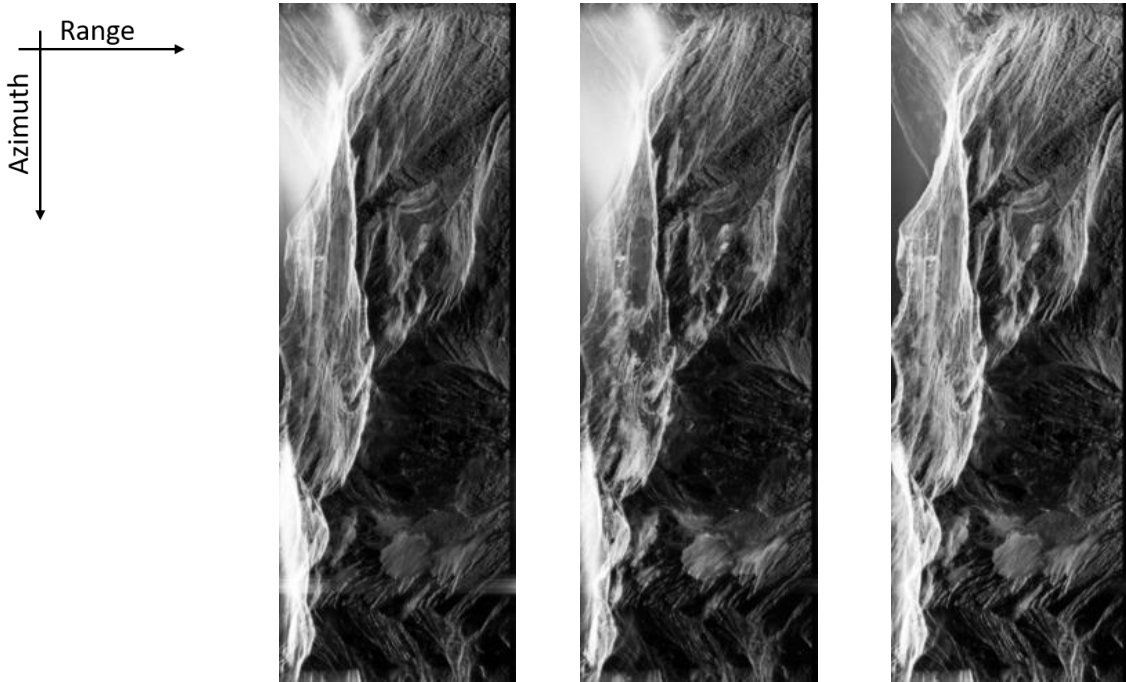


Figure 5-6: Simulated single-look complex (SLC) product of geosynchronous SAR (resolution: 0.5 m x 0.5 m; samples: 24320 x 7536) from F-SAR data of flight 5 with track 10 for different polarisations. From left to right: HH, HV, VV.



Figure 5-7: For comparison an F-SAR single pass, single-look complex (SLC) image (resolution: 0.5 m x 0.5 m; samples: 24320 x 7536) of flight 5 with track 10 for different polarisations. From left to right: HH, HV, VV.

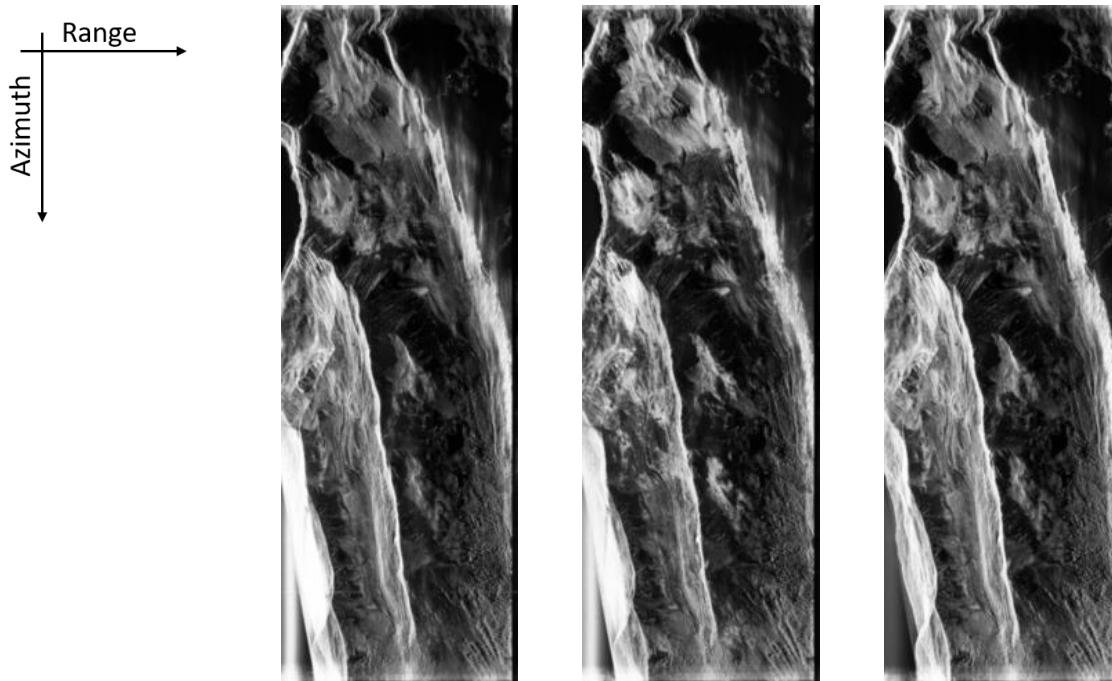


Figure 5-8: Simulated single-look complex (SLC) product of geosynchronous SAR (resolution: 0.5 m x 0.5 m; samples: 20224 x 7536) from F-SAR data of flight 5 with track 11 for different polarisations. From left to right: HH, HV, VV.

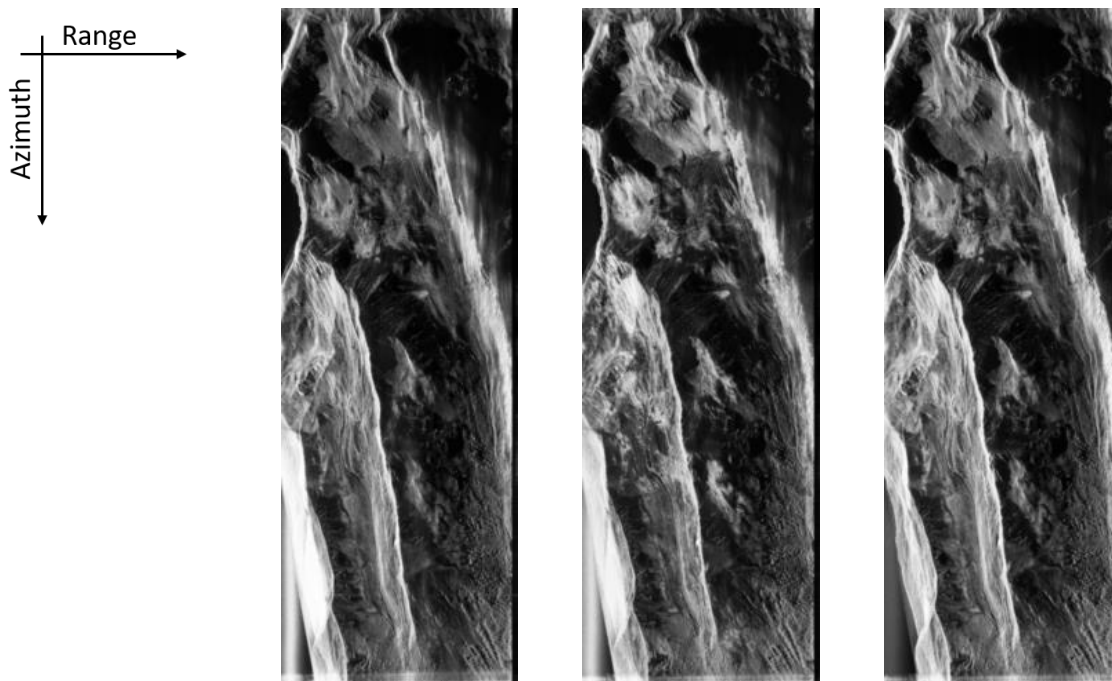


Figure 5-9: For comparison an F-SAR single pass, single-look complex (SLC) image (resolution: 0.5 m x 0.5 m; samples: 20224 x 7536) of flight 5 with track 11 for different polarisations. From left to right: HH, HV, VV.

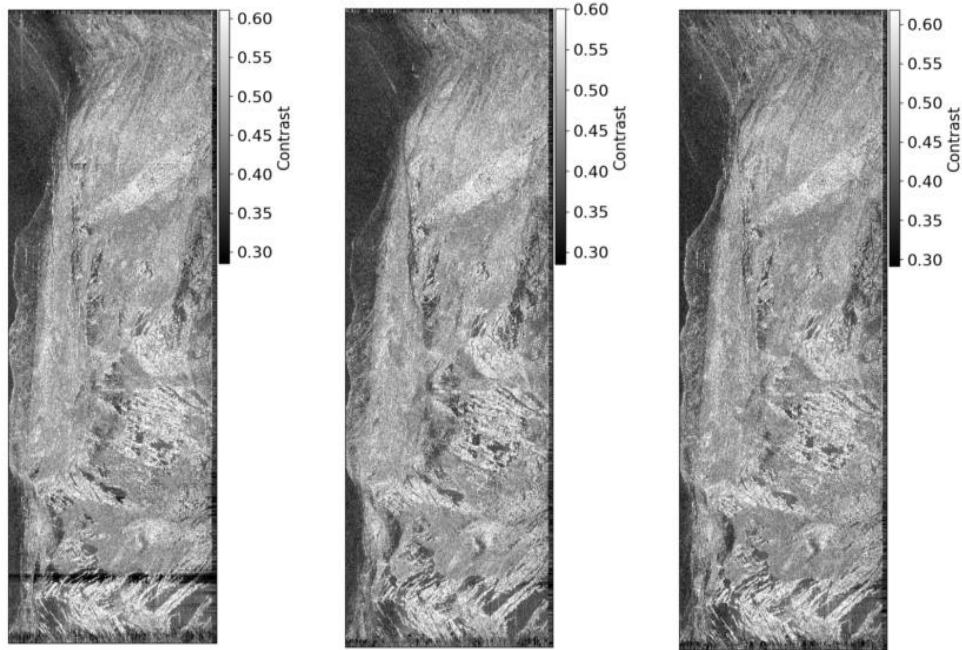


Figure 5-10: Contrast of simulated geosynchronous SAR SLC product of flight 2 with track 10 for different polarisations. From left to right: HH, HV, VV.

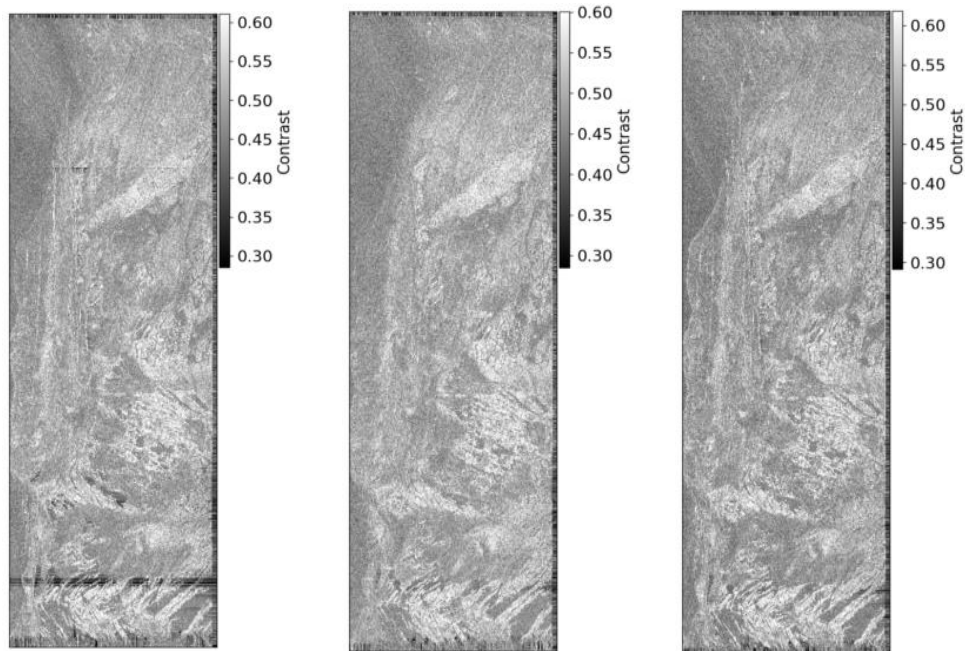


Figure 5-11: Contrast of a single pass SLC image of flight 2 with track 10 for different polarisations. From left to right: HH, HV, VV.

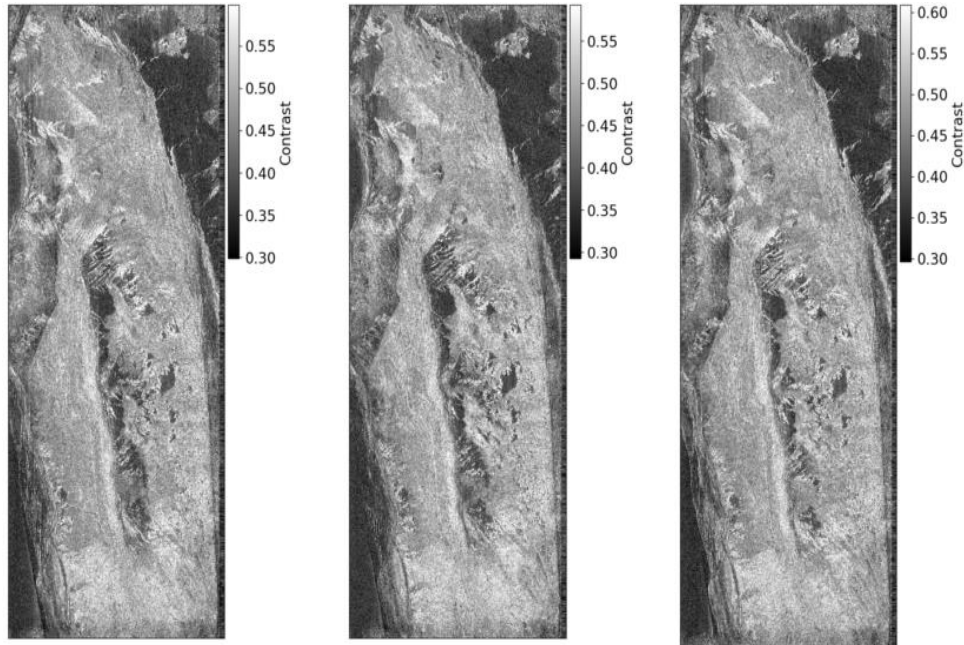


Figure 5-12: Contrast of simulated geosynchronous SAR SLC product of flight 2 with track 11 for different polarisations. From left to right: HH, HV, VV.

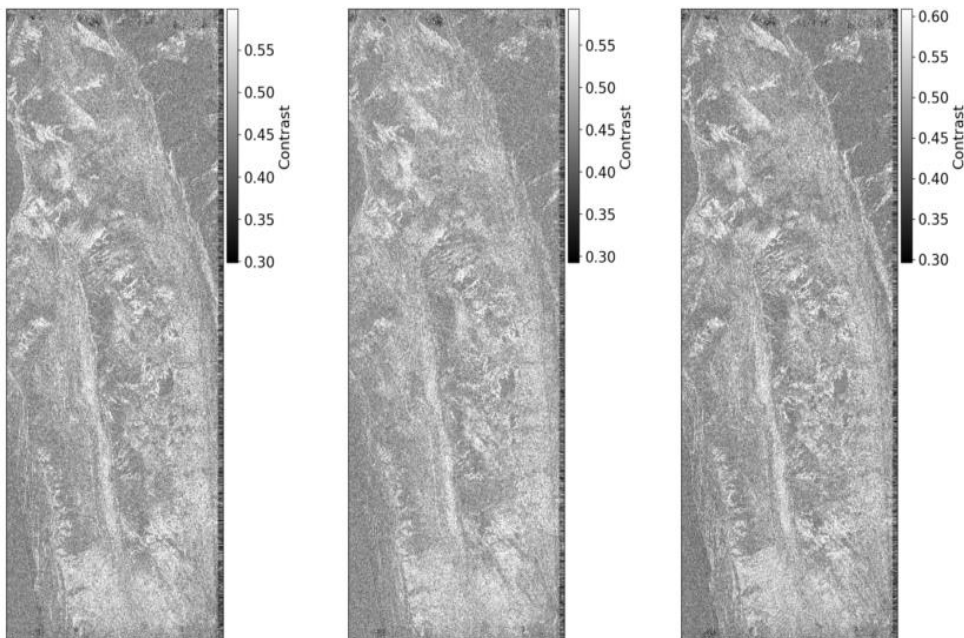


Figure 5-13: Contrast of a single pass SLC image of flight 2 with track 11 for different polarisations. From left to right: HH, HV, VV.

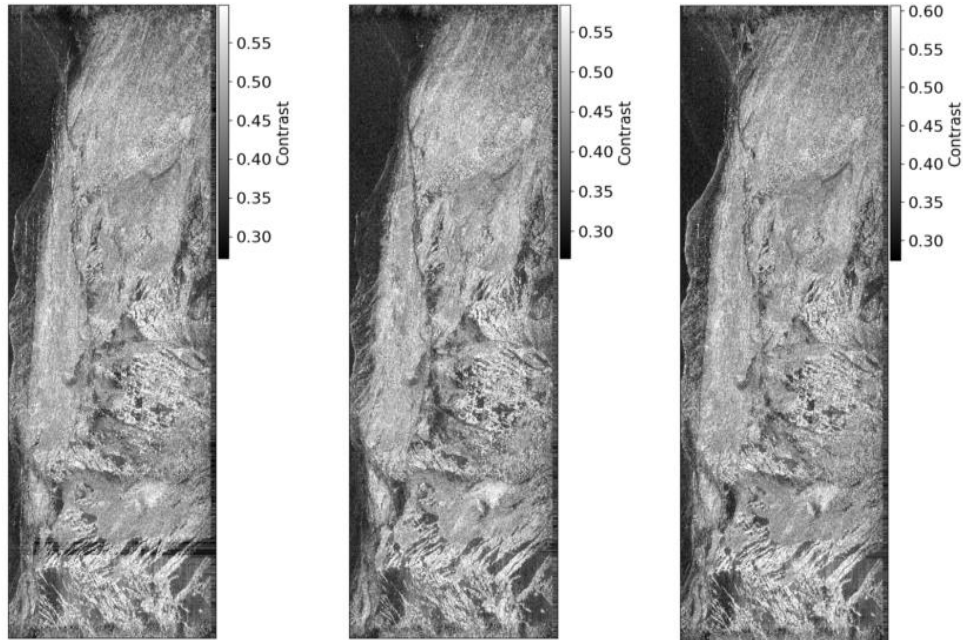


Figure 5-14: Contrast of simulated geosynchronous SAR SLC product of flight 5 with track 10 for different polarisations. From left to right: HH, HV, VV.

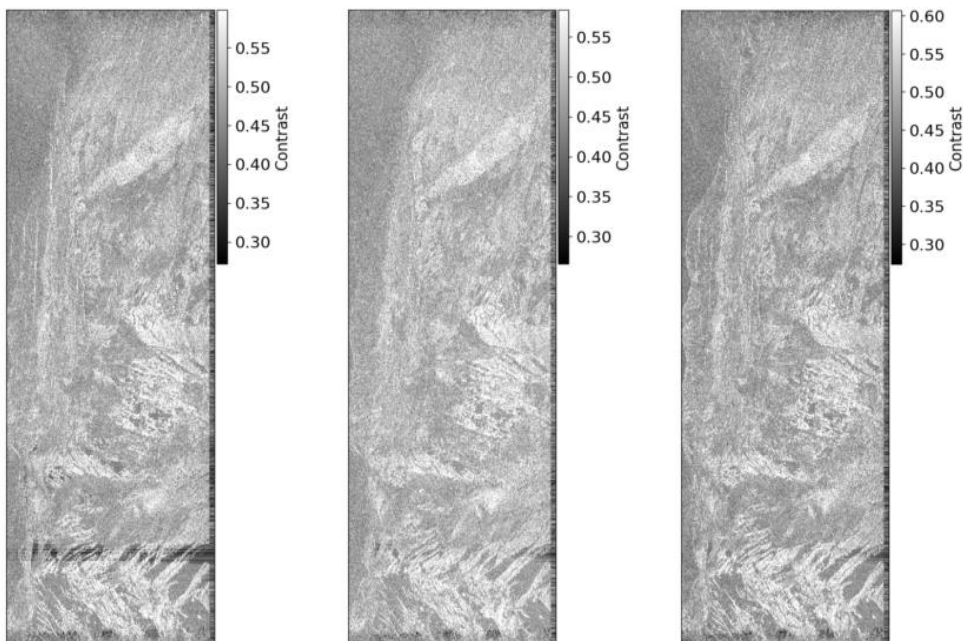


Figure 5-15: Contrast of a single pass SLC image of flight 5 with track 10 for different polarisations. From left to right: HH, HV, VV.

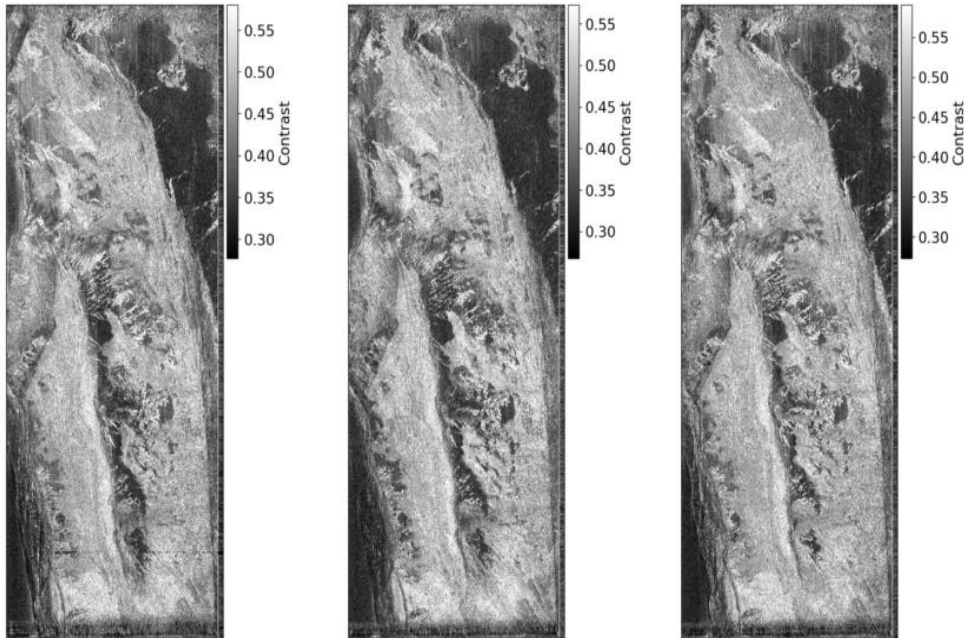


Figure 5-16: Contrast of simulated geosynchronous SAR SLC product of flight 5 with track 11 for different polarisations. From left to right: HH, HV, VV.

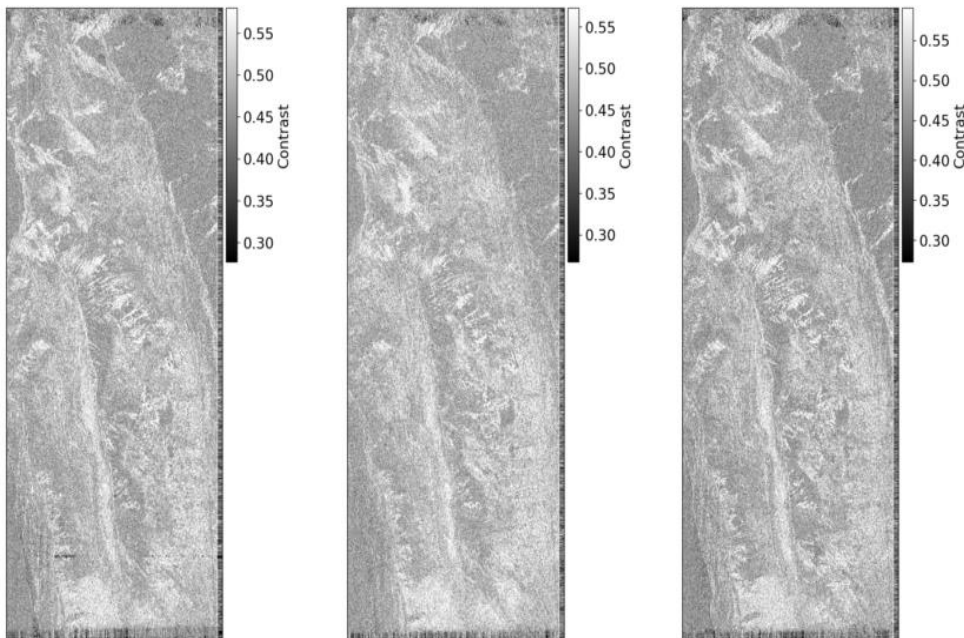


Figure 5-17: Contrast of a single pass SLC image of flight 5 with track 11 for different polarisations. From left to right: HH, HV, VV.

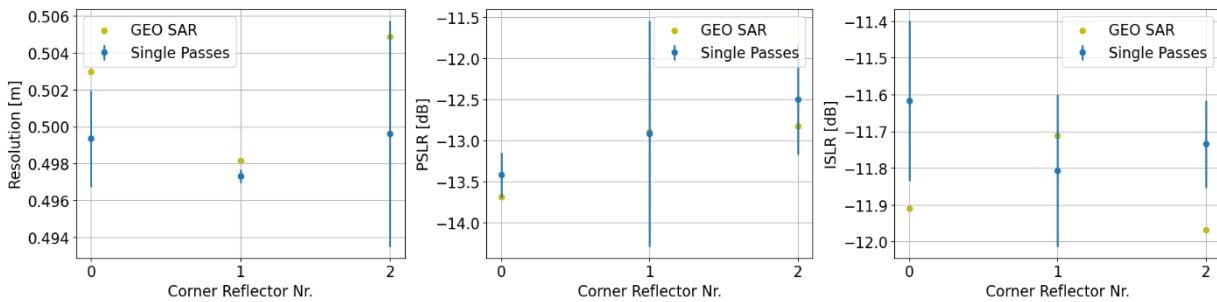


Figure 5-18: Azimuth impulse response function parameters of corner reflectors inside the test scene of flight 2 with track 10 for the HH polarization. For single passes the dot represents the mean and the error bar the 3σ . (Note: For the mapping of CR numbers refer to Table 5-3.)

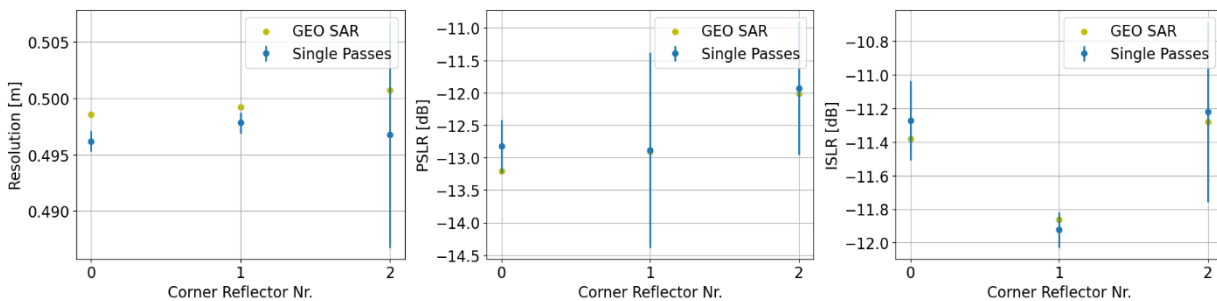


Figure 5-19: Azimuth impulse response function parameters of corner reflectors inside the test scene of flight 2 with track 10 for the VV polarization. For single passes the dot represents the mean and the error bar the 3σ .

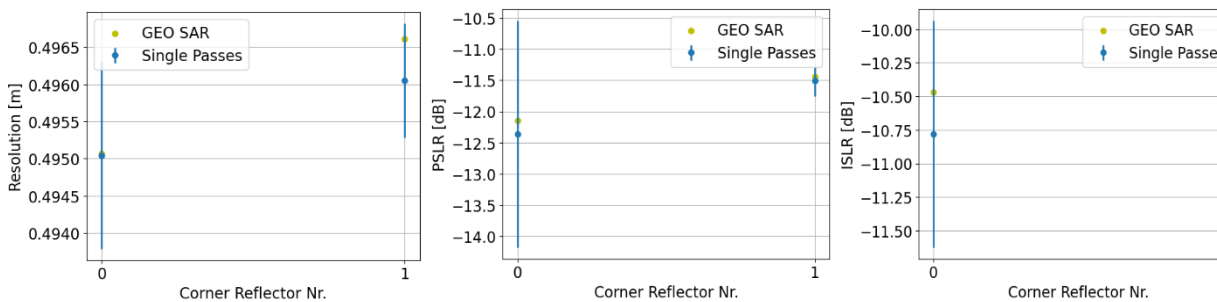


Figure 5-20: Azimuth impulse response function parameters of corner reflectors inside the test scene of flight 2 with track 11 for the HH polarization. For single passes the dot represents the mean and the error bar the 3σ . (Note: For the mapping of CR numbers refer to Table 5-3.)

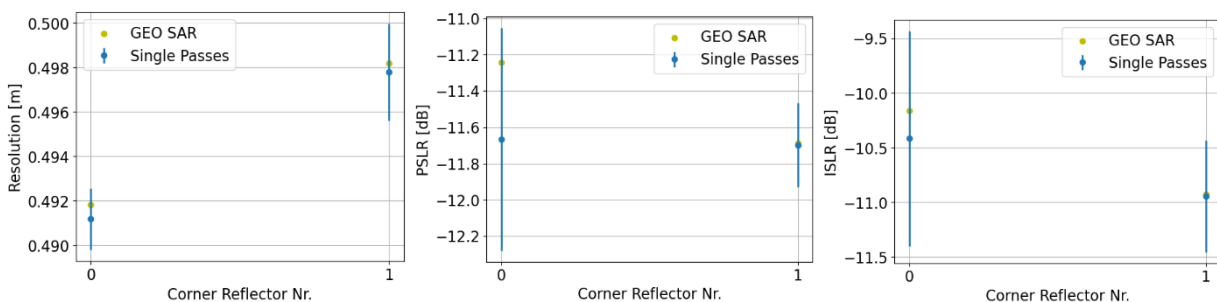


Figure 5-21: Azimuth impulse response function parameters of corner reflectors inside the test scene of flight 2 with track 11 for the VV polarization. For single passes the dot represents the mean and the error bar the 3σ .

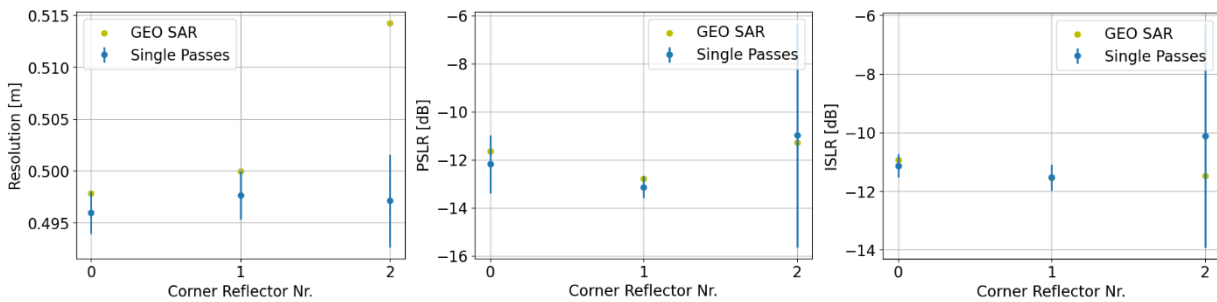


Figure 5-22: Azimuth impulse response function parameters of corner reflectors inside the test scene of flight 5 with track 10 for the HH polarization. For single passes the dot represents the mean and the error bar the 3σ . (Note: For the mapping of CR numbers refer to Table 5-3.)

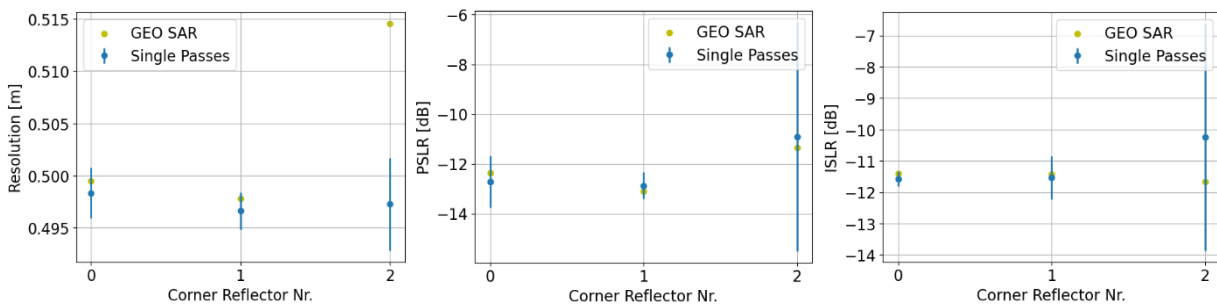


Figure 5-23: Azimuth impulse response function parameters of corner reflectors inside the test scene of flight 5 with track 10 for the VV polarization. For single passes the dot represents the mean and the error bar the 3σ .

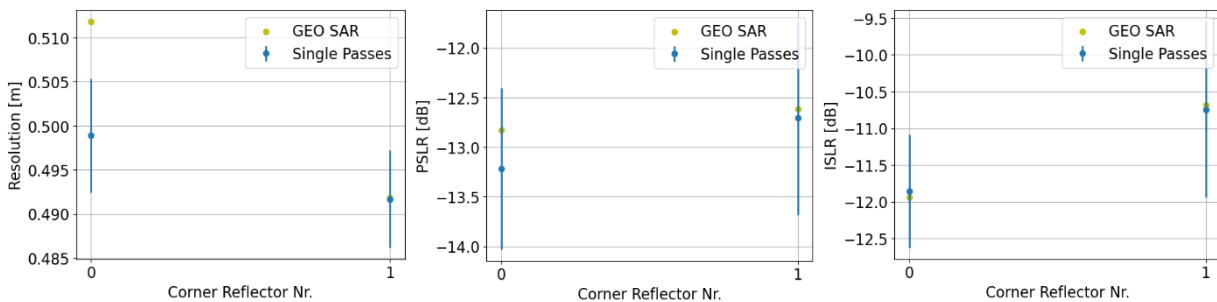


Figure 5-24: Azimuth impulse response function parameters of corner reflectors inside the test scene of flight 5 with track 11 for the HH polarization. For single passes the dot represents the mean and the error bar the 3σ . (Note: For the mapping of CR numbers refer to Table 5-3.)

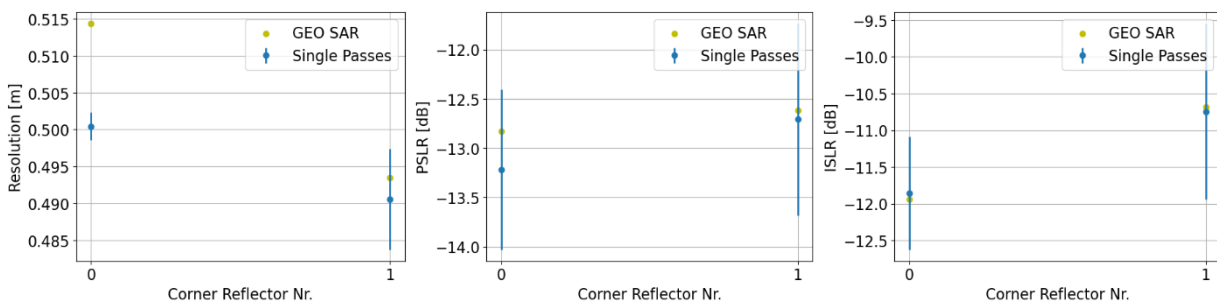


Figure 5-25: Azimuth impulse response function parameters of corner reflectors inside the test scene of flight 5 with track 11 for the VV polarization. For single passes the dot represents the mean and the error bar the 3σ .

5.3.2 Interferometric Geosynchronous SAR Products

In this subsection the interferometric coherence and the interferometric phase of simulated geosynchronous SAR images of all interferometric pairs, which were defined in Section 5.1, are presented. These data sets will also be delivered to ESA. Here the interferometric coherence and phase of the whole test scene are shown. However, in a mountainous test site layover and shadowing occurs. For further analysis only scatterers with valid incidence angles should be considered. In Figure 5-26 the local incidence angle maps of flight 1 for both tracks are visualized. These maps can be used to mask out invalid pixels. The local incidence angle maps will be delivered to ESA for all flights and all tracks.

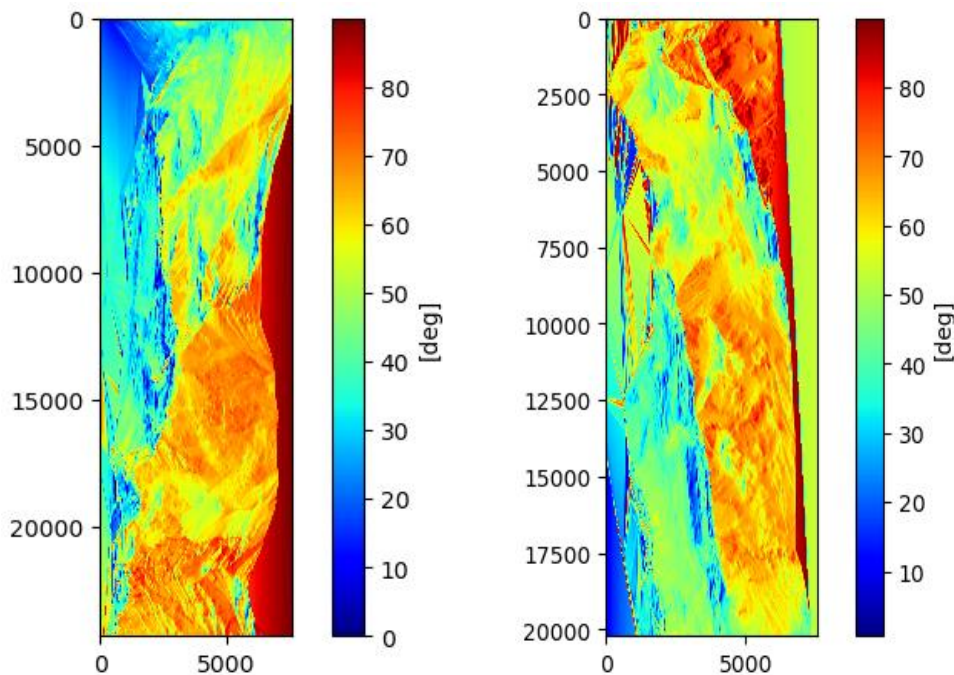


Figure 5-26: Local incidence angle map in degrees for flight 1 and track 10 (left) and for flight 1 and track 11 (right).

In Figure 5-27 the interferometric coherence between the simulated GEO SAR product of flight 1 and flight 5 for track 10 is shown for the polarisations HH, HV and VV. The interferometric phase of the same pair is demonstrated in Figure 5-28. The interferometric coherence and phase between the simulated GEO SAR product of flight 1 and flight 5 for track 11 are visualized in Figure 5-29 and Figure 5-30. The coherence and interferometric phase between the simulated GEO SAR products of flight 2 and 8 for both tracks are shown in Figure 5-31, Figure 5-32, Figure 5-33 and Figure 5-34. Figure 5-35, Figure 5-36, Figure 5-37 and Figure 5-38 demonstrate the interferometric coherence and phase between the simulated GEO SAR products of flight 3 and 4 for both tracks. The interferometric coherence and phase between the simulated GEO SAR products of flight 6 and 7 for both tracks can be found in Figure 5-39, Figure 5-40, Figure 5-41 and Figure 5-42.

The coherence between flight 2 and flight 8 is the lowest, as is visible in Figure 5-31 and Figure 5-33. This is because the time lag between those two flights is the longest, as was described in Chapter 4. In Figure 5-30 and Figure 5-38 a negative phase signal is strongly visible for areas with a high coherence. When processing the C-band stack of flight 3 and flight 4, track 11, the constant phase offsets could not be estimated properly, because non-valid passes had been included in the residual baseline error estimation. (Remark: This was corrected for later on by reprocessing.) However, caution is still advised when combining these data to Hydroterra products and when performing phase analysis.

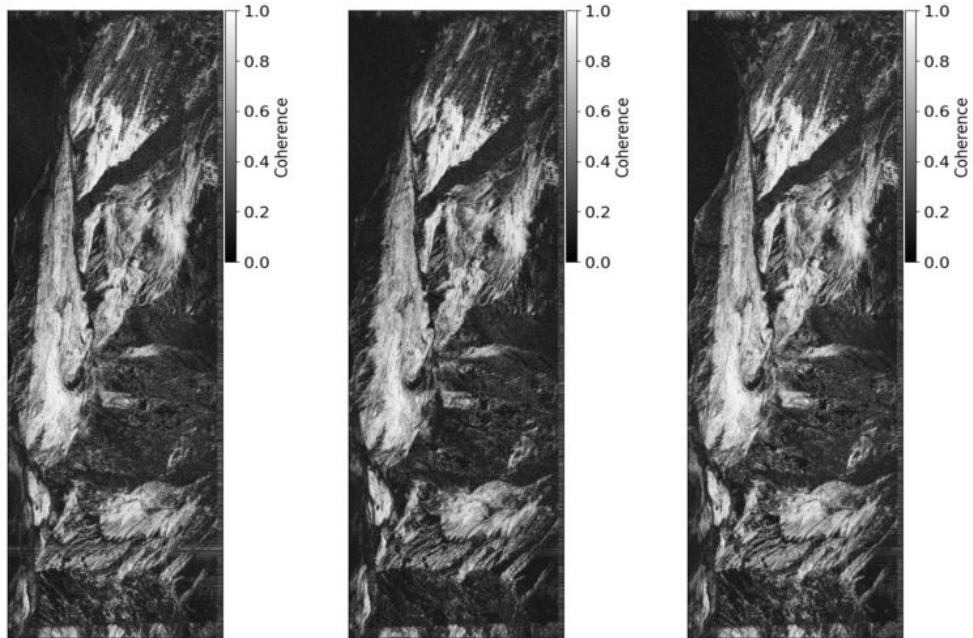


Figure 5-27: Interferometric coherence between simulated geosynchronous SAR SLCs of flight 1 and flight 5 of track 10 for different polarisations. From left to right: HH, HV, VV.

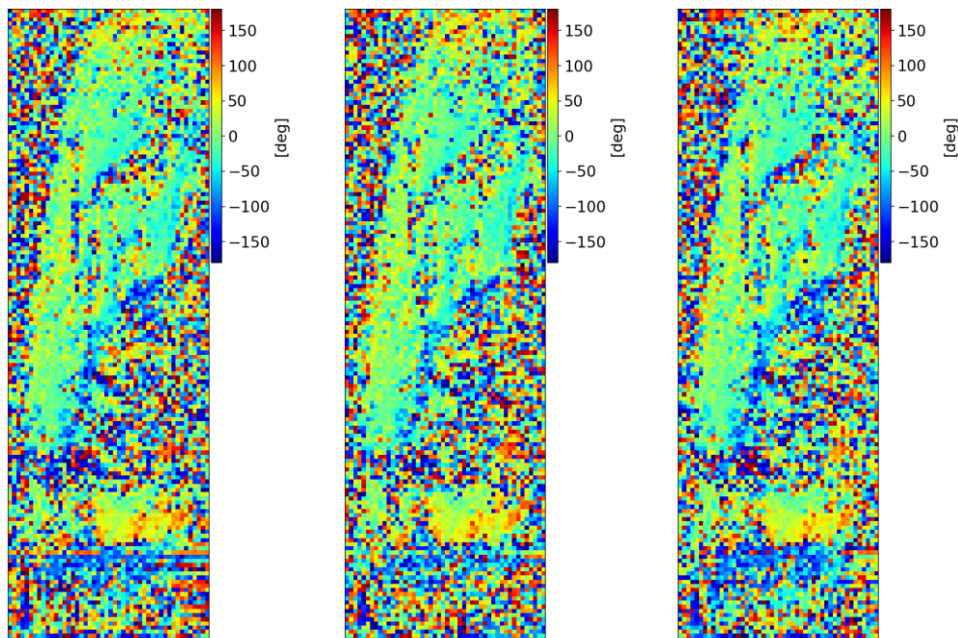


Figure 5-28: Interferometric phase between simulated geosynchronous SAR SLCs of flight 1 and flight 5 of track 10 for different polarisations. From left to right: HH, HV, VV. Time lag: 4 days. Snowfall between both flights.

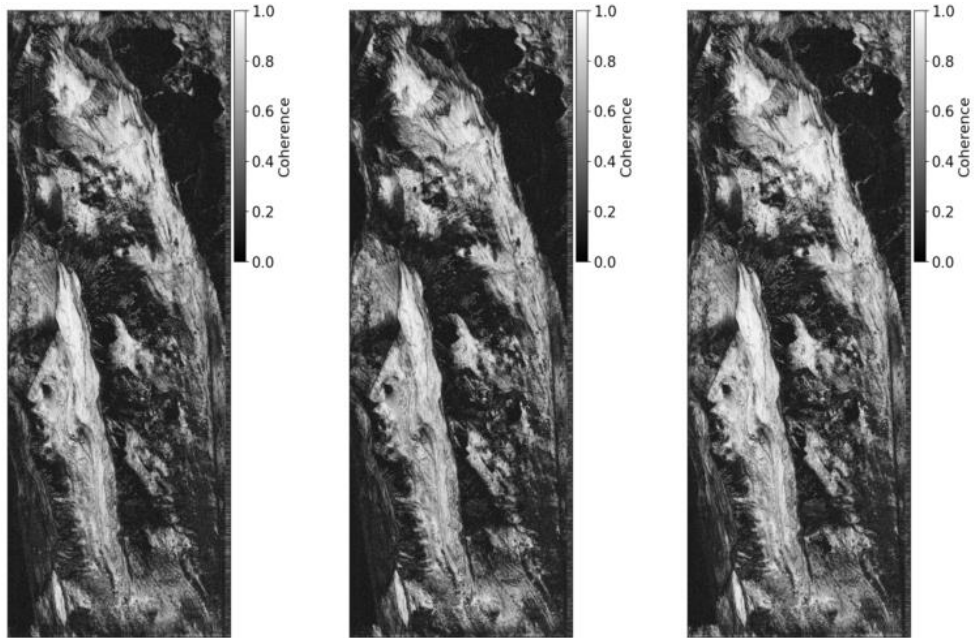


Figure 5-29: Interferometric coherence between simulated geosynchronous SAR SLCs of flight 1 and flight 5 of track 11 for different polarisations. From left to right: HH, HV, VV.

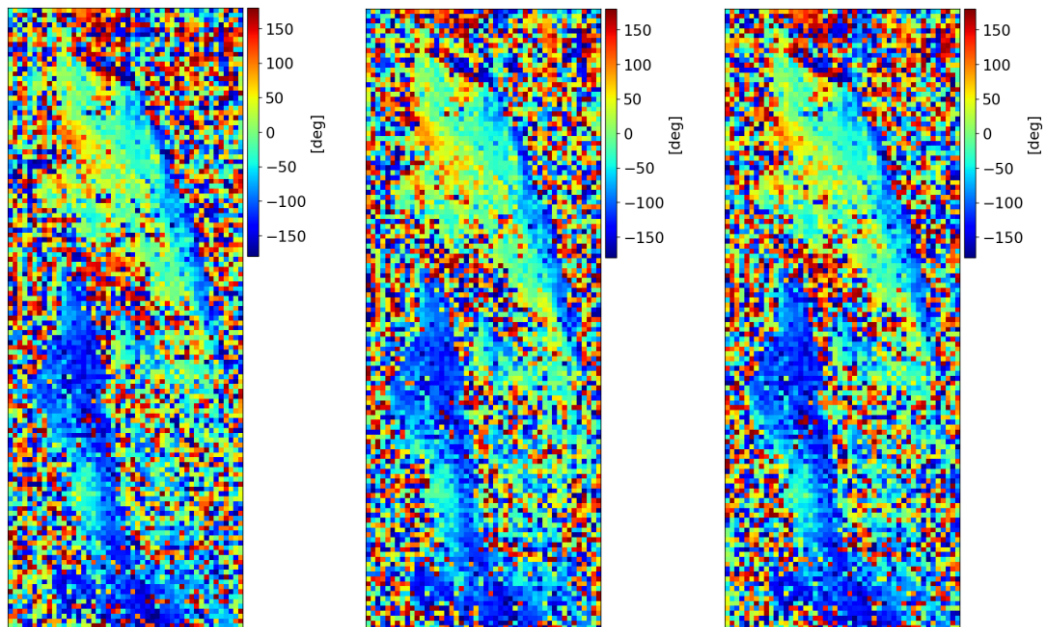


Figure 5-30: Interferometric phase between simulated geosynchronous SAR SLCs of flight 1 and flight 5 of track 11 for different polarisations. From left to right: HH, HV, VV. Time lag: 4 days. Snowfall between both flights.

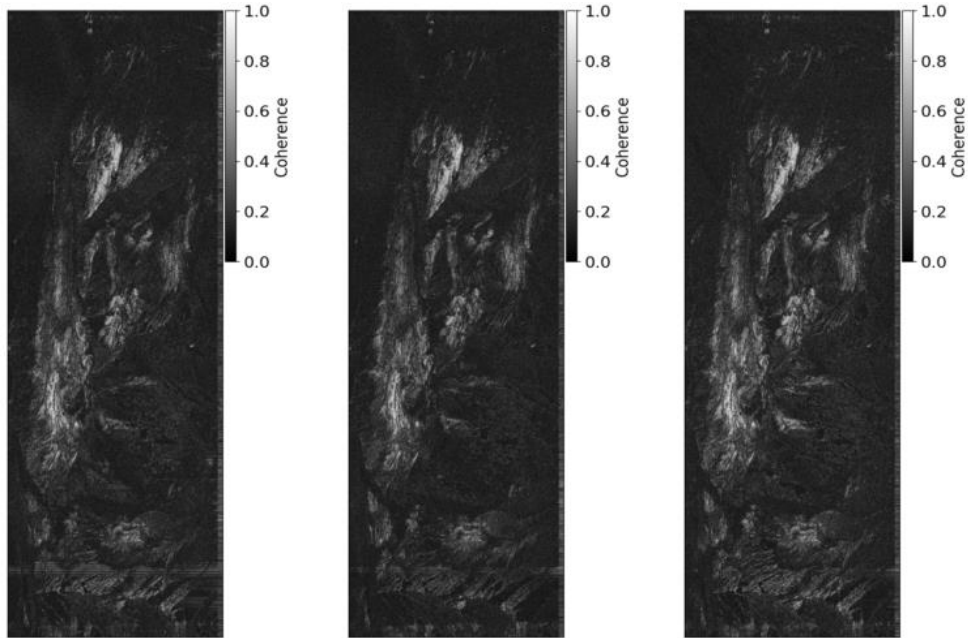


Figure 5-31: Interferometric coherence between simulated geosynchronous SAR SLCs of flight 2 and flight 8 of track 10 for different polarisations. From left to right: HH, HV, VV.

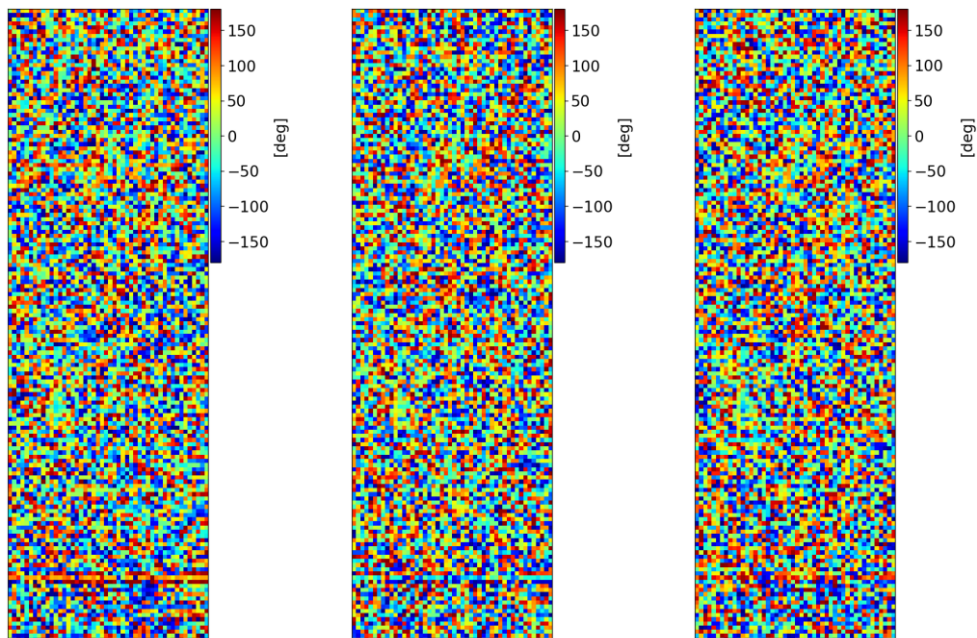


Figure 5-32: Interferometric phase between simulated geosynchronous SAR SLCs of flight 2 and flight 8 of track 10 for different polarisations. From left to right: HH, HV, VV. Time lag: 16 days. Snowfall between both flights.

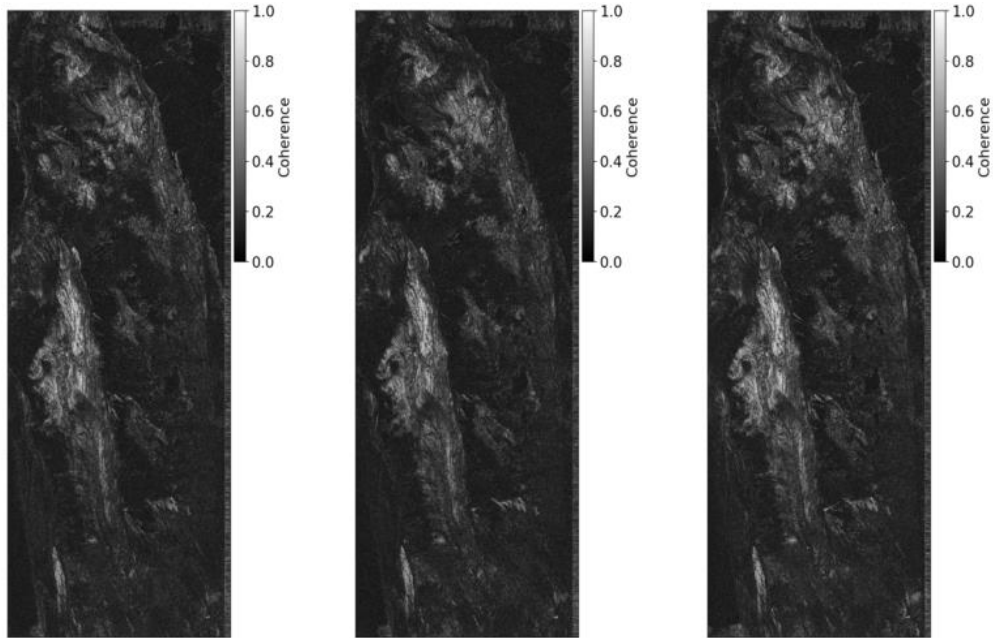


Figure 5-33: Interferometric coherence between simulated geosynchronous SAR SLCs of flight 2 and flight 8 of track 11 for different polarisations. From left to right: HH, HV, VV.

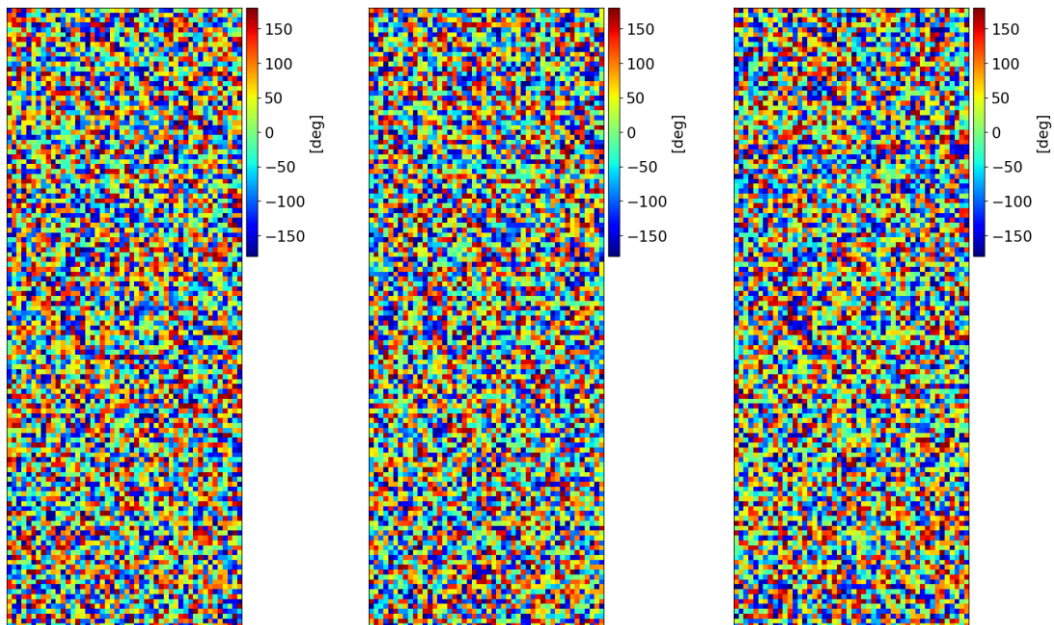


Figure 5-34: Interferometric phase between simulated geosynchronous SAR SLCs of flight 2 and flight 8 of track 11 for different polarisations. From left to right: HH, HV, VV. Time lag: 16 days. Snowfall between both flights.

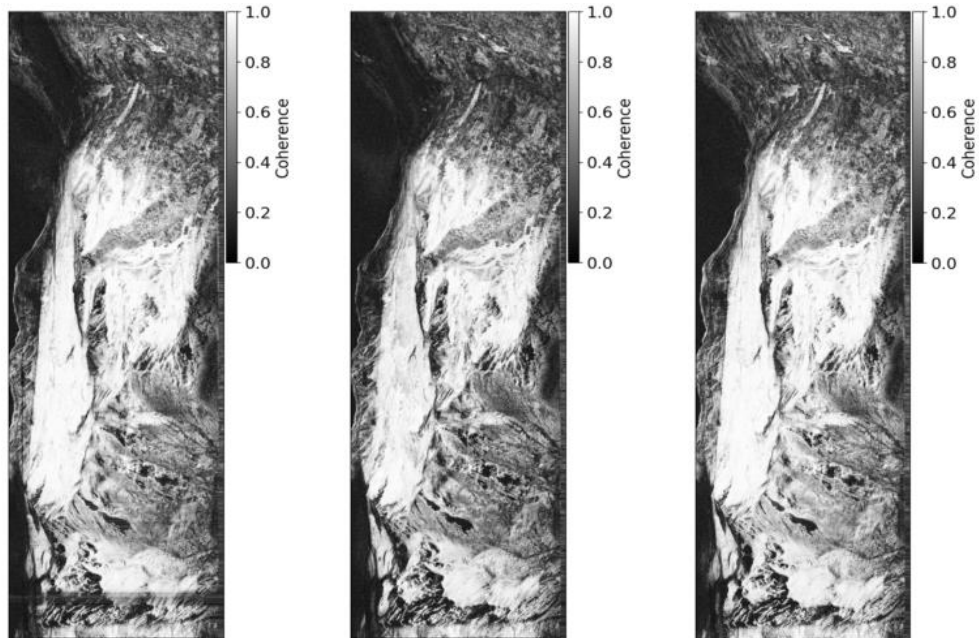


Figure 5-35: Interferometric coherence between simulated geosynchronous SAR SLCs of flight 3 and flight 4 of track 10 for different polarisations. From left to right: HH, HV, VV.

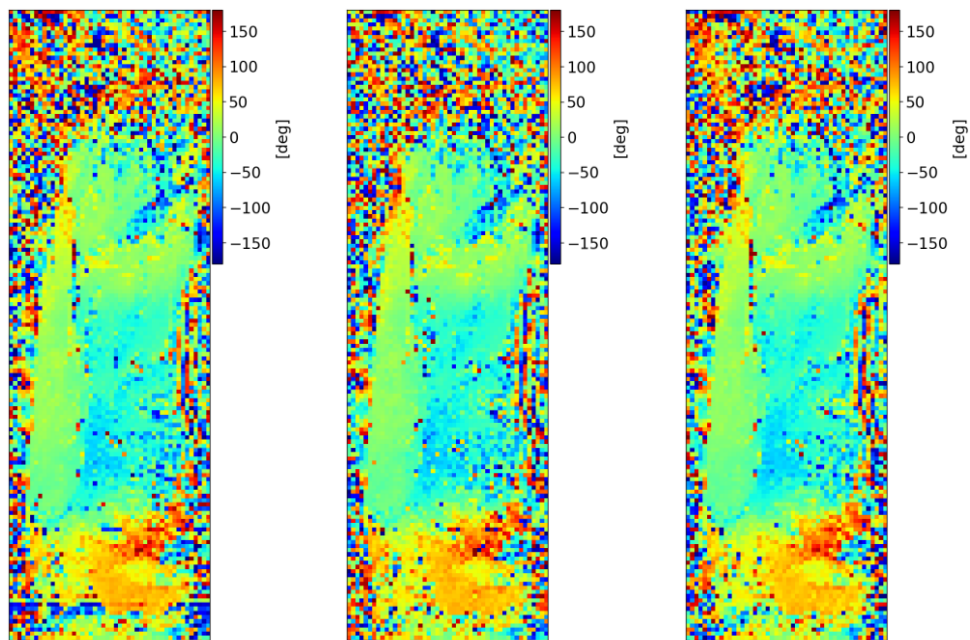


Figure 5-36: Interferometric phase between simulated geosynchronous SAR SLCs of flight 3 and flight 4 of track 10 for different polarisations. From left to right: HH, HV, VV. Time lag: 0.5 days. No snowfall between both flights.

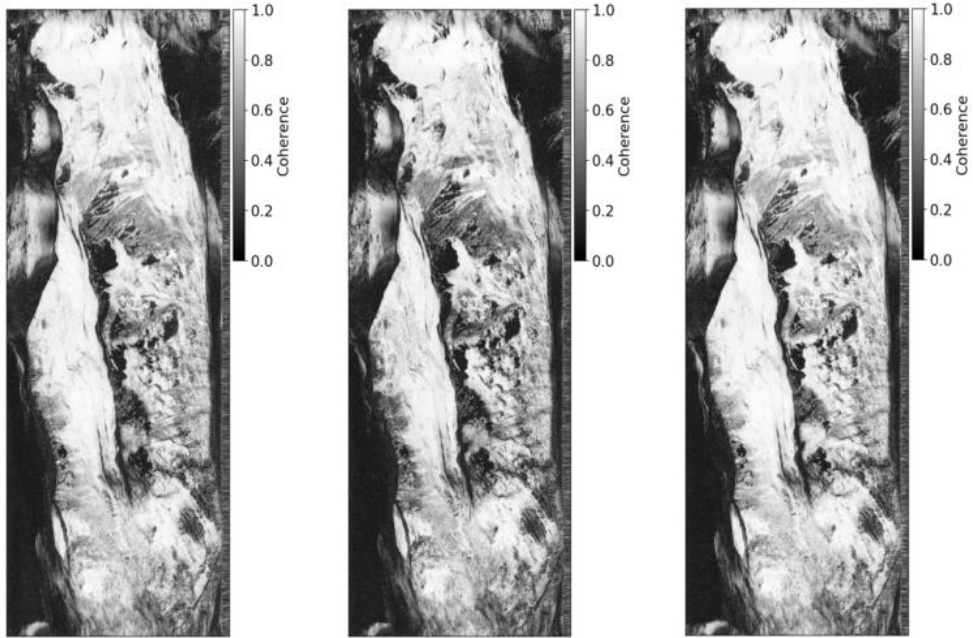


Figure 5-37: Interferometric coherence between simulated geosynchronous SAR SLCs of flight 3 and flight 4 of track 11 for different polarisations. From left to right: HH, HV, VV.

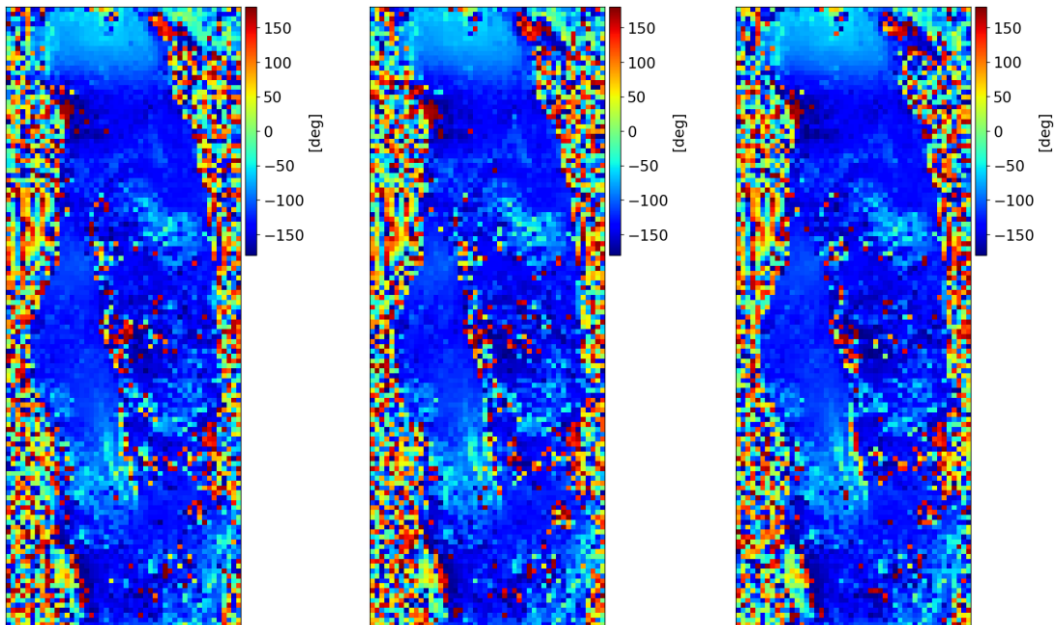


Figure 5-38: Interferometric phase between simulated geosynchronous SAR SLCs of flight 3 and flight 4 of track 11 for different polarisations. From left to right: HH, HV, VV. Time lag: 0.5 days. No snowfall between both flights.

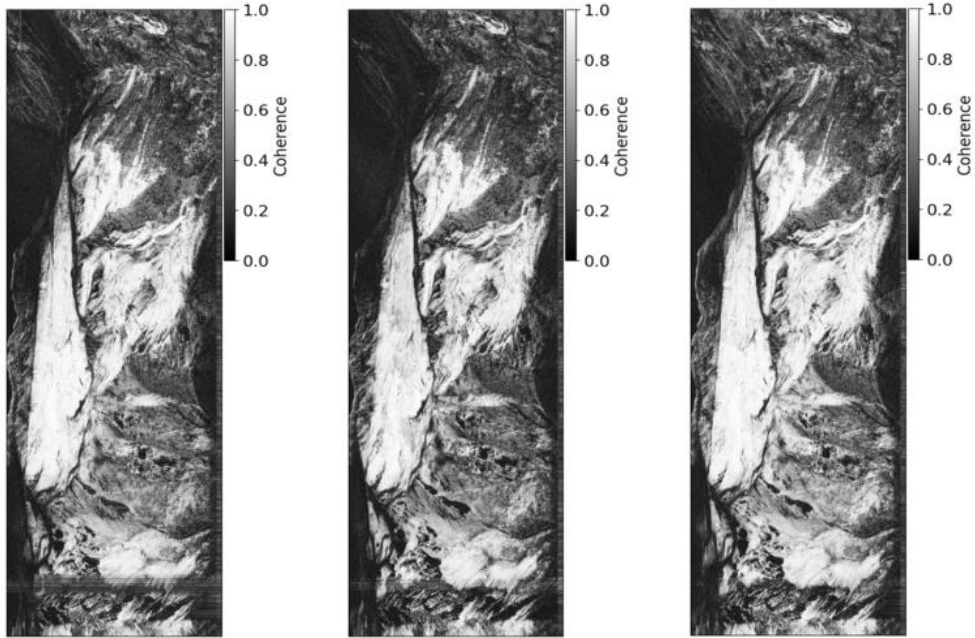


Figure 5-39: Interferometric coherence between simulated geosynchronous SAR SLCs of flight 6 and flight 7 of track 10 for different polarisations. From left to right: HH, HV, VV.

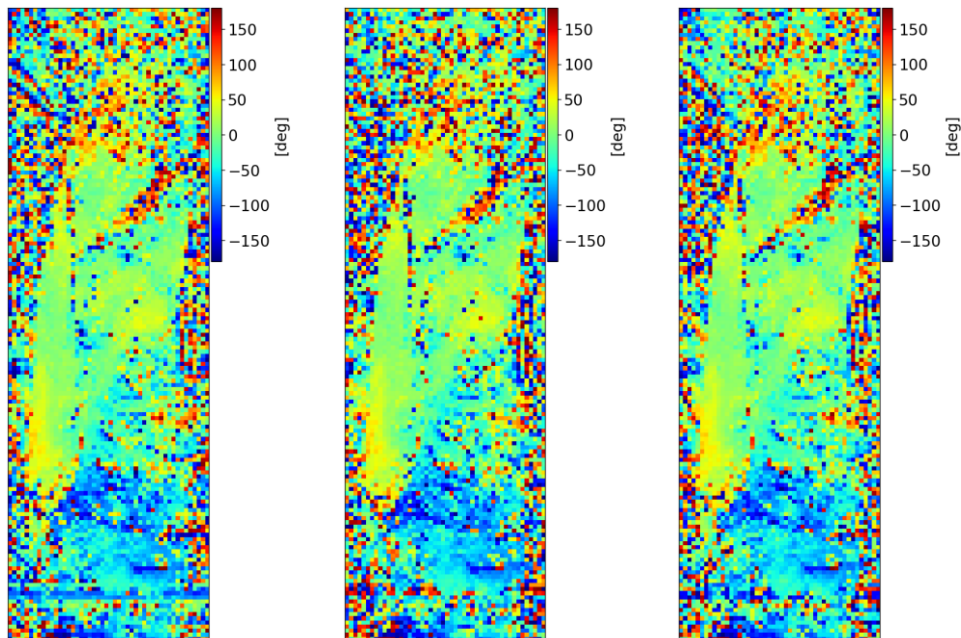


Figure 5-40: Interferometric phase between simulated geosynchronous SAR SLCs of flight 6 and flight 7 of track 10 for different polarisations. From left to right: HH, HV, VV. Time lag: 1 day. No snowfall between both flights.

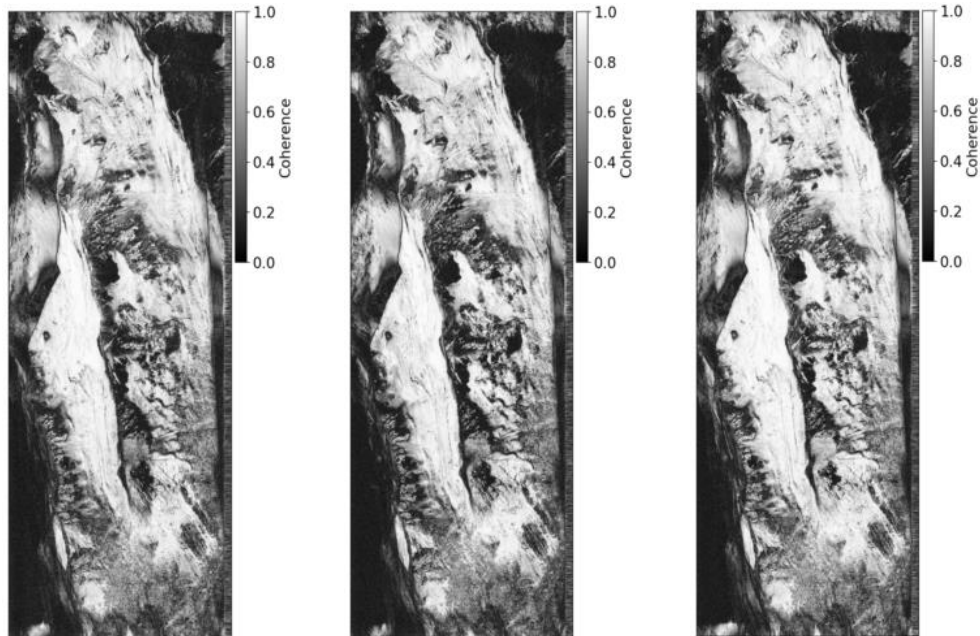


Figure 5-41: Interferometric coherence between simulated geosynchronous SAR SLCs of flight 6 and flight 7 of track 11 for different polarisations. From left to right: HH, HV, VV.

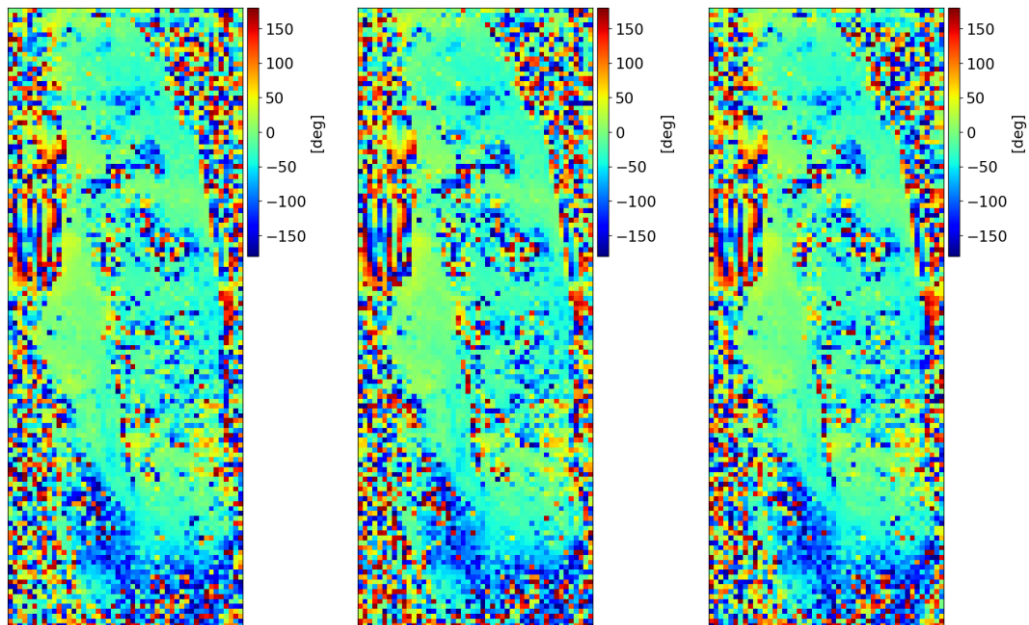


Figure 5-42: Interferometric phase between simulated geosynchronous SAR SLCs of flight 6 and flight 7 of track 10 for different polarisations. From left to right: HH, HV, VV. Time lag: 1 day. No snowfall between both flights.

	<p>SARSimHT-NG – Simulation of Hydroterra SAR System Performance in the Mediterranean and the Alps Based on Experimental Airborne SAR Data</p> <p>D1: Data Acquisition Report of SWE Experiment</p>	<p>Doc.: DLR-HR-TR-SARSimHT-NG-01 Issue: 2.0 Date: 25.11.2021 Page: 93 of 110</p>
---	---	--

5.4 Simulated Hydroterra Products

To analyse the potential to retrieve SWE from Hydroterra data, Hydroterra products were simulated and are described in this section. The difference between these products and the ones from Section 5.3 is that here not only the long integration time is simulated, but also the resolution, sampling, number of samples and NESZ is adjusted to the ones of the Hydroterra system. The products from this section are therefore referred to as Hydroterra products. To simulate the Hydroterra products, the parameters of the scenario 4 of the interferometric type (Glacier flow / Landslides) [7] were used. In Table 5-4 the relevant parameters are summarized.

The simulated Hydroterra products of all flights will be delivered to ESA. In this report exemplarily, the products of flight 2 and flight 5 are demonstrated, because flight 2 is one of the two flights with the shortest integration time and flight 5 is one of the two flights with the longest integration time. Figure 5-43 shows the single-look complex (SLC) Hydroterra products of flight 2 for track 10 and for all polarisations. Figure 5-44 demonstrates the multi-look (ML) detected images of flight 2 for track 10 and for all polarisations. The simulated Hydroterra SLC and ML images of flight 2 for track 11 and for all polarisations are visible in Figure 5-45 and Figure 5-46. Figure 5-47, Figure 5-48, Figure 5-49 and Figure 5-50 show the simulated Hydroterra SLC and ML images of flight 5 for both tracks.

Figure 5-52 to Figure 5-66 show the interferometric Hydroterra products of all interferometric pairs and for all polarisations. Figure 5-51, Figure 5-53, Figure 5-55, Figure 5-57, Figure 5-59, Figure 5-61, Figure 5-63 and Figure 5-65 visualize the interferometric coherence. The interferometric phase of the different pairs can be found in Figure 5-52, Figure 5-54, Figure 5-56, Figure 5-58, Figure 5-60, Figure 5-62, Figure 5-64 and Figure 5-66. More noise is visible in the simulated interferometric Hydroterra products, because of the higher NESZ. The signal between flight 2 and flight 8 is completely decorrelated, as is visible in Figure 5-55, Figure 5-56, Figure 5-57 and Figure 5-58.

Table 5-4: Relevant parameters of scenario 4 of the interferometric type used for Hydroterra product simulation.

Parameters	Values
Single-look azimuth resolution	5 m
Multi-look azimuth resolution	50 m
Number of looks in azimuth	10
Range bandwidth	6 MHz
Single-look slant range resolution	22.2 m
Multi-look slant range resolution	22.2 m
Number of looks in range	1
Noise Equivalent Sigma Zero	-21.1 dB

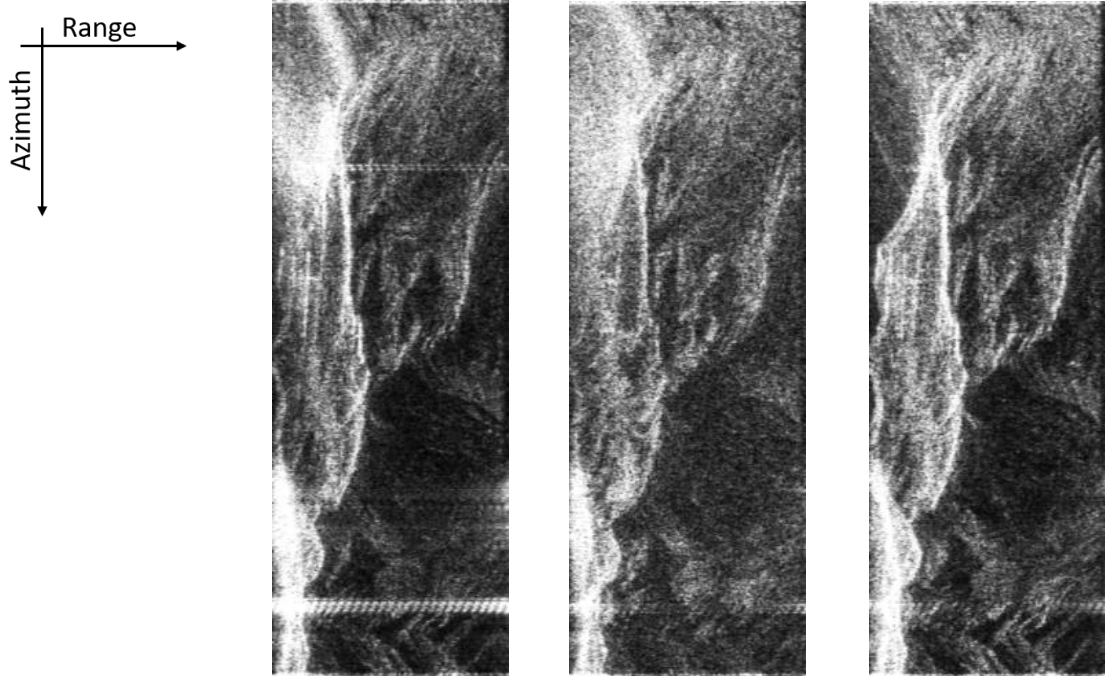


Figure 5-43: Simulated single-look complex (SLC) Hydroterra product of scenario 4 (resolution: 5 m x 22 m; samples: 1738 x 118) of flight 2 with track 10 for different polarisations. From left to right: HH, HV, VV.

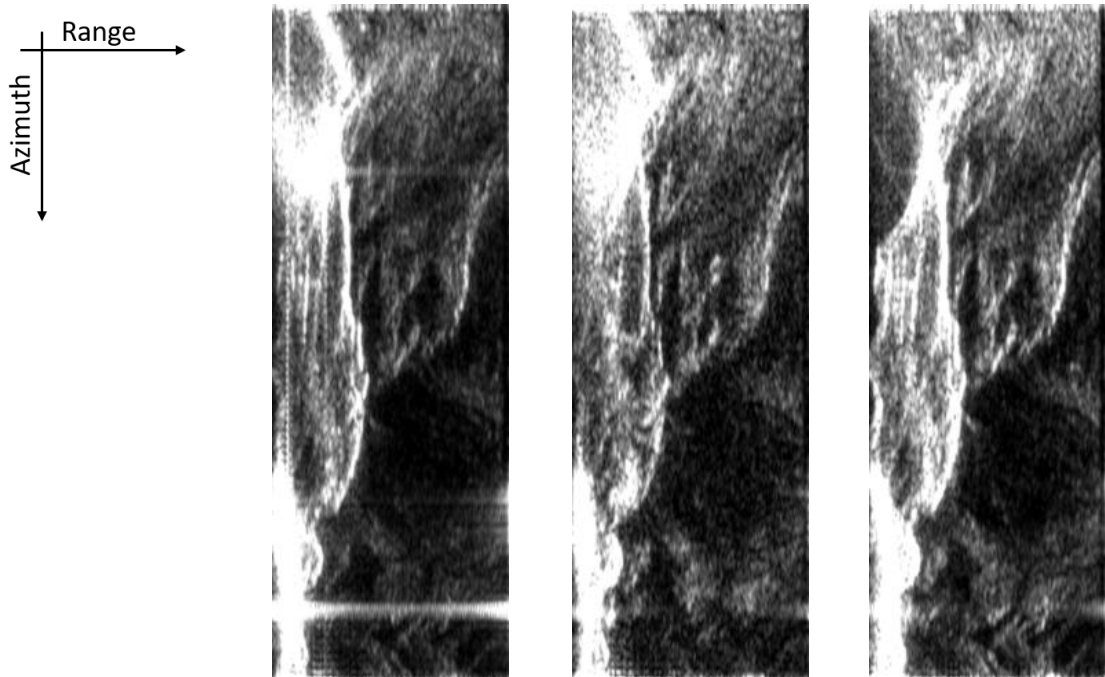


Figure 5-44: Simulated multi-look detected (ML) Hydroterra product of scenario 4 (resolution: 50 m x 22 m) of flight 2 with track 10 for different polarisations. From left to right: HH, HV, VV.

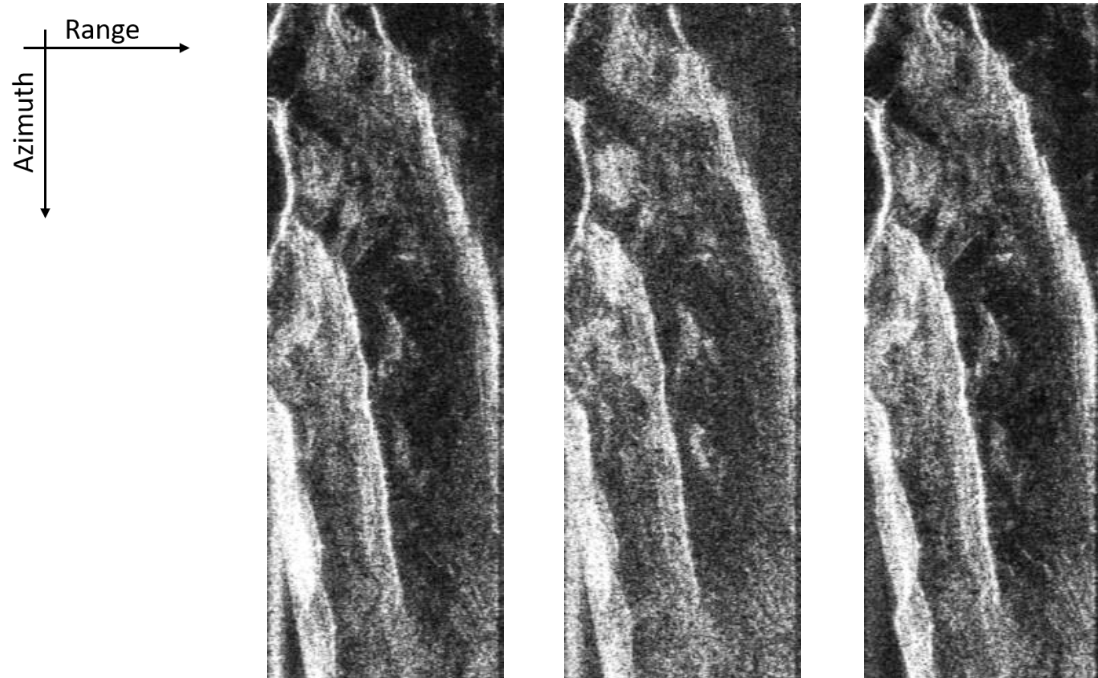


Figure 5-45: Simulated single-look complex (SLC) Hydroterra product of scenario 4 (resolution: 5 m x 22 m; samples: 1738 x 118) of flight 2 with track 11 for different polarisations. From left to right: HH, HV, VV.

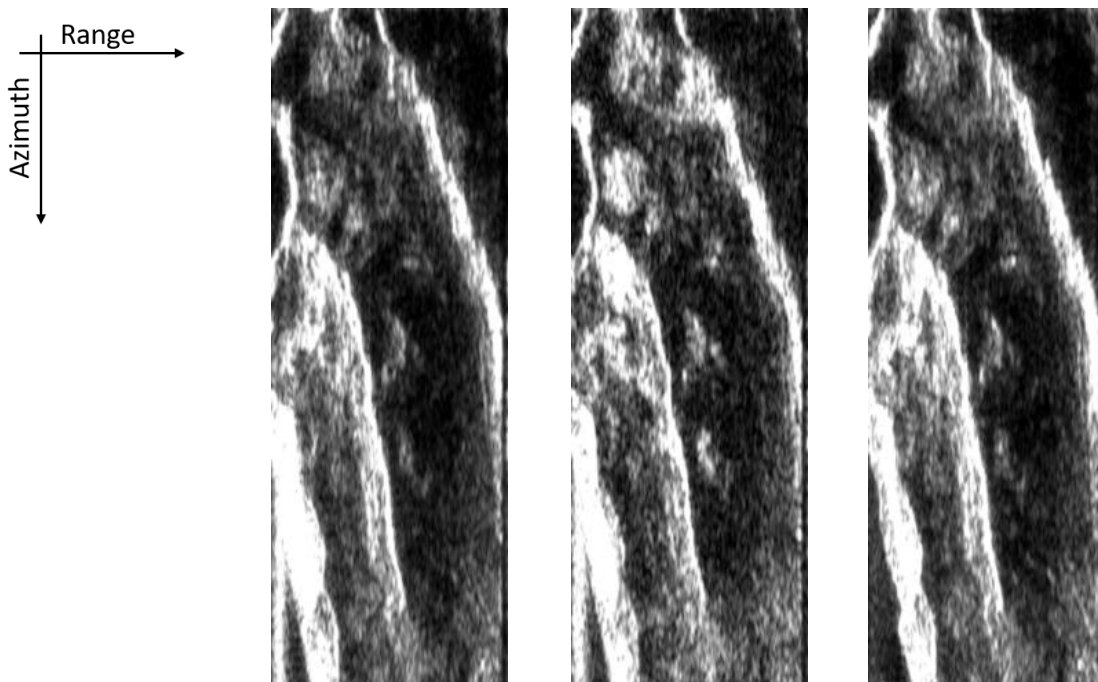


Figure 5-46: Simulated multi-look detected (ML) Hydroterra product of scenario 4 (resolution: 50 m x 22 m) of flight 2 with track 11 for different polarisations. From left to right: HH, HV, VV.

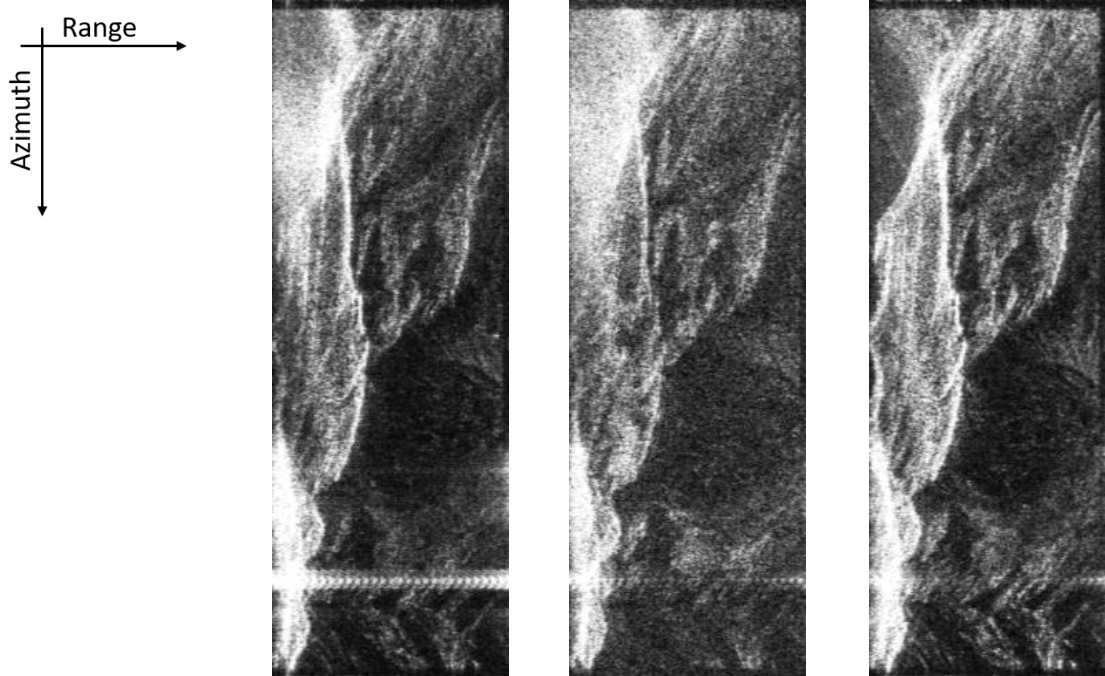


Figure 5-47: Simulated single-look complex (SLC) Hydroterra product of scenario 4 (resolution: 5 m x 22 m; samples: 1738 x 118) of flight 5 with track 10 for different polarisations. From left to right: HH, HV, VV.

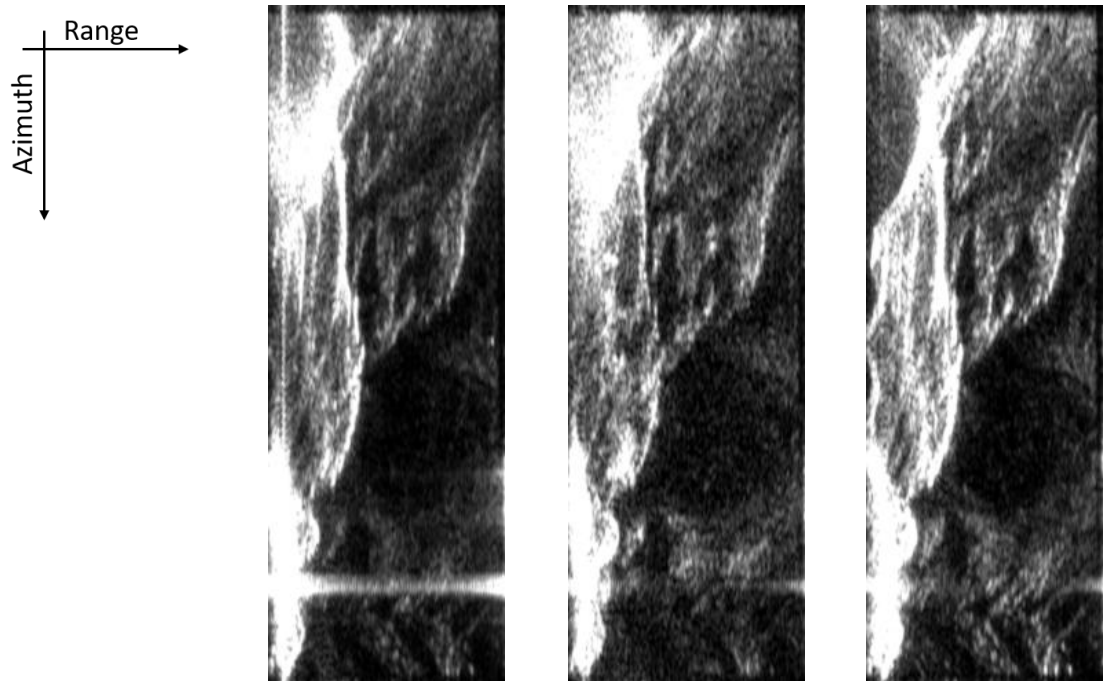


Figure 5-48: Simulated multi-look detected (ML) Hydroterra product of scenario 4 (resolution: 50 m x 22 m) of flight 5 with track 10 for different polarisations. From left to right: HH, HV, VV.

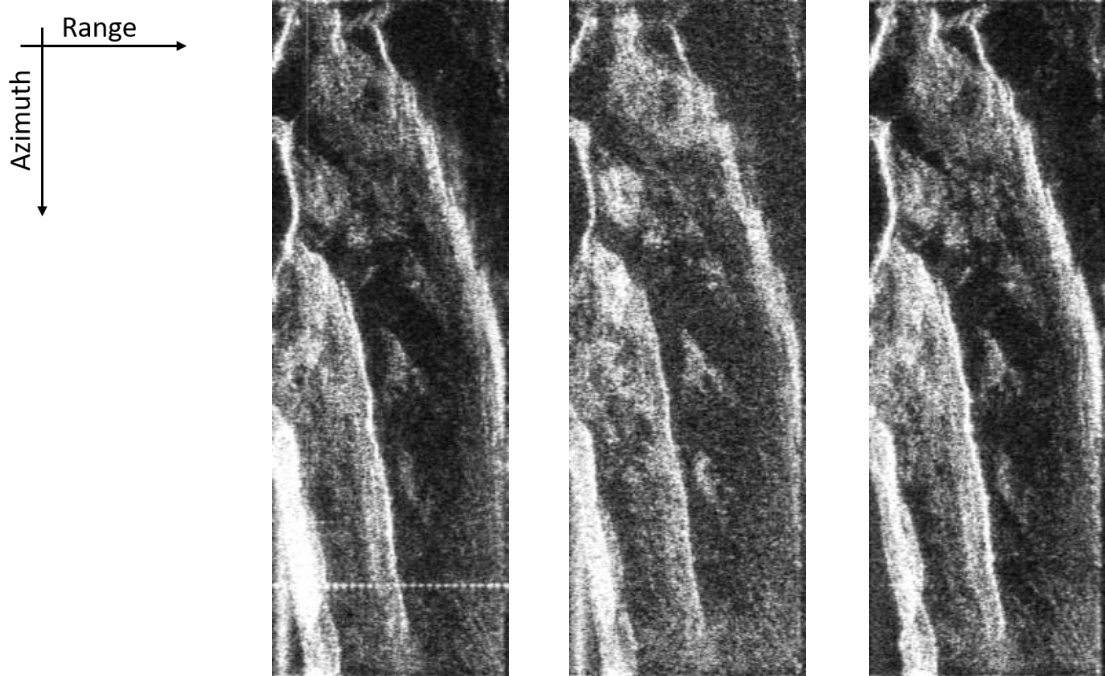


Figure 5-49: Simulated single-look complex (SLC) Hydroterra product of scenario 4 (resolution: 5 m x 22 m; samples: 1738 x 118) of flight 5 with track 11 for different polarisations. From left to right: HH, HV, VV.

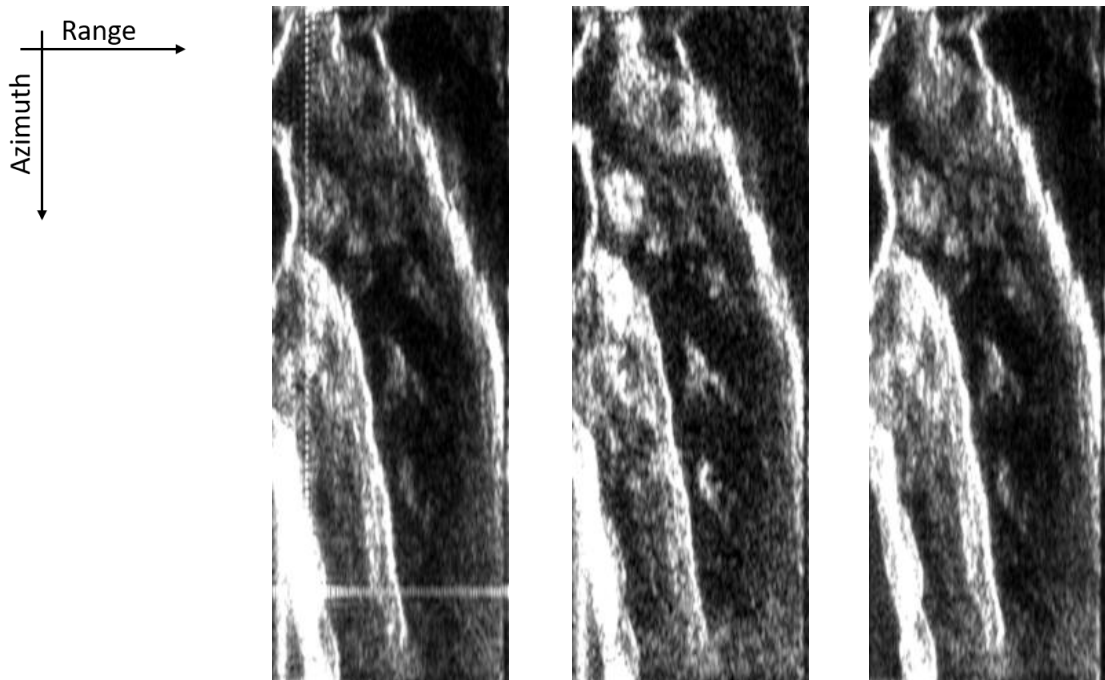


Figure 5-50: Simulated multi-look detected (ML) Hydroterra product of scenario 4 (resolution: 50 m x 22 m) of flight 5 with track 11 for different polarisations. From left to right: HH, HV, VV.

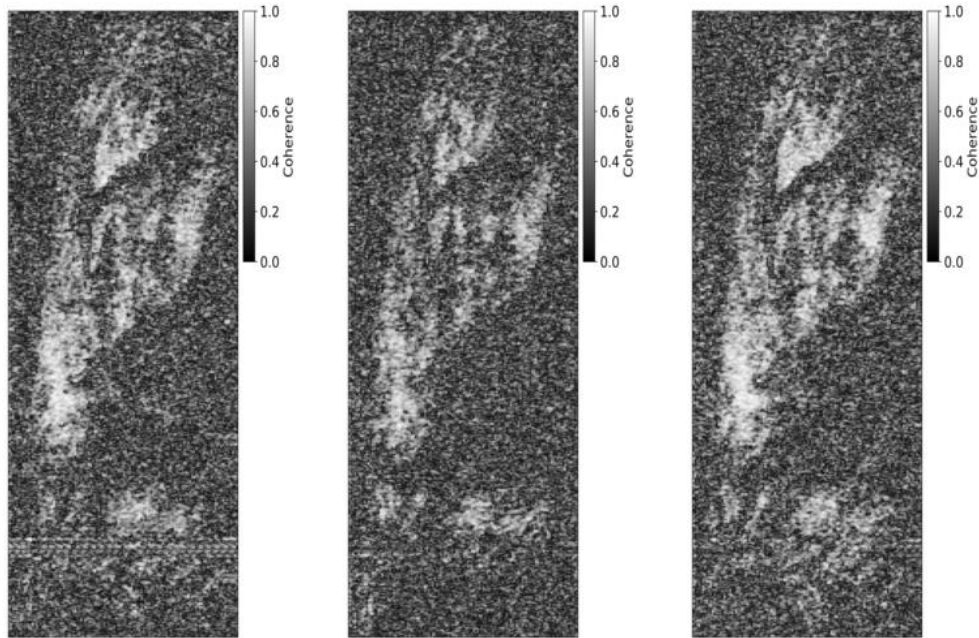


Figure 5-51: Interferometric coherence between simulated Hydroterra products of flight 1 and flight 5 of track 10 for different polarisations. From left to right: HH, HV, VV.

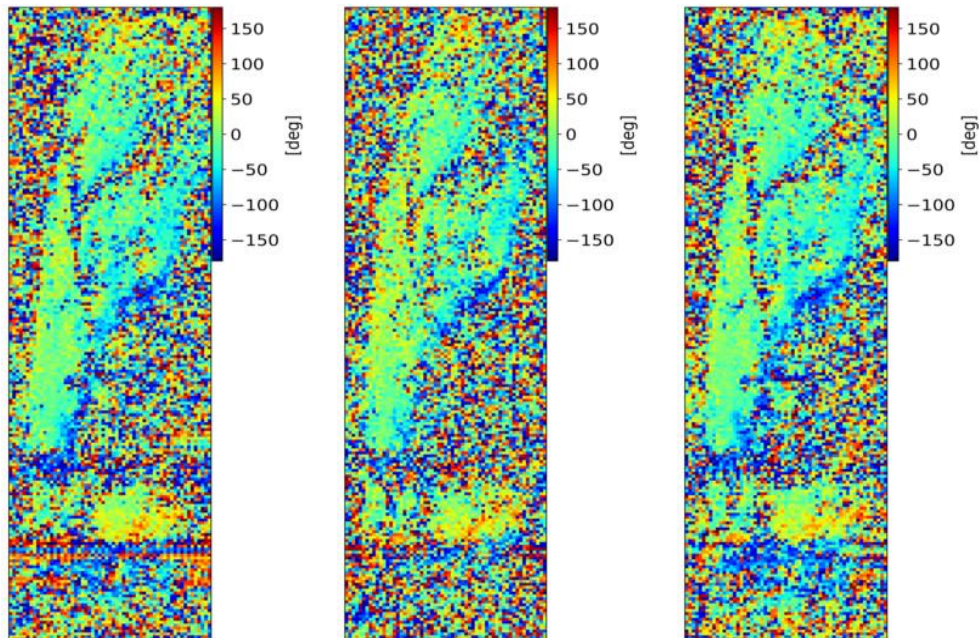


Figure 5-52: Interferometric phase between simulated Hydroterra products of flight 1 and flight 5 of track 10 for different polarisations. From left to right: HH, HV, VV. Time lag: 4 days. Snowfall between both flights.

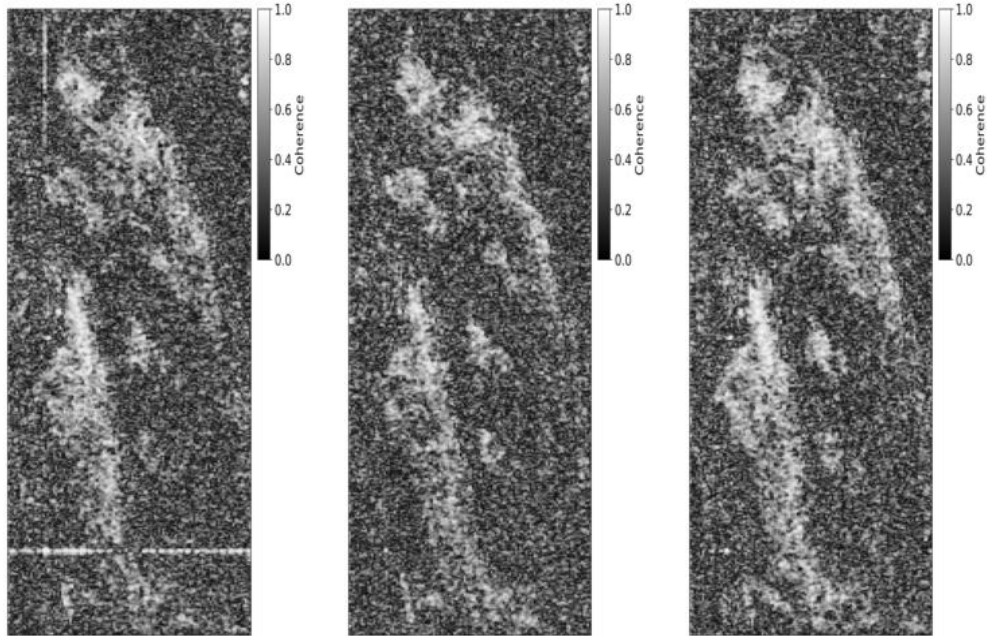


Figure 5-53: Interferometric coherence between simulated Hydroterra products of flight 1 and flight 5 of track 11 for different polarisations. From left to right: HH, HV, VV.

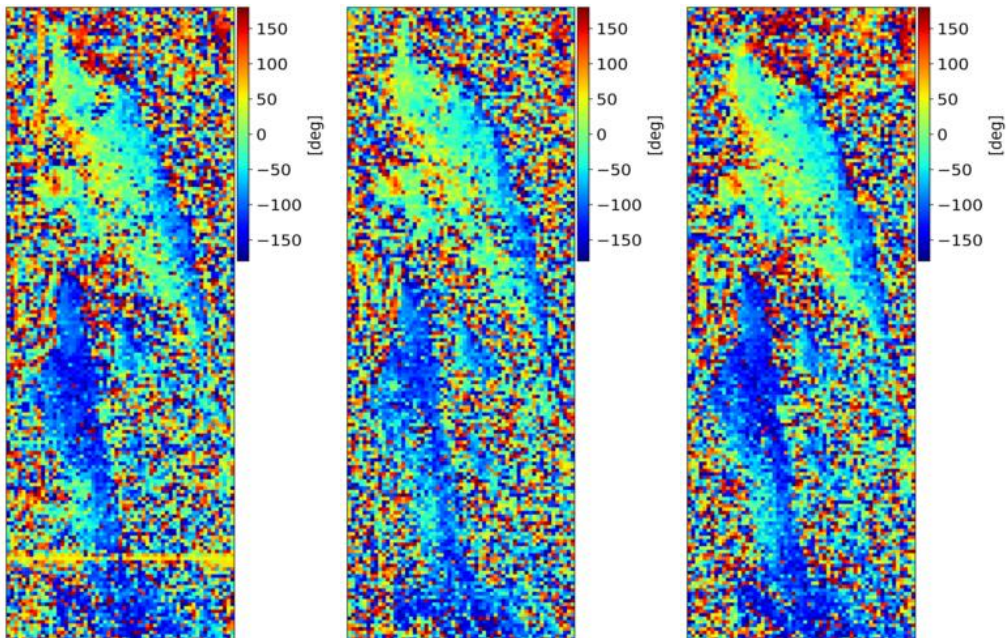


Figure 5-54: Interferometric phase between simulated Hydroterra products of flight 1 and flight 5 of track 11 for different polarisations. From left to right: HH, HV, VV. Time lag: 4 days. Snowfall between both flights.

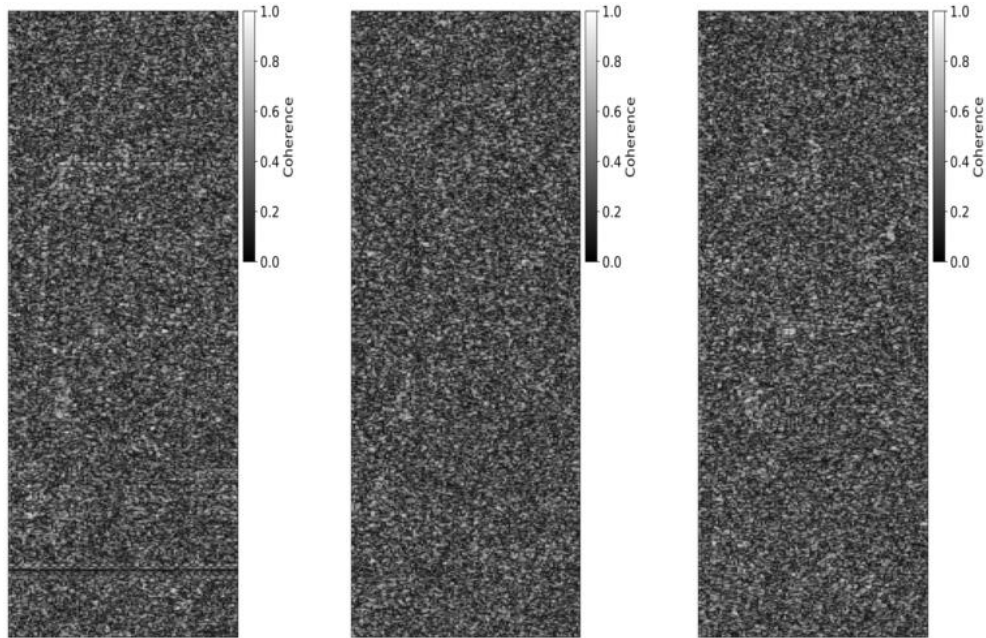


Figure 5-55: Interferometric coherence between simulated Hydroterra products of flight 2 and flight 8 of track 10 for different polarisations. From left to right: HH, HV, VV.

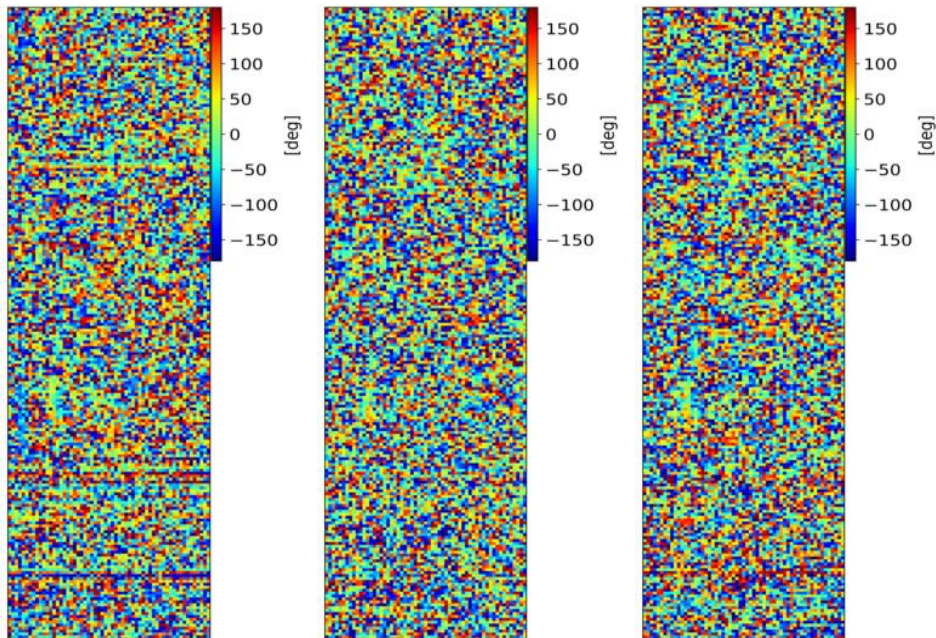


Figure 5-56: Interferometric phase between simulated Hydroterra products of flight 2 and flight 8 of track 10 for different polarisations. From left to right: HH, HV, VV. Time lag: 16 days. Snowfall between both flights.

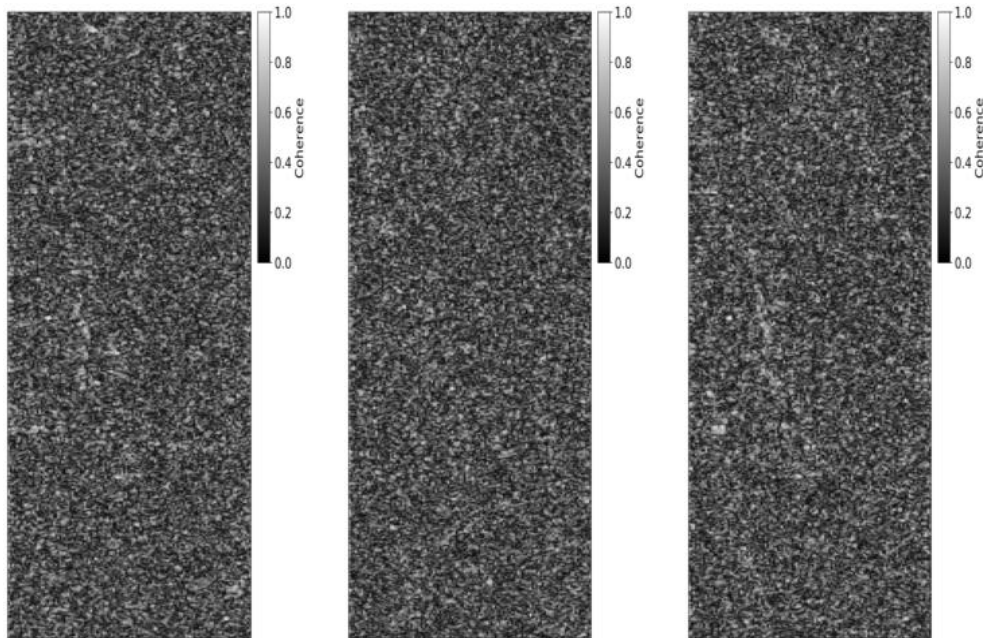


Figure 5-57: Interferometric coherence between simulated Hydroterra products of flight 2 and flight 8 of track 10 for different polarisations. From left to right: HH, HV, VV.

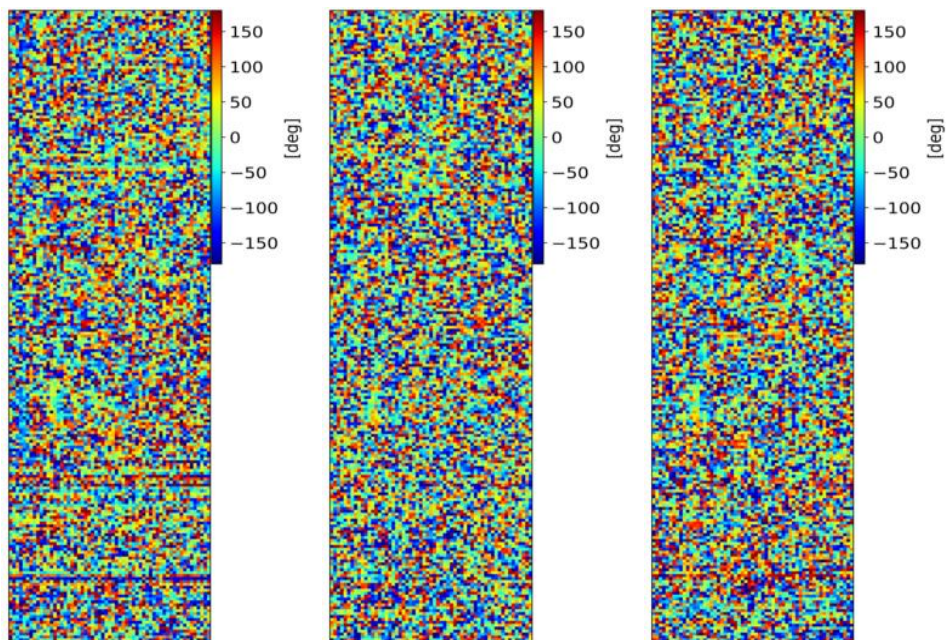


Figure 5-58: Interferometric phase between simulated Hydroterra products of flight 2 and flight 8 of track 10 for different polarisations. From left to right: HH, HV, VV. Time lag: 16 days. Snowfall between both flights.

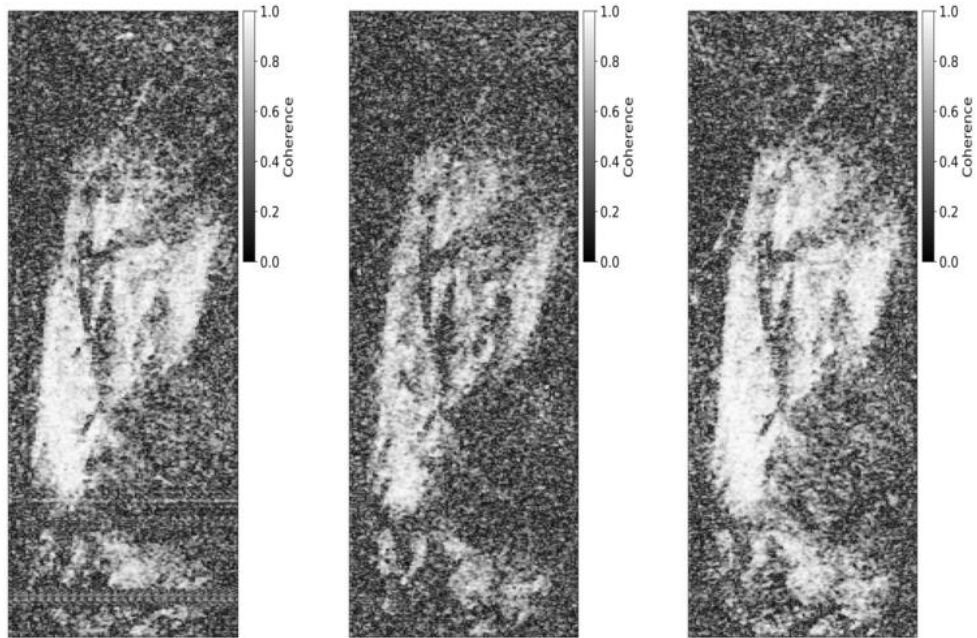


Figure 5-59: Interferometric coherence between simulated Hydroterra products of flight 3 and flight 4 of track 10 for different polarisations. From left to right: HH, HV, VV.

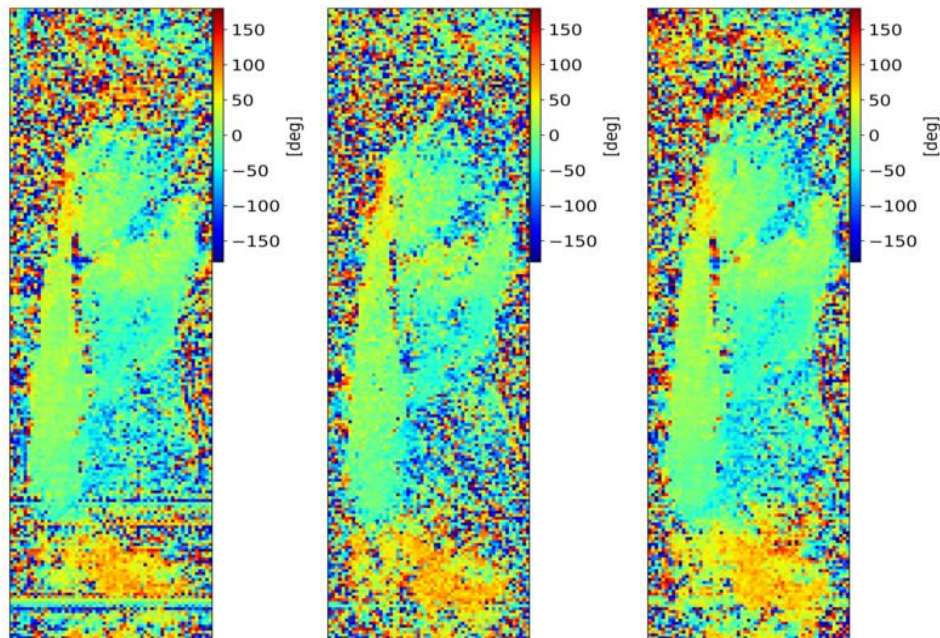


Figure 5-60: Interferometric phase between simulated Hydroterra products of flight 3 and flight 4 of track 10 for different polarisations. From left to right: HH, HV, VV. Time lag: 0.5 days. No snowfall between both flights.

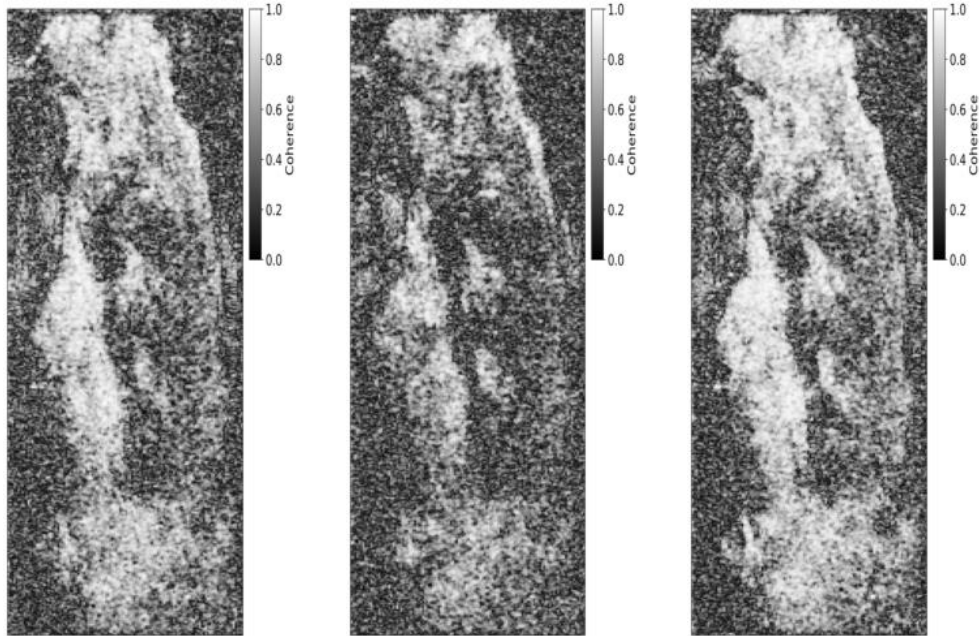


Figure 5-61: Interferometric coherence between simulated Hydroterra products of flight 3 and flight 4 of track 11 for different polarisations. From left to right: HH, HV, VV.

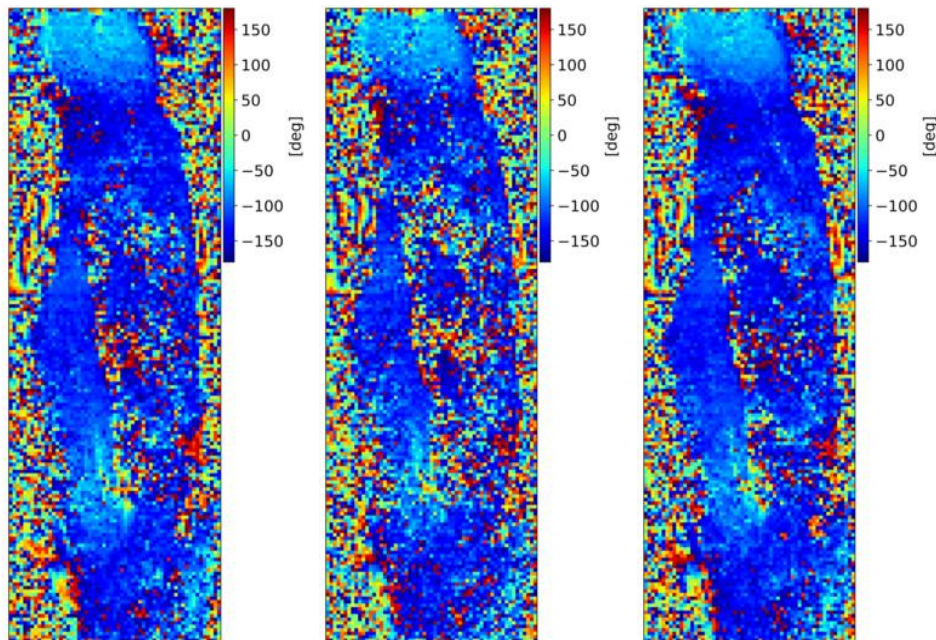


Figure 5-62: Interferometric phase between simulated Hydroterra products of flight 3 and flight 4 of track 11 for different polarisations. From left to right: HH, HV, VV. Time lag: 0.5 days. No snowfall between both flights.

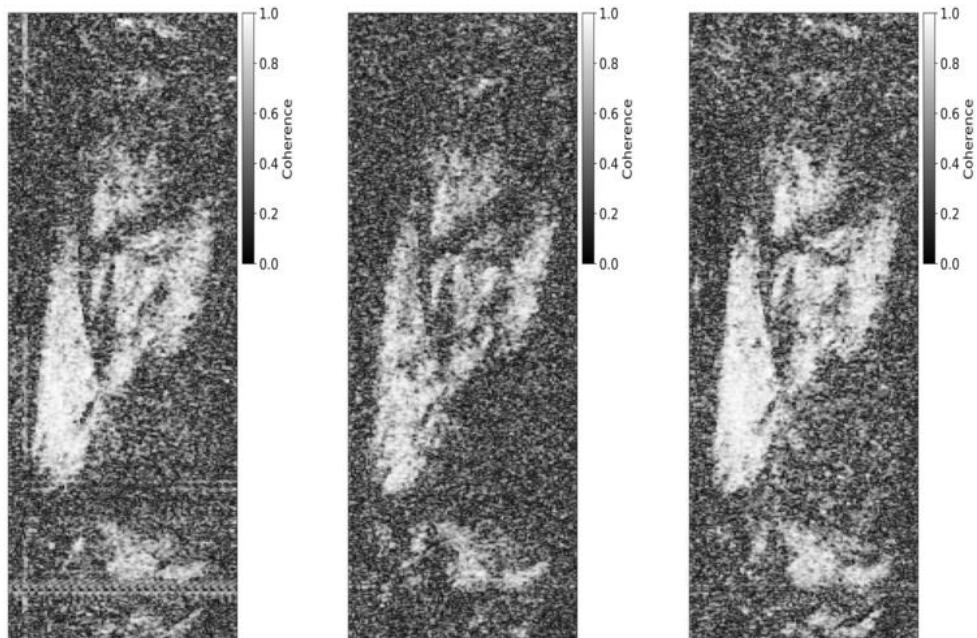


Figure 5-63: Interferometric coherence between simulated Hydroterra products of flight 6 and flight 7 of track 10 for different polarisations. From left to right: HH, HV, VV.

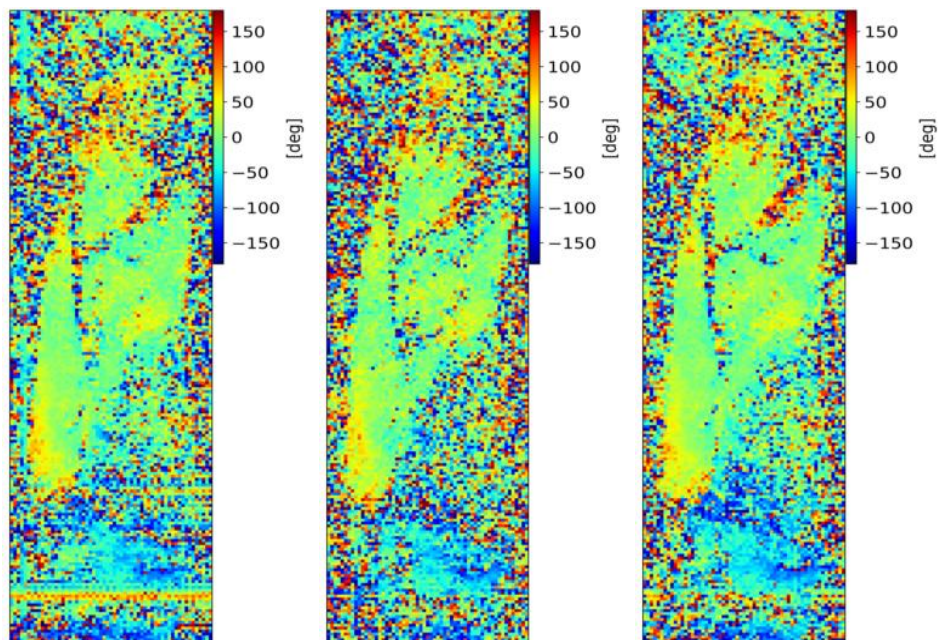


Figure 5-64: Interferometric phase between simulated Hydroterra products of flight 6 and flight 7 of track 10 for different polarisations. From left to right: HH, HV, VV. Time lag: 1 day. No snowfall between both flights.

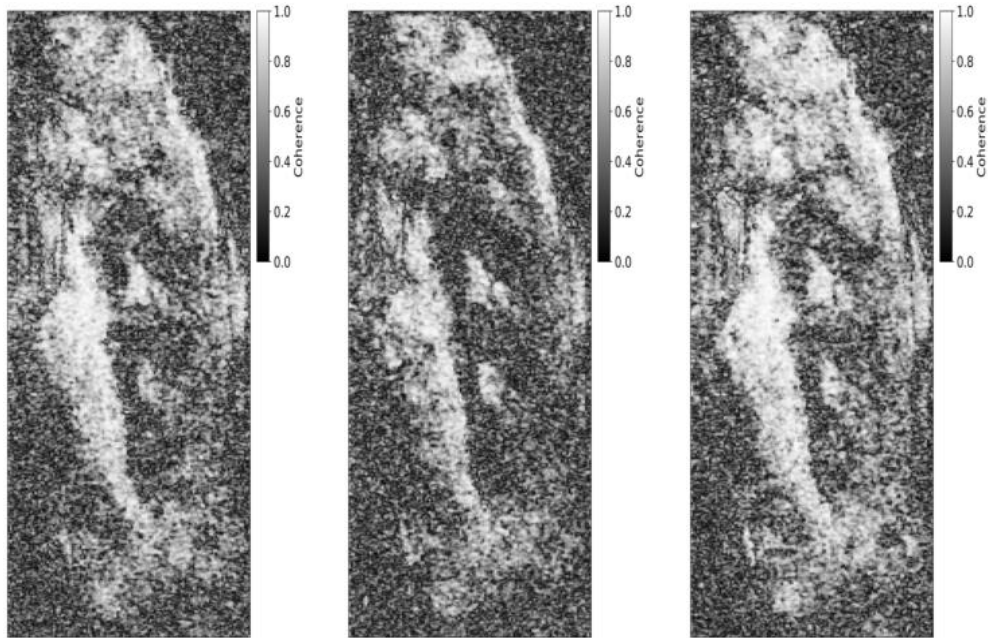


Figure 5-65: Interferometric coherence between simulated Hydroterra products of flight 6 and flight 7 of track 11 for different polarisations. From left to right: HH, HV, VV.

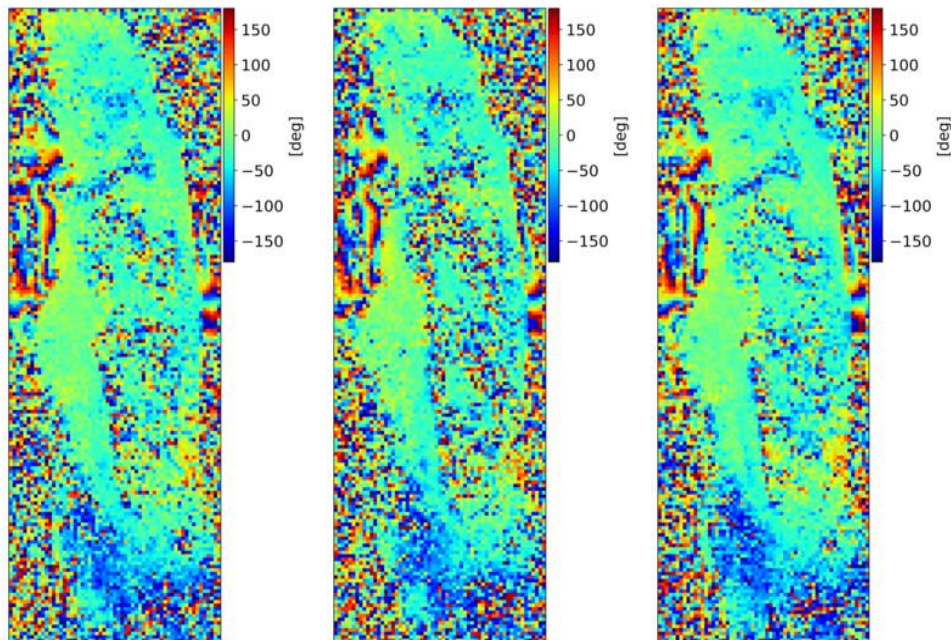


Figure 5-66: Interferometric phase between simulated Hydroterra products of flight 6 and flight 7 of track 11 for different polarisations. From left to right: HH, HV, VV. Time lag: 1 day. No snowfall between both flights.

	<p>SARSimHT-NG – Simulation of Hydroterra SAR System Performance in the Mediterranean and the Alps Based on Experimental Airborne SAR Data</p> <p>D1: Data Acquisition Report of SWE Experiment</p>	<p>Doc.: DLR-HR-TR-SARSimHT-NG-01 Issue: 2.0 Date: 25.11.2021 Page: 106 of 110</p>
---	---	---

5.5 Data Products Format

This section summarizes the data which will be delivered to ESA and describes its format.

From the simulation of geosynchronous SAR products with F-SAR resolution, the following data will be delivered to ESA:

- slc_geo_fIAA_trackCC_DD.rat
- slc_par_geo_fIAA_trackCC_DD.xml
- coh_geo_fIAA_fIBB_trackCC_DD.rat
- pha_geo_fIAA_fIBB_trackCC_DD.rat
- ppinsar_geo_fIAA_fIBB_trackCC_DD.xml

Here "AA" corresponds to the flight number, "CC" is the track number and "DD" the polarization. For interferometric products "AA" is the primary and "BB" the secondary flight. "slc_geo*.rat" are the simulated SLCs, "coh_geo_fIAA_fIBB *.rat" refers to the interferometric coherence and "pha_geo*.rat" to the interferometric phase. "slc_par_geo_fIAA_trackCC_DD.xml" is the xml file with all parameters. The file "ppinsar_geo_fIAA_fIBB_trackCC_DD.xml" is the xml file with all INSAR parameters. The structure and the parameters of all xml files and the rat format are described in [8].

Additionally, the following images will be delivered to ESA:

- slc_geo_fIAA_trackCC_DD.png
- coh_geo_fIAA_fIBB_trackCC_DD.png
- pha_geo_fIAA_fIBB_trackCC_DD.png
- contrast_geo_fIAA_trackCC_DD.png
- contrast_pass0_fIAA_trackCC_DD.png
- res_geo_fIAA_trackCC_DD.png
- PSLR_geo_fIAA_trackCC_DD.png
- ISLR_geo_fIAA_trackCC_DD.png

"slc_geo_fIAA_trackCC_DD.png", "coh_geo_fIAA_fIBB_trackCC_DD.png" and "pha_geo_fIAA_fIBB_trackCC_DD.png" are the quick looks of the corresponding data sets.

"coh_geo_pass0_fIAA_trackCC_DD.png" shows the coherence between the geosynchronous SAR SLC and the SLC of the first pass.

"contrast_geo_fIAA_trackCC_DD.png" visualizes the contrast of GEO SAR SLC. The contrast of the SLC of the first pass is shown in "contrast_pass0_fIAA_trackCC_DD.png".

The analysis of the azimuth impulse response function parameters for flight "AA" are shown in "res_geo_fIAA_trackCC_DD.png", "PSLR_geo_fIAA_trackCC_DD.png" and "ISLR_geo_fIAA_trackCC_DD.png".

In "res_geo_fIAA_trackCC_DD.png" the azimuth resolution is evaluated, in "PSLR_geo_fIAA_trackCC_DD.png" the azimuth peak-to-sidelobe ratio and in "ISLR_geo_fIAA_trackCC_DD.png" the integrated sidelobe ratio is analysed.

 	<p>SARSimHT-NG – Simulation of Hydroterra SAR System Performance in the Mediterranean and the Alps Based on Experimental Airborne SAR Data</p> <p>D1: Data Acquisition Report of SWE Experiment</p>	<p>Doc.: DLR-HR-TR-SARSimHT-NG-01 Issue: 2.0 Date: 25.11.2021 Page: 107 of 110</p>
--	---	---

From the simulation of Hydroterra products, the following data will be delivered to ESA:

- slc_ht_fIAA_trackCC_DD.rat
- slc_par_ht_fIAA_trackCC_DD.xml
- ml_ht_fIAA_trackCC_DD.rat
- ml_par_ht_fIAA_trackCC_DD.xml
- coh_ht_fIAA_fIBB_trackCC_DD.rat
- pha_ht_fIAA_fIBB_trackCC_DD.rat
- ppinsar_ht_fIAA_fIBB_trackCC_DD.xml

Additionally, the following images will be delivered to ESA:

- slc_ht_fIAA_trackCC_DD.png
- ml_ht_fIAA_trackCC_DD.png
- coh_ht_fIAA_fIBB_trackCC_DD.png
- pha_ht_fIAA_fIBB_trackCC_DD.png
- contrast_ht_fIAA_trackCC_DD.png
- contrast_pass0_fIAA_trackCC_DD.png

The description of the data and images is equivalent to the one of GEO SAR.

“ml_ht_fIAA_trackCC_DD.rat” is the multi-look detected product.

“ml_par_ht_fIAA_trackCC_DD.xml” is the xml file with all multi-look parameters.

	<p>SARSimHT-NG – Simulation of Hydroterra SAR System Performance in the Mediterranean and the Alps Based on Experimental Airborne SAR Data</p> <p>D1: Data Acquisition Report of SWE Experiment</p>	<p>Doc.: DLR-HR-TR-SARSimHT-NG-01 Issue: 2.0 Date: 25.11.2021 Page: 108 of 110</p>
---	---	---

5.6 Delivered Simulation Products

The following simulation products are delivered.

No.	Geosynchronous SAR - Simulation Product	Flight	Track	INF	Size
1	/mnt/HydroTerra/simulation_data/geo_fl01_track10	1	10	-	11G
2	/mnt/HydroTerra/simulation_data/geo_fl01_track11	1	11	-	9.1G
3	/mnt/HydroTerra/simulation_data/geo_fl05_track10	5	10	fl01-fl05	22G
4	/mnt/HydroTerra/simulation_data/geo_fl05_track11	5	11	fl01-fl05	19G
5	/mnt/HydroTerra/simulation_data/geo_fl02_track10	2	10	-	11G
6	/mnt/HydroTerra/simulation_data/geo_fl02_track11	2	11	-	9.1G
7	/mnt/HydroTerra/simulation_data/geo_fl08_track10	8	10	fl02-fl08	22G
8	/mnt/HydroTerra/simulation_data/geo_fl08_track11	8	11	fl02-fl08	19G
9	/mnt/HydroTerra/simulation_data/geo_fl03_track10	3	10	-	11G
10	/mnt/HydroTerra/simulation_data/geo_fl03_track11	3	11	-	9.2G
11	/mnt/HydroTerra/simulation_data/geo_fl04_track10	4	10	fl03-fl04	22G
12	/mnt/HydroTerra/simulation_data/geo_fl04_track11	4	11	fl03-fl04	19G
13	/mnt/HydroTerra/simulation_data/geo_fl06_track10	6	10	-	11G
1	/mnt/HydroTerra/simulation_data/geo_fl06_track11	6	11	-	9.1G
15	/mnt/HydroTerra/simulation_data/geo_fl07_track10	7	10	fl06-fl07	22G
16	/mnt/HydroTerra/simulation_data/geo_fl07_track11	7	11	fl06-fl07	19G

No.	HydroTerra SAR - Simulation Product	Flight	Track	INF	Size
1	/mnt/HydroTerra/simulation_data/ht_fl01_track10	1	10	-	52M
2	/mnt/HydroTerra/simulation_data/ht_fl01_track11	1	11	-	46M
3	/mnt/HydroTerra/simulation_data/ht_fl05_track10	5	10	fl01-fl05	71M
4	/mnt/HydroTerra/simulation_data/ht_fl05_track11	5	11	fl01-fl05	51M
5	/mnt/HydroTerra/simulation_data/ht_fl02_track10	2	10	-	52M
6	/mnt/HydroTerra/simulation_data/ht_fl02_track11	2	11	-	46M
7	/mnt/HydroTerra/simulation_data/ht_fl08_track10	8	10	fl02-fl08	72M
8	/mnt/HydroTerra/simulation_data/ht_fl08_track11	8	11	fl02-fl08	63M
9	/mnt/HydroTerra/simulation_data/ht_fl03_track10	3	10	-	52M
10	/mnt/HydroTerra/simulation_data/ht_fl03_track11	3	11	-	46M
11	/mnt/HydroTerra/simulation_data/ht_fl04_track10	4	10	fl03-fl04	71M
12	/mnt/HydroTerra/simulation_data/ht_fl04_track11	4	11	fl03-fl04	63M
13	/mnt/HydroTerra/simulation_data/ht_fl06_track10	6	10	-	52M
1	/mnt/HydroTerra/simulation_data/ht_fl06_track11	6	11	-	46M
15	/mnt/HydroTerra/simulation_data/ht_fl07_track10	7	10	fl06-fl07	71M
16	/mnt/HydroTerra/simulation_data/ht_fl07_track11	7	11	fl06-fl07	63M

 	SARSimHT-NG – Simulation of Hydroterra SAR System Performance in the Mediterranean and the Alps Based on Experimental Airborne SAR Data D1: Data Acquisition Report of SWE Experiment	Doc.: DLR-HR-TR-SARSimHT-NG-01 Issue: 2.0 Date: 25.11.2021 Page: 109 of 110
--	--	--

Regarding Group 03 (FL03 – FL04), we decided to deliver both the initially processed data stacks (including passes 0323 and 0409) and the re-processed stacks (excluding passes 0323 and 0409). However, the associated simulation products delivered were generated based on the re-processed stacks only.

 	<p>SARSimHT-NG – Simulation of Hydroterra SAR System Performance in the Mediterranean and the Alps Based on Experimental Airborne SAR Data</p> <p>D1: Data Acquisition Report of SWE Experiment</p>	<p>Doc.: DLR-HR-TR-SARSimHT-NG-01</p> <p>Issue: 2.0</p> <p>Date: 25.11.2021</p> <p>Page: 110 of 110</p>
--	---	---

6 Summary

In this Data Acquisition Report the airborne experiment, the ground truth measurements, the processed data products and the simulated geosynchronous SAR products with F-SAR resolution and simulated Hydroterra products of the SWE experiment are described.

In total eight flights were performed with DLR's F-SAR airborne radar system, where for each flight two different tracks were flown. The Wörgetal test site was illuminated from opposite look directions, from the east and the west. The collected data sets in L- and C-band were focused to obtain 368 fully polarimetric F-SAR products.

During the airborne experiment, six corner reflectors were deployed as ground control points and a ground-truth measurement team was present to measure the snow and air temperature, snow density, stratigraphy and the snow depth.

The processed C-band SAR images were used to simulate geosynchronous SAR products with F-SAR resolution as well as Hydroterra image quality. In total, 32 geosynchronous SAR product sets were generated, 16 with F-SAR resolution and 16 with Hydroterra image quality.

These products were used to compute interferometric products (phase and coherence) for each polarisation. The processed SAR images were also employed to simulate Hydroterra images and Hydroterra interferometric products. A preliminary analysis of the simulated data sets is provided.

The described ground-truth data, the processed airborne SAR data and the simulated products will be delivered to ESA.